A reporter cell system for TREM2 reveals differential effects of disease-associated variants on receptor signaling and activation by antibodies against the stalk region

Dissertation

zur

Erlangung des Doktorgrades (Dr. rer. nat.)

der

Mathematisch-Naturwissenschaftlichen Fakultät

der

Rheinischen Friedrich-Wilhelms-Universität Bonn

vorgelegt von

Melanie Sandra Ibach

aus Krefeld

Bonn 2020

Angefertigt mit Genehmigung der Mathematisch-Naturwissenschaftlichen Fakultät
der Rheinischen Friedrich-Wilhelms-Universität Bonn

1. Gutachter: Prof. Dr. Jochen Walter
2. Gutachter: Prof. Dr. Walter Witke

Tag der Promotion: 05.05.2021
Erscheinungsjahr: 2021

Table of contents

Summary

The triggering receptor expressed on myeloid cells 2 (TREM2) is an immune receptor expressed on myeloid-derived cell types. The extracellular immunoglobulin-like domain of TREM2 binds anionic ligands including Apolipoprotein E (APOE) and Amyloid-β (Aβ). The transmembrane domain interacts with its adaptor protein DAP12/TYROBP that is responsible for propagation of downstream signaling upon ligand interaction. Several sequence variants of TREM2 have been linked to different neurodegenerative diseases including Alzheimer's disease.

In this study, HEK 293 Flp-In cell lines were generated stably expressing human TREM2 and DAP12 using a bicistronic construct with a T2A linker sequence allowing initial expression of both proteins in stoichiometric amounts. Cell biological and biochemical analyses revealed transport of TREM2 to the cell surface, and canonical sequential proteolytic processing and shedding of TREM2 (sTREM2). Interestingly, the TREM2 G145W variant showed to possibly affect the cleavage and processing by ADAM proteases. Furthermore, the H157Y variant results in a more complex glycosylation as compared to the common variant in the reporter cell system. Using the cell model, we could further demonstrate that TREM2 is mainly degraded via the autophagy-lysosomal pathway. We verified the functionality of this cell system by detection of reactive oxygen species upon challenge with necrotic neural debris as well as by detection of phosphorylated spleen tyrosine kinase (SYK) upon stimulation of TREM2 with the anionic membrane lipid phosphatidylserine or anti-TREM2 antibodies. Using this cell model, we demonstrated impaired signaling of disease associated TREM2 variants. We also identified a monoclonal antibody against the stalk region of TREM2 with agonistic activity that induced phosphorylation of SYK by cross-linking. Activation of TREM2-DAP12 signaling with the monoclonal antibody and the partial loss-of-function of disease associated variants were recapitulated in induced pluripotent stem cell (iPSC) derived microglia. Thus, this reporter cell model represents a suitable experimental system to investigate signaling of TREM2 variants, and for the identification of ligands and compounds that modulate TREM2-DAP12 signaling.

1 Introduction

1.1 Common characteristics of neurodegenerative diseases

Neurodegenerative diseases are fatal, neurological disorders that share hallmarks at the neuropathological level, commonly characterized by accumulation of aggregated proteins forming fibrils (Takalo et al., 2013). These fibrils are termed amyloids, which are characterized by a cross-β structure along the fibril axis. Different proteins can adopt the structure of amyloids, thereby likely damaging neurons in the brain. Due to this specific common cross-β structure, dyes like Congo red or Thioflavin T specifically label amyloid structures irrespective of the nature of the different proteins in the respective disease (Saiki et al., 2005). Huntington's Disease (HD) is associated with protein aggregates of huntingtin protein with more than 36 CAG repeats. The length of the CAG repeats correlates with the severity and presence of inclusions, mainly found in the striatum (Ross & Poirier, 2004; Vonsattel et al., 1985). In Alzheimer's disease (AD), a dementing illness, there are different types of aggregated proteins. In early stages of the disease, degeneration of neurons is particularly found in the basal forebrain and hippocampus. Extracellular plaques and intracellular neurofibrillary tangles, consistent mostly of amyloid β (Aβ) and tau protein, respectively, are the major kinds of protein aggregates involved in AD (Ross & Poirier, 2004; Soto, 2003). In some cases of the progressive fatal disease amyotrophic lateral sclerosis (ALS), mutations in the superoxide dismutase 1 (SOD1) gene lead to aggregation of SOD1 protein that might cause degeneration of lower motor neurons and upper motor neurons in the spinal cord and cerebral cortex, respectively (Ross & Poirier, 2004). Another common neurodegenerative disease associated with protein aggregation is Parkinson's disease (PD). In this disease, misfolded α-synuclein aggregates/fibrils accumulate in so called Lewy bodies (Ross & Poirier, 2004). Aggregation of α-synuclein can occur as a result of high temperature or low pH (Ma et al., 2003). The most affected brain region in PD is the substantia nigra of the mid brain, though the disease is not limited to this area (Forno, 1996). Many neurodegenerative diseases also present inflammation in the central nervous system (CNS). This inflammation can have beneficial roles, however, it can lead to crucial damage of the CNS and neuronal connections (Stephenson et al., 2018; Wyss-Coray & Mucke, 2002).

1.2 Alzheimer's disease (AD)

Back in 1906, the neuropathologist Dr. Alois Alzheimer first described a form of dementia that was later named after him, Alzheimer's disease. His first AD patient was a 51-year old woman, Auguste Deter (Hippius & Neundörfer, 2003; Stelzmann et al., 1995). Since then, AD has become the most common cause of dementia, with 60-80 % of all cases, affecting over 30 million people worldwide (Prince et al., 2015; The Alzheimer's Association, 2020). Approximately 5-8 % of the world population over the age of 60 years will be living with dementia (Hebert et al., 2013; Prince et al., 2015). The advances in medical research and care and the social and environmental conditions in the current time will lead to a growing population above their 80's, also resulting in an increased number of AD patients (The Alzheimer's Association, 2020). The first clinical symptoms of the disease include mild memory loss and cognitive impairment, followed by abnormal social behavior and impairment of language skills (The Alzheimer's Association, 2020). The symptoms become more severe over time, as AD is a progressive disease with currently no available treatment. Patients eventually rely on others as they become unable to care for themselves, leading to social and economic burden.

The main neuropathological hallmarks of the disease are extracellular amyloid plaques and intraneuronal neurofibrillary tangles (NFTs), already described by Alois Alzheimer himself (Hippius & Neundörfer, 2003; Stelzmann et al., 1995). The amount of NFTs, consisting of hyperphosphorylated tau protein, highly correlates with the progression of clinical AD (Braak & Braak, 1991; Nelson et al., 2012; Tomlinson et al., 1970), whereas a strong association of the genetic background of AD and amyloid plaque formation was described (Nelson et al., 2012). In addition, neuroinflammation supposedly contributes equally to AD pathogenesis as amyloid plaques and NFTs (Heneka et al., 2015; Zhang et al., 2013). Amyloid-β (Aβ) peptides are the main component of the amyloid plaques (LaFerla et al., 2007). In the early 1990s, the Aβ cascade hypothesis was first described (Hardy & Higgins, 1992). This hypothesis states that Aβ peptides, generated by proteolytic cleavage of the amyloid precursor protein (APP), accumulate into extracellular senile plaques, disrupting the neuronal connections and initiating several neurotoxic events, including oxidative stress and decreased neuroplasticity, eventually leading to neuronal death (Paula et al., 2009; Rhein & Eckert, 2007). However, the accumulation and aggregation of Aβ

peptides is not the only trigger for these neurotoxic events, as it has been shown that the soluble Aβ oligomers appear to exert the main toxicity of all Aβ forms (Paula et al., 2009). Inside neurons, NFTs mainly consist of the tau protein (Brion et al., 1985; Grundke-Iqbal et al., 1987; Kosik et al., 1986; Wood et al., 1986). Under physiological conditions, tau is a microtubule-associated protein, stabilizing microtubules and regulating vesicular transport along the axons (Weingarten et al., 1975). When tau is hyperphosphorylated, its ability to bind, stabilize and promote microtubule assemblies is decreased (Grundke-Iqbal et al., 1987; Köpke et al., 1993). Hyperphosphorylation of tau might also lead to tau aggregation and formation of NFTs, as tau is more prone to aggregate when it is not bound to microtubules (Mandelkow & Mandelkow, 2012). The connection between AD and the immune system has been described, as inflammatory pathways seem to be highly involved in the pathogenesis of AD (Heneka et al., 2015). Also, several genes related to inflammatory processes were found to be associated with an increased risk of developing AD (Bradshaw et al., 2013; Guerreiro et al., 2013; Jonsson et al., 2013).

1.2.1 Genetic factors involved in AD

Even though age is the greatest known risk factor for the development of AD, it might not directly be the cause of it (Hebert et al., 2013). AD can be separated into two different forms, early-onset AD (EOAD) or familial AD and late-onset AD (LOAD) or sporadic AD. EOAD occurs in patients younger than 65 years. However, this describes the minority of all AD cases. In 1991, the first evidence was found that mutations in APP are involved in the development of EOAD (Goate et al., 1991). Further on, mutations in genes for presenilin 1 and 2 (PS1 and PS2) were linked to EOAD (Tanzi & Bertram, 2001). Mutations in all three described genes are involved in the generation or aggregation of Aβ, the main component of amyloid plaques in AD brains (Haass & De Strooper, 1999). However, the majority of AD patients develop LOAD. While the cause for this form of AD is not well understood, it has been suggested that environmental factors, lifestyle and the combination with genetic factors might contribute to the development of LOAD. The most important genetic risk factor is the ε4 isoform of the Apolipoprotein E (APOE) gene. The APOE gene is localized on chromosome 19, and has three different main isoforms in the human population: APOE ε2, APOE ε3 and APOE ε4 (Strittmatter et al., 1993). The most common form of APOE is APOE ε3. When one allele carries the APOE ε4 form, the

risk of developing AD is increased about fourfold, whereas the presence of APOE ε4 on both alleles increases the risk by more than 10-fold. In contrast to this, APOE ε2 showed to have a protective effect on the development of LOAD (Corder et al., 1994). Different gene sets were highly associated with AD risk, including lipid metabolism and regulation of APP trafficking or catabolic processes (Carbon et al., 2017; Jansen et al., 2019). Amongst others, SORL1 and ABCA7, involved in regulation of Aβ peptide production and transport of lipids across membranes, respectively, were identified as risk factors for EOAD (Bellenguez et al., 2017; Pottier et al., 2012; Steinberg et al., 2015). As described above, genes involved in immune responses were found to have an impact on the pathogenesis of AD as well. The triggering receptor expressed on myeloid cells 2 (TREM2) was identified in genome-wide association studies (GWAS) linked to LOAD (Guerreiro et al., 2013; Jonsson et al., 2013). TREM2 rare variant R47H increased the risk for developing AD comparable to one allele of the APOE ε4 form (Jonsson et al., 2013).

1.2.2 APP and Aβ generation

Amyloid plaques mainly consist of the Aβ peptide that is generated by sequential cleavage of APP. APP is a type I transmembrane protein with one large amino terminal ectodomain, a single transmembrane domain, and a small carboxy terminal tail within the cytosol of the cell (Dyrks et al., 1988; Kang et al., 1987). In neurons, APP has been shown to modulate the synaptic activity, formation and function and implies an important role in axonal transport of vesicles (Priller et al., 2006; Satpute-Krishnan et al., 2006; P. Wang, 2005). Alternative splicing of APP can lead to several isoforms. In the brain, APP695 is mainly expressed by neurons and represents one of the shorter isoforms. In contrast, APP770 is the longest isoform and together with APP751 mainly produced by peripheral cells or platelets and non-neuronal brain cells (Esch et al., 1990; Ponte et al., 1988; Selkoe, 2001). The Aβ region in APP lies partly within the ectodomain and the transmembrane domain (Kang et al., 1987). Additionally, APP can be proteolytically processed by several proteases, resulting in the generation of different proteolytic derivatives (Figure 1). In the non-amyloidogenic pathway, α-secretase cleaves APP within the ectodomain. Proteases, harboring the α-secretase activity are several members of the ADAM (a disintegrin and metallo proteinases) family, including ADAM9, ADAM10, ADAM17 and ADAM19 (Allinson et al., 2003). The cleavage site of α-secretase in APP is located within the Aβ region.

Thus, cleavage by α-secretase prevents the production of potentially harmful Aβ species (Roberts et al., 1994). Following α-secretase cleavage, soluble APPα (sAPPα) is released into the extracellular fluid. Additionally, a α-C-terminal-fragment (α-CTF, C83) is generated, still anchored to the cellular membrane. In contrast, the amyloidogenic pathway describes the initial cleavage of APP by β-secretase, resulting in the release of sAPPβ and a membrane-tethered β-CTF, also called C99. The β-site APP-cleaving enzyme (BACE) has been identified as the main β-secretase processing APP (Vassar et al., 1999; Yan et al., 1999). After processing by α- or β-secretase, the respective α- and β-CTFs can be further cleaved by γ-secretase, leading to the production of p3 (3 kDa) and Aβ (4 kDa), respectively (Haass et al., 1993). P3 and Aβ peptides are released into the extracellular fluid whereas an APP intracellular domain (AICD) remains cytosolic, acting as a transcription factor (Furukawa et al., 2002; LaFerla et al., 2007; Mattson, 1997; Pardossi-Piquard & Checler, 2012). The γ-secretase represents a protein complex consisting of four proteins essential for the enzymatic activity, called APH-1, PEN-2, nicastrin and PS1 or PS2 (De Strooper, 2003; Edbauer et al., 2003). As mentioned earlier, mutations of PS1 and PS2 are associated with the development of EOAD (Haass & De Strooper, 1999; Tanzi & Bertram, 2001).

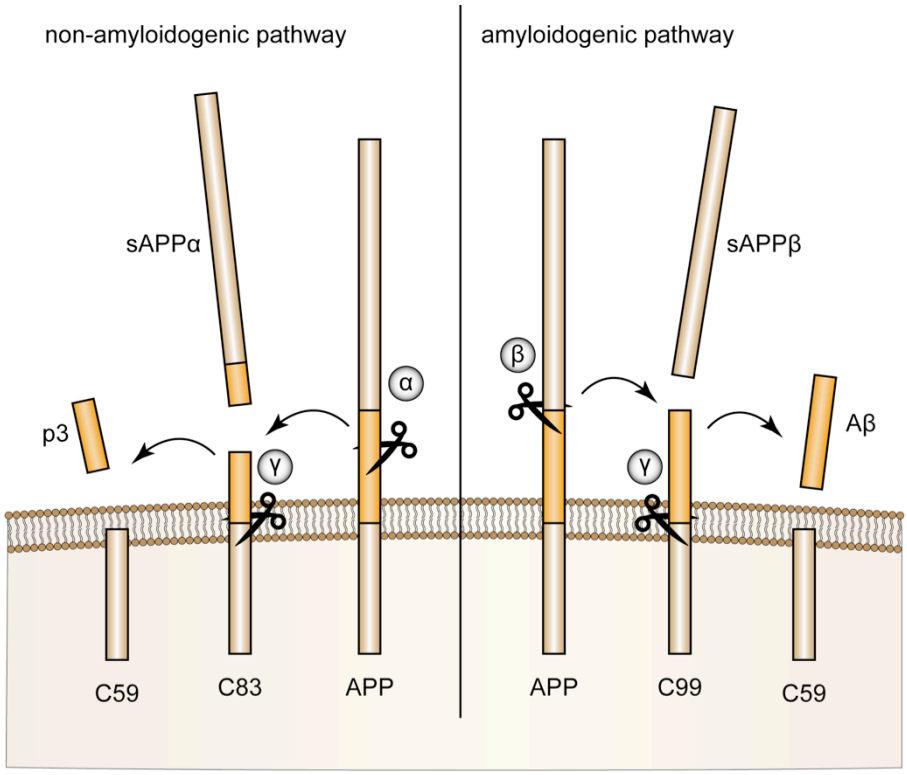

Figure 1: Proteolytic processing of APP. In the non-amyloidogenic pathway, APP is initially cleaved by α-secretase, leading to the release of sAPPα into the extracellular space and generation of a α-CTF (C83) within the plasma membrane. The amyloidogenic pathway starts with generation of sAPPβ and a membrane bound fragment C99 by proteolytic cleavage of β-secretase. In both pathways, γ-secretase conducts a subsequent cleavage of the respective CTFs, leading to the release of p3 and Aβ in the non-amyloidogenic and amyloidogenic pathway, respectively (Image adapted from LaFerla et al., 2007).

The Aβ peptide, generated by the amyloidogenic pathway, can be of different lengths, ranging between 37 and 49 amino acids. The most abundant species are Aβ40 and Aβ42, with the latter to a much lower extent (Citron et al., 1996; Wiltfang et al., 2002). The generation of Aβ40 and Aβ42 occurs through endoproteolysis in a stepwise process, possibly due to inaccurate cleavage by the respective enzymes. The first cleavage occurs at aa48 or 49, followed by cleavage at position 45 or 46, eventually resulting in a peptide with 38, 40 or 42 amino acids in length (Kummer & Heneka, 2014; Qi-Takahara, 2005). It has been shown, that even though Aβ42 is less abundant, it is more toxic to neurons. Due to the last two amino acids, the peptide becomes more hydrophobic and thus is more prone to aggregate and deposit in amyloid plaques (Barrow et al., 1992; Haass & Selkoe, 2007; Jarrett et al., 1993).

Aβ can undergo several post-translational modifications (PTM). Among others, phosphorylation at Serine 8 and Serine 26 (Kumar et al., 2011, 2013; Milton, 2001),

nitration (Kummer et al., 2011), pyroglutamylation (Mori et al., 1992) and N-terminal truncation can occur (Güntert et al., 2006; Schieb et al., 2011). Some PTMs have been shown to increase the aggregation rate of Aβ. Truncation of Aβ at its N-terminus makes up the majority of Aβ species in AD brains (Sergeant et al., 2003). Truncations, producing Aβ 2-x, 3-x, 4-x, 5-x and even larger amino acid deprivations, have been described in AD patients as well as transgenic mouse models (Kummer & Heneka, 2014). In *in vitro* studies, N-terminally truncated species have an increased aggregation propensity as compared to Aβ peptides starting at Asp1, the first amino acid of the Aβ domain (Pike et al., 1995). Oxidation of Aβ has been described in AD patients at early stages of the disease. In neurodegenerative diseases, increased oxidative stress possibly plays an important role in the initiation and progression of the disease (Kim et al., 2015). As the brain depends on a large amount of oxygen to properly fulfill its functions, it is more prone to generate free radicals or reactive oxygen species (ROS) (Singh et al., 2019). However, oxidation of methionine at position 35 (Met35) prevents the formation of Aβ fibrils (Hou et al., 2002; Palmblad et al., 2002). This might confirm that oligomeric Aβ species exert more toxic effects on neurons compared to amyloid fibrils. Phosphorylation of Aβ can occur at two positions within the peptide, serine residue 8 (Ser8) and 26 (Ser26). Some studies described effects of both PTMs on AD pathology. In AD brains and the NT-2 neuronal cell line, phosphorylation of Ser26 was reported (Kumar et al., 2016; Milton, 2001). This PTM showed to stabilize the formation of Aβ oligomers and thus increased neurotoxic effects (Kumar et al., 2016; Rezaei-Ghaleh et al., 2014). Phosphorylation of Aβ at Ser8 was observed in amyloid plaques, but could also be found inside neurons, just like phosphorylation at Ser26 (Kumar et al., 2011, 2013, 2016). Tyr10 in the Aβ peptide can be nitrated. This possibly occurs by the enzyme nitric oxide synthase-2 that has been shown to be up-regulated in AD (Fernández-Vizarra et al., 2004; Heneka et al., 2001). Another PTM is pyroglutamylation at position 3 or 11 of the Aβ peptide (3pE-Aβ, 11pE-Aβ). In N-terminally truncated Aβ, glutamate is converted into pyroglutamate, making the peptide less soluble (Mori et al., 1992; Saido et al., 1995). The increased propensity to form aggregates might be explained due to the loss of charges and thus the gain in hydrophobicity at the N-terminus of the peptide (He & Barrow, 1999). Furthermore, presence of 3pE-Aβ in amyloid plaques was described in postmortem brains of aged individuals (Saido et al., 1995). Mouse models that generate 3pE-Aβ showed progressive accumulation

and formation of amyloid plaques, accompanied by severe neurotoxic effects (Alexandru et al., 2011; Wirths et al., 2009). Interestingly, presence of pyroglutamylated Aβ was already found in preclinical stages of AD, whereas phosphorylated Ser8 species could be exclusively detected in the clinical stage of AD (Rijal Upadhaya et al., 2014). Thus, phosphorylation of Ser8 possibly represents an important step in the transition of preclinical AD to clinical AD.

1.3 Microglia

As inflammation in the CNS is also a hallmark of neurodegenerative diseases, microglia, the resident immune cells of the brain have gained high interest. Neurons and glia cells (microglia, astrocytes and oligodendrocytes) are the main cells in the CNS (Jäkel & Dimou, 2017). Microglia represent 5-20 % of all cells in the CNS and exert main functions in its homeostasis (Perry, 1998; Perry et al., 2010). Just one century ago, the origin of microglia cells has been identified. Microglia arise from primitive myeloid precursors in the yolk-sac during early hematopoiesis and further infiltrate the CNS, where they differentiate and build connections to other cells in the CNS (Ginhoux et al., 2010; Ransohoff & Cardona, 2010). Subsequently, the blood-brain-barrier (BBB) develops, leading to a separation of microglia in the CNS and the immune cells in other tissues. During brain development, microglia fulfill many different functions. When blood vessels are built throughout the brain, microglia control this process by clearing excess vessels (Fantin et al., 2010). In addition, microglia control the number of neurons by releasing growth factors, or phagocytosing excess neural stem cells (Cunningham et al., 2013; Ueno et al., 2013). Furthermore, synapse formation and synapse pruning of neurons is regulated by microglia cells (Stevens et al., 2007; Tremblay et al., 2010). Involvement of microglia in the process of myelination has also been described, as they promote the maturation of oligodendrocyte precursor cells into oligodendrocytes (Pang et al., 2013; Shigemoto-Mogami et al., 2014). In their resting state, their most important function is the surveillance of the CNS and maintaining its homeostasis (Nimmerjahn et al., 2005).

When microglia are resting, they are highly ramified, with long processes and small cell bodies, constantly scanning their environment (Tremblay et al., 2011). However, once they become activated, they acquire an amoeboid morphology with shorter

processes and an increasing cell body volume. Depending on the CNS region, age of the individual and conditions of heath and disease, microglia can adopt different functions (Stratoulias et al., 2019). In general, microglia can exert the classical type of immune reaction, as they lead to the production of pro-inflammatory cytokines. This pathway is mainly initiated by lipopolysaccharide (LPS) from gram-negative bacteria, leading to release of tumor necrosis factor-α (TNF-α), interleukin-1β (IL-1β), superoxide, nitric oxide (NO), or reactive oxygen species (ROS) (Block et al., 2007). In contrast, microglia can also produce opposed cytokines, leading to an anti-inflammatory reaction. This phenotype is usually activated by IL-4 or IL-13 (Colton, 2009; Ponomarev et al., 2007). It is suggested that several microglia subtypes exist under steady state and disease conditions, thus reacting differently to stimuli by expression of diverse genes (Stratoulias et al., 2019).

1.4 Microglia in AD

Recent research demonstrated the contribution of inflammation in the development and pathogenesis of AD and other neurodegenerative diseases (Heneka et al., 2015; Heppner et al., 2015). A connection between the immune system and AD was indicated by the detection of activated microglia with a pro-inflammatory phenotype in close proximity to amyloid plaques (Frautschy et al., 1998; Solito & Sastre, 2012). It was suggested that microglia form a protective barrier around those plaques and thereby prevent neurotoxic effects of amyloid accumulations (Condello et al., 2015). Accordingly, an integrative network-based approach revealed an increase of genes involved in inflammatory processes in postmortem brains of AD patients (Zhang et al., 2013).

Recent GWAS and exome sequencing analyses provided further evidence for an important contribution of microglia in AD, as a number of genes expressed in this cell type were shown to be associated with an increased risk for developing AD. Comparison of AD patients and healthy controls revealed association of TREM2 and the myeloid cell surface antigen CD33 variants with AD (Bertram et al., 2008; Guerreiro et al., 2013; Jonsson et al., 2013). Interestingly, inflammatory mediators such as cytokines were detected at earlier stages of the disease where patients showed mild cognitive impairment (MCI). Thus, enhanced levels of cytokines possibly represent a risk for disease progression from MCI to AD (Brosseron et al.,

2014; Tarkowski et al., 2003). One study even reported that in mice, a systemic immune reaction could be the cause of AD pathology including amyloid deposition and tau aggregation (Krstic et al., 2012).

Microglia express various receptors, including toll-like receptors and CD36, which bind soluble or fibrillar Aβ (El Khoury et al., 2003; Stewart et al., 2010). This binding leads to the release of inflammatory mediators *in vitro*. In addition, one study showed that microglia have been involved in the clearance of Aβ plaques in hippocampal brain slices (Hellwig et al., 2015). In brain slices of wild-type (wt) mice that were exposed to synthetic Aβ42, Aβ plaque formation has not been detected. However, depletion of microglia in respective brain sections and subsequent application of synthetic Aβ42 induced the formation of Aβ deposits within 14 days (Hellwig et al., 2015), highlighting the importance of microglia in the clearance of amyloid plaques. Additionally, uptake and transport of Aβ into lysosomes of microglia cells was detected, further indicating the involvement of microglia in AD pathology (Hellwig et al., 2015; J.-H. Lee et al., 2010; Pickford et al., 2008). Interestingly, Hellwig et al. also showed that depletion of microglia in brain slices and replenishment with wt-microglia reversed the Aβ plaque formation. However, replenishment of respective brain slices with microglia from an AD mouse model showed opposing effects. Here, AD-microglia were not able to clear Aβ deposits, in contrast, they led to an increase of Aβ plaques (Hellwig et al., 2015). This effect has already been described with isolated microglia from two different AD mouse models, as isolated microglia showed impaired phagocytic activity and uptake of Aβ (Krabbe et al., 2013; Orre et al., 2014). Thus, microglia that are constantly exposed to high amounts of plaques become unable to cope with the load of Aβ and along with this become functionally impaired. In addition to phagocytosis of fibrillar Aβ, soluble Aβ can be degraded by cell surface or secreted proteases expressed by microglia. These Aβ degrading enzymes are neprilysin (NEP) and insulin-degrading enzyme (IDE) (C. Y. D. Lee & Landreth, 2010). In a transgenic mouse model with depleted NEP, increased Aβ levels were detected, whereas NEP overexpressing mice showed a reduction of soluble Aβ and plaque deposition (Farris et al., 2007; Iwata et al., 2001; Leissring et al., 2003). Beside binding and degradation of insulin (Sladek et al., 2007), IDE has also been reported to degrade soluble Aβ, however, with a lower efficiency compared to insulin (Iwata et al., 2000). Interestingly, patients with type-2 diabetes have a higher risk to

develop AD (Qiu & Folstein, 2006). This might be explained by the higher amount of insulin that is preferentially degraded by IDE, wherefore IDE cannot degrade soluble Aβ anymore (C. Y. D. Lee & Landreth, 2010; Taubes, 2003).

Another pathway for clearance of soluble Aβ is the uptake through constitutive macropinocytosis by microglia with subsequent degradation in lysosomal compartments (Mandrekar et al., 2009). Furthermore, the low-density lipoprotein receptor-related protein 1 (LRP1) can export soluble Aβ through the BBB into the peripheral circulation (Deane et al., 2004). The receptor is highly expressed in brain capillary endothelium and has been known to efficiently bind APOE (Zerbinatti & Bu, 2005). Thus, in a complex with APOE, Aβ is more efficiently exported by LRP1-mediated transcytosis (Shibata et al., 2000).

1.5 Triggering receptor expressed on myeloid cells 2 (TREM2)

TREM2 belongs to the immunoglobulin superfamily of cell surface receptors encoded by a gene cluster located on chromosome 6p21 (Allcock et al., 2003; Klesney-Tait et al., 2006). It is expressed on monocyte-derived cell types, including dendritic cells, osteoclasts, tissue macrophages, and microglia (Colonna, 2003b; Colonna & Wang, 2016; Paloneva et al., 2003). The receptor represents a type I membrane protein with an extracellular region containing a single immunoglobulin-like domain which binds anionic lipids and lipoproteins, including APOE (Atagi et al., 2015; Y. Wang et al., 2015; Yeh et al., 2016). Just recently, Aβ and galecin-3 have been identified as TREM2 ligands (Boza-Serrano et al., 2019; Y. Zhao et al., 2018; Zhong et al., 2018). The short cytoplasmic domain of TREM2 has no known signaling function. However, TREM2 associates with its co-receptor DAP12/TYROBP (DNAX activation protein of 12 kDa, TYRO protein tyrosine kinase binding protein) via interactions of charged residues within the transmembrane domains of both proteins (Paloneva et al., 2002). The cytoplasmic domain of DAP12 contains a characteristic immunoreceptor tyrosine-based activation motif (ITAM), which is phosphorylated upon ligand binding to TREM2, recruiting spleen tyrosine kinase (SYK), which is further phosphorylated. Phosphorylated SYK (pSYK) activates downstream signaling molecules, thereby regulating several intracellular signaling pathways that control cell proliferation and differentiation, survival, phagocytosis and cytoskeletal remodeling as well as calcium

mobilization and cytokine production (Colonna, 2003a; Jay et al., 2017; J. Walter, 2016).

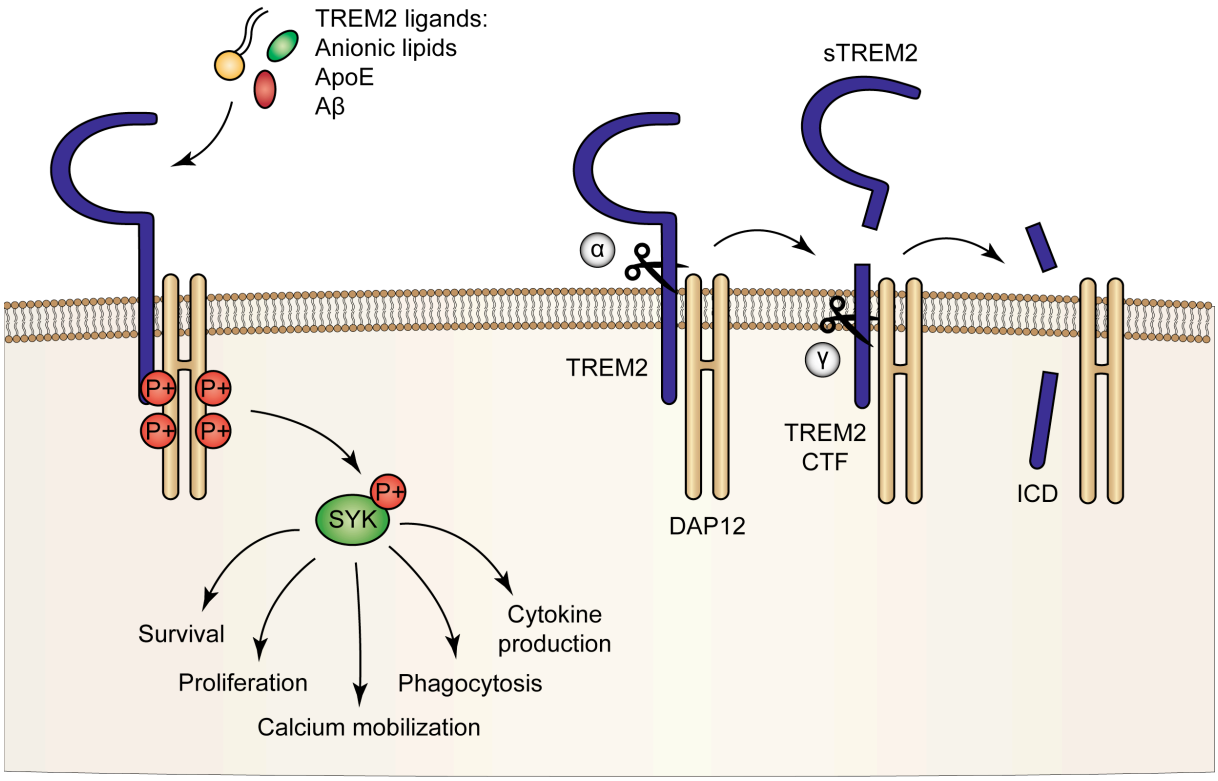

Figure 2: TREM2 signaling pathway and processing. TREM2 forms a complex with its co-receptor DAP12. Upon ligand binding, including anionic lipids, ApoE or Aβ, the ITAM motif in the cytoplasmic domain of DAP12 gets phosphorylated, further leading to phosphorylation of SYK. This leads to phosphorylation and activation of several signaling adapters, eventually leading to survival and proliferation of microglia, accompanied by calcium mobilization, phagocytosis and cytokine production. TREM2 can be proteolytically processed by α-secretase ADAM10 or ADAM17, releasing sTREM2 into the extracellular space and generating a membrane bound CTF. Furthermore, γ-secretase cleaves the remaining CTF, releasing an ICD. SYK, spleen tyrosine kinase; CTF, C-terminal fragment; ICD, intracellular domain.

TREM2 is mainly found intracellularly either within the Golgi or in exocytic vesicles (Prada et al., 2006). TREM2 can undergo proteolytic cleavage between amino acids H157 and S158 by members of the ADAM family, including ADAM10 and ADAM17 (Schlepckow et al., 2017; Thornton et al., 2017). This cleavage results in the release of a soluble TREM2 ectodomain (sTREM2) into extracellular fluids, and generation of a membrane-tethered C-terminal fragment (CTF) (Kleinberger et al., 2014; Wunderlich et al., 2013). TREM2 CTF represents a substrate for intramembranous proteolysis by γ-secretase that is also expressed in microglia (Farfara et al., 2011;

Kemmerling et al., 2017; Nadler et al., 2008; J. Walter et al., 2017) and further leads to generation of an intracellular domain (ICD, (Wunderlich et al., 2013). Notably, γ-secretase cleavage represents an important step in proteolytic processing of TREM2, as accumulation of CTFs could trap DAP12 at the plasma membrane, interfering with proper TREM2-DAP12 signaling.

1.5.1 Soluble TREM2 (sTREM2)

It was first thought that sTREM2 might function as a decoy receptor, blocking ligand binding to full-length TREM2 at the cell surface. This function has already been shown for TREM1, as sTREM1 competes with full-length plasma membrane TREM1 for ligands, thereby influencing TREM1 signaling (Bouchon et al., 2001; Piccio et al., 2008). Though, it was shown that sTREM2 could exert additional biological functions. In response to a viral infection in the lung, macrophages showed increased expression of TREM2 and secretion of sTREM2, which prevented macrophage apoptosis (Wu et al., 2015). In line with this, it has been described that sTREM2 can promote microglial survival and lead to the production of inflammatory cytokines, suggesting an important role in the immune response of microglial cells in neurodegenerative diseases (Zhong et al., 2017). The effect of sTREM2 was independent of full-length TREM2 at the cell surface, as these functions were described in a TREM2-deficient mouse model. Meaning, sTREM2 binds to a yet unknown receptor on microglia cells.

The role of sTREM2 became more important in the progression of AD when levels of sTREM2 have been shown to be elevated in cerebrospinal fluids (CSFs) of AD patients (Heslegrave et al., 2016; Piccio et al., 2016; Suárez-Calvet et al., 2016). Thus, CSF sTREM2 might also serve as a potential biomarker for AD (Zhong & Chen, 2019). Interestingly, sTREM2 levels correlate with the amount of phosphorylated tau and peak in the early stages of the disease, where patients develop MCI (Suárez‐Calvet et al., 2016). In contrast, the amounts of sTREM2 did not correlate with Aβ levels in CSF, suggesting the involvement of sTREM2 in pathological processes subsequent to the accumulation of Aβ (Suárez‐Calvet et al., 2016; Zhong & Chen, 2019). In inflammatory conditions in the CNS, such as multiple sclerosis, sTREM2 levels were found to be elevated as well (Piccio et al., 2008). Thus, the amount of sTREM2 in CSFs might also represent a biomarker for other

inflammatory diseases. Interestingly, it has been proposed that sTREM2 modulates AD pathology, as in early-stage AD brains with high levels of sTREM2, reduction of the hippocampal volume was attenuated, in line with reduced cognitive decline (Ewers et al., 2019). In a transgenic mouse model of AD, sTREM2 could reduce Aβ plaque burden, which was shown to be dependent on microglia, as depletion of microglia abrogated the neuroprotective effects (Zhong et al., 2019).

In a GWAS study, the gene cluster membrane-spanning 4-domains superfamily A (MS4A) was associated with sTREM2 levels in CSF (Deming et al., 2019). Variants of the MS4A gene cluster were already linked to the risk of developing LOAD (Hollingworth et al., 2011; Naj et al., 2011). The overexpression of MS4A genes led to an increase in sTREM2 and, in accordance with this, silencing of the MS4A gene cluster reduced the amounts of sTREM2 in the CSF (Deming et al., 2019). However, those observations were obtained with a quite small sample size. As MS4A proteins are transmembrane proteins, it might be possible that α-secretases are regulated by MS4A proteins and therefore the amount of sTREM2 is modulated (Zhong & Chen, 2019).

1.5.2 TREM2 variants and risk for neurodegenerative diseases

Interestingly, several mutations in TREM2 have been linked to different neurodegenerative diseases. Loss-of-function mutations were first identified in Nasu-Hakola disease (NHD, also known as polycystic lipomembraneous osteodysplasia with sclerosing leukoencephalopathy, PLOSL) (Hakola et al., 2009; Nasu et al., 1973), characterized by bone cysts, fractures, and dementia associated with axonal degeneration, increased microglial activation, and neuroinflammation (Kaneko et al., 2010; Satoh et al., 2011). Similar neurological symptoms have been discovered in frontotemporal dementias (FTDs) (Humphrey et al., 2015). The TREM2 variants Y38C and T66M have been shown to be a cause for NHD or FTD in homozygous carriers (Guerreiro et al., 2013; Le Ber et al., 2014). T66M shows a decreased cell surface expression, caused by impaired protein folding and decreased transport from the ER to the plasma membrane (Kleinberger et al., 2014; Kober et al., 2016). Accordingly, the T66M variant showed significantly lower secretion of sTREM2 (Kleinberger et al., 2014). TREM2 variant Q33X has been associated with NHD and

FTD and results in a complete loss of TREM2 expression due to insertion of a stop codon (Guerreiro et al., 2013).

Some rare TREM2 variants are associated with an increased risk of developing AD. Here, the R47H variant increases the risk for AD 2-3 fold, comparable to the effect of the APOE ε4 allele (Guerreiro et al., 2013; Yeh et al., 2017). The R47H substitution is located in the ligand-binding site within the Ig-like domain. It does not alter TREM2 translocation to the cell surface or overall structure of the ectodomain, but decreases the interaction with anionic lipids (Kober et al., 2016). In AD mouse models, it was identified that microglia with a heterozygous expression of TREM2 R47H showed decreased abundance around amyloid plaques. Brains of these mice showed less dense core plaques but instead more diffuse amyloid plaques, accompanied by increased plaque-associated neuritic dystrophy (Cheng-Hathaway et al., 2018). Those effects were also described in a TREM2-deficient mouse model of AD, highlighting the importance of TREM2 in preventing neuritic damage (Y. Wang et al., 2016). In addition to effects on full-length TREM2, the R47H variant was shown to impair functions of sTREM2 regarding microglial survival and inflammatory responses (Zhong et al., 2017). TREM2 R62H is another variant with an increased risk for LOAD. It is also located within the ligand binding site and showed similar impairment in immune responses and microglia activation as the R47H variant (Sims et al., 2017).

Another AD risk-associated variant is TREM2 H157Y (Jiang, Hou, et al., 2016). Interestingly, the cleavage of TREM2 occurs after histidine at position 157, and the H157Y variant substitution results in increased shedding and higher levels of sTREM2 (Schlepckow et al., 2017; Thornton et al., 2017). Concerning the amount of TREM2 CTFs for this variant, both publications identified opposing effects. Whereas one group described a reduction of CTF levels, possibly due to enhanced degradation (Schlepckow et al., 2017), the other group showed increased levels, explained by enhanced cleavage and generation of sTREM2 (Thornton et al., 2017). Recently, a novel TREM2 variant linked to familial AD has been identified. The G145W mutation appears to cause changes in the protein conformation, thus affecting the function and signaling of TREM2 (Karsak et al., 2020). The mutation is located within an intrinsically disordered region (IDR) where it appears to shorten the IDR compared to the common protein. Interestingly, TREM2 variant T96K

supposedly reduces the risk of developing AD and is rather protective (Jin et al., 2014). The positively charged lysine residue possibly influences ligand binding.

1.6 Protein transport mechanisms and glycosylation

Proteins that are destined to reach the plasma membrane or get secreted can undergo the classical protein secretion (CPS) or the unconventional secretory pathway (USP). The CPS is the best characterized mechanism in protein secretion, where proteins start in the ER, get delivered to the Golgi apparatus (GA), further to the *trans*-Golgi network (TGN) through cisternae maturation before they will finally reach the plasma membrane via secretory vesicles (Burgess & Kelly, 1987; Kelly, 1985; Palade, 1975; Viotti, 2016). In the case of secretory or plasma membrane proteins, a signal recognition particle (SRP) recognizes the signal peptide while the protein is being synthesized and induces translocation through translocon pores into the ER lumen or integrated into the ER membrane (G. Blobel & Sabatini, 1971; Günter Blobel & Dobberstein, 1975; Nyathi et al., 2013). Further maturation and folding occurs through molecular chaperones that prevent aggregation and ensure protein quality control. Misfolded proteins can be degraded through the ER-associated degradation (ERAD) pathway, translocating the misfolded proteins to the cytosol where they get degraded by the ubiquitin-proteasome system (P. Walter & Ron, 2011). Properly folded membrane and soluble proteins leave the ER by coat protein complex II (COPII)-mediated vesicular transport mechanisms. Several proteins, including the GTPase Sar1p, and complexes Sec23p and Sec13p, are involved in the formation of COPII-coated vesicles that can form at specific ER-exit sites (Barlowe et al., 1994). Those vesicles reach and fuse with the ER-Golgi-intermediate compartment (ERGIC) on the way to the Golgi compartments (Presley et al., 1997). The ERGIC is a distinct organelle, possibly executing further protein quality control steps before the protein is transported to the GA (Appenzeller-Herzog & Hauri, 2006; Breuza et al., 2004). The GA consists of several cisternae, with the *cis*-Golgi, the entry site, and the *trans*-Golgi, the exit site (Klumperman, 2011). In the TGN proteins are sorted into vesicles with three different destinations, the plasma membrane, endosomes, or lytic compartments (Viotti, 2016).

Starting in the ER already during translation, many proteins undergo glycosylation, which is the most common but also most complex PTM (Spiro, 2002). During the

process of glycosylation, glycans, also called polysaccharides, are attached by glycosyltransferases. Most glycoproteins are found on the plasma membrane where they have divers functions. Glycosylation plays a critical role in protein stability and protection against proteolytic degradation, but also activity and function of the protein. Several monosaccharides are used for the generation of glycan residues (Varki et al., 2015). There are two types of protein glycosylation, N-linked and O-linked glycosylation. During N-linked glycosylation, N-acetylglucosamine (GlcNAc) is attached to the nitrogen atom of an Asn (N) residue, within the amino acid sequence of Asn-X-Ser/Thr, where the X can be any amino acid except of Pro (Shakin-Eshleman et al., 1996). The core of N-glycans consists of two GlcNAc and three Mannose (Man) residues (Figure 3, Sethi & Fanayan, 2015). Based on this core, three different subgroups of N-glycans can be classified: high-mannose N-glycan, complex N-glycan or hybrid N-glycan (Goldberg et al., 2009). The first process of N-glycan synthesis takes place in the ER, where the core is formed and further Man residues are attached to the core, forming a high-mannose N-glycan. The glycoprotein is then transported to the *cis*-Golgi, as reorganization and modulation take place in the Golgi compartments (Stanley, 2011). There, trimming of Man occurs back to the core of the N-glycan and further maturation and addition of monosaccharides is mediated by transferases in the *medial*- and *trans*-Golgi (Helenius & Aebi, 2001, 2004). Monosaccharides involved in the formation of complex N-glycans are GlcNAc, N-acetylgalactosamine (GalNAc), galactose, fucose, and N-acetylneuraminic acid (Neu5Ac). Complex N-glycans can consist of two to five antennae growing from the core mannoses (Goldberg et al., 2009). Hybrid N-glycans are a combination of high-mannose and complex residues (Stanley et al., 2009).

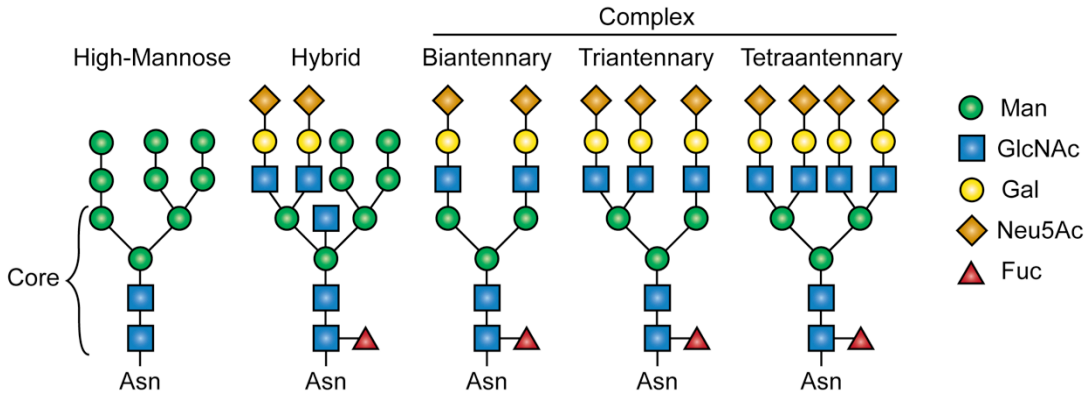

Figure 3: Different types of N-linked glycans. The most common forms of N-linked glycans are high-mannose, hybrid and complex glycan types. Man, mannose; GlcNAc, N-acetylglucose; Gal, galactose; Neu5Ac, N-acetylneuraminic acid; Fuc, fucose (Image adapted from Sethi & Fanayan, 2015).

The O-linked glycosylation is more heterogeneous and complex and typically occurs in the Golgi compartments. GlcNAc, fucose, Man and GalNAc get attached to hydroxyl groups of Ser or Thr. The most common types of O-linked glycosylations are GalNAc glycans, also called mucin-type O-glycans. They are highly abundant on many plasma membrane and secreted proteins (Bennett et al., 2012; Vasudevan & Haltiwanger, 2014). When many of these mucin-type O-glycans are present, a barrier is formed that protects the glycoprotein and the cell surface from pathogens, external stress and proteolytic degradation (Amore et al., 2017; Reily et al., 2019). As O-linked glycosylation occurs at Ser or Thr, it competes with phosphorylation of these amino acids (Reily et al., 2019).

1.7 Protein quality control mechanisms

Protein homeostasis, or proteostasis, is very important for cellular functions. The conformation and concentration of proteins as well as their interactions with binding partners needs to be tightly controlled (Balch et al., 2008). An important process in proteostasis is protein folding and regulation of protein synthesis and degradation rates. Several chaperones and enzymes are involved in properly folding proteins to prevent their aggregation (Voisine et al., 2010). During stress conditions, including exposure to pathogens and presence of aggregation-prone proteins, stress sensors like heat shock proteins help maintain the cellular proteostasis (Westerheide & Morimoto, 2005). Turnover of proteins provides new amino acids to obtain protein

homeostasis and prevent abnormal accumulation. Degradation pathways are controlled by complex regulatory mechanisms to circumvent excessive breakdown of cellular components (Lecker et al., 2006). The ubiquitin-proteasome system (UPS) and autophagy-lysosomal pathway are the two major pathways for proteolytic degradation. The UPS degrades most cellular proteins. However, entire organelles and protein aggregates are more likely to be degraded by the autophagy-lysosomal pathway (Kraft et al., 2009).

1.7.1 Ubiquitin-proteasome system (UPS)

Proteasomes, large catalytic protease complexes, are present inside the cytoplasm as well as the nucleus of eukaryotic cells (Wójcik & DeMartino, 2003). The 26S proteasome consists of two major subunits, the core complex which is the 20S proteasome, and the regulatory subunit, the 19S proteasome cap (Heinemeyer et al., 2004; Murata et al., 2009). The core is mainly responsible for protein digestion and is composed of α and β subunits, guiding proteins through the degradation machinery (Groll et al., 2000). Additionally, a cap subunit prevents nonspecific degradation of proteins that are not ubiquitinated. Hence, degradation by the 20S core proteasome is a highly selective process (Glickman & Ciechanover, 2002). The majority of cytosolic proteins gets degraded by this pathway (Rock et al., 1994). A series of interaction partners are involved in proteolytic degradation. Ubiquitin (Ub) is a major cofactor for the proteasome. For degradation of proteins, Ub is covalently bound to proteins and marks them for recognition by the 26S proteasome. Subsequently, the proteasome degrades ubiquitinated proteins into smaller fragments that can further be hydrolyzed by proteases, resulting in the generation of single amino acids available for synthesis of new proteins (Baumeister et al., 1998; Glickman & Ciechanover, 2002). The process of Ub binding is controlled by three enzymatic components. The Ub-activating enzymes (E1) and Ub-carrier proteins (E2) are responsible for preparing Ub for conjugation by the Ub-protein ligases (E3). E3 specifically recognizes proteins selected for degradation and leads to transfer and binding of Ub to those proteins (Hershko & Ciechanover, 1992; Lecker et al., 2006).

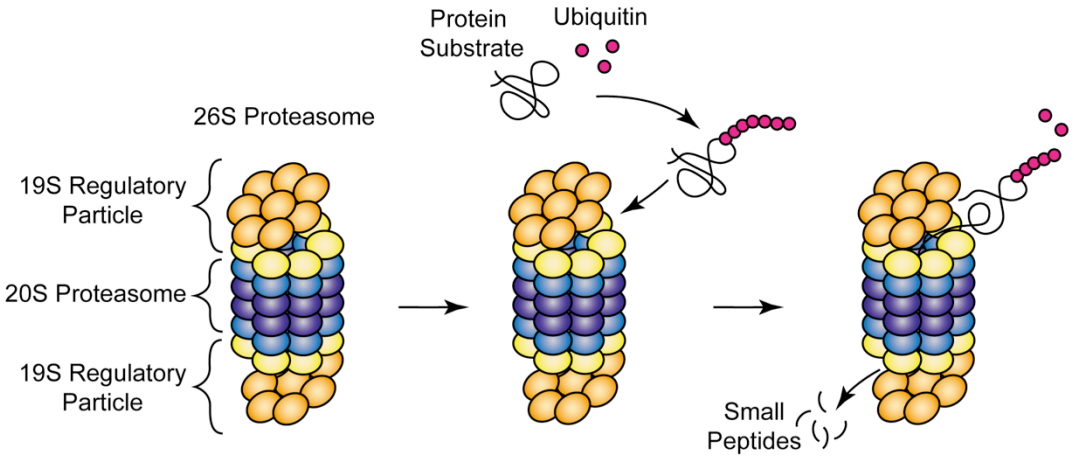

Figure 4: Ubiquitin-proteasome system. The 26S proteasome consists of a 20S core proteasome and a 19S regulatory subunit that allow specific degradation of proteins. Through covalent binding, a protein substrate gets polyubiquitinated and can thus be recognized by the 19S subunit. The protein is further unfolded, ubiquitin is released and the protein is translocated through the proteasome and degraded into smaller peptides (Image adapted from Murata et al., 2009).

1.7.2 Autophagy-lysosomal pathway

Macroautophagy, hereafter referred to as autophagy, is an evolutionarily conserved pathway in eukaryotic cells that can be induced by cellular stress factors, such as starvation or infection by pathogens. It is important for providing nutrients to the cell but also for the selective degradation of aggregated proteins or damaged organelles (Klionsky, 2007; Zaffagnini & Martens, 2016). Therefore, autophagy has to be tightly regulated (D. Wang et al., 2015). During the autophagy pathway, a double-membrane organelle, called autophagosome, is formed and fuses with lysosomes to build an autophagolysosome, degrading contents in the inside of the organelle (Figure 5). Proteins of the family of autophagy-related genes (Atg) are involved in initiation and autophagosome formation (Klionsky et al., 2011). The ULK1 kinase complex induces autophagy after being dephosphorylated depending on the nutrient availability inside the cell (Kraft & Martens, 2012). The phosphorylation is catalyzed by the mammalian target of rapamycin complex 1 (mTORC1) in a nutrient-rich condition, thus being a negative regulator of autophagy. Accordingly, inhibition of mTORC1 with rapamycin leads to induction of autophagy (Klionsky & Emr, 2000). Besides others, Raptor (regulator-associated protein of mTOR) is the main component of mTORC1. While a lot is known about mTORC1, the mTOR complex 2 (mTORC2) is not well investigated. Besides its components including Rictor

(rapamycin-insensitive companion of mTOR), only little is known about its signaling pathway (Sarkar, 2013; Takei & Nawa, 2014). Formation of phagophores is not only regulated by mTOR-dependent but also by mTOR-independent pathways. Furthermore, the autophagy-initiating class III PI3K complex is involved in induction of autophagy. Beclin-1 is an important interaction partner, enhancing the activity of other components in this complex (Sarkar, 2013). Formation of phagophores is regulated by several Atg genes (Kraft & Martens, 2012). Phagophores are formed by activation of the Atg12-Atg5-Atg16 complex. This complex is needed for conjugation of LC3 I with phosphatidylethanolamine (PE) into PE conjugated LC3 II (Sarkar, 2013). LC3 II localizes to autophagosomes and autophagolysosomes and thus serves as a specific marker for autophagy (Kabeya et al., 2003). Once autophagosomes are formed, autophagic cargo is engulfed. Ubiquitinated and polyubiquitinated proteins are recognized and bound to p62 via its ubiquitin-associated domain. Consequentially, the p62 protein, also called sequestosome 1, is found in protein aggregate-rich inclusion bodies. Subsequently, p62 directly binds to LC3 II located in the membrane of phagophores (Pankiv et al., 2007). After engulfment of autophagic cargo autophagosomes fuse with late endosomes and lysosomes. The formed amphisomes or autophagolysosomes, respectively, lead to degradation of cargo by lysosomal hydrolases (Sarkar, 2013).

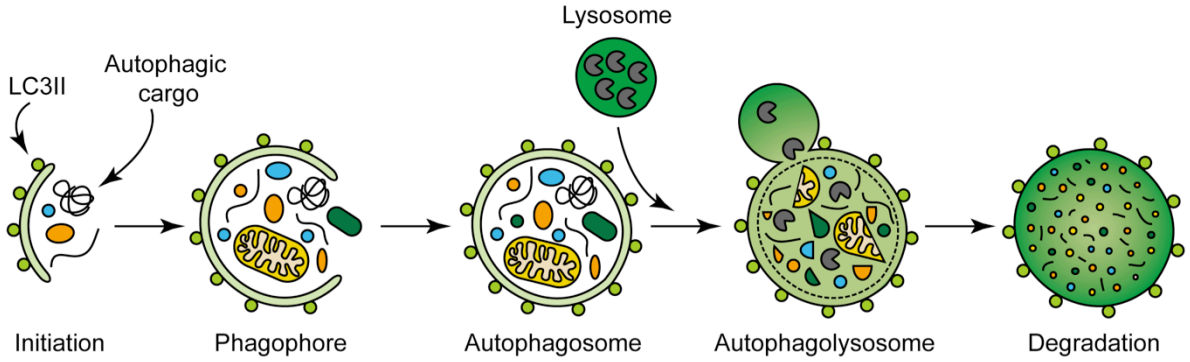

Figure 5: Autophagy-lysosomal pathway. The first step of autophagy is the initiation and formation of a phagophore. For this, PE-conjugated LC3II is localized to the phagophore membrane, coating autophagic cargo like aggregation-prone proteins or mitochondria. Autophagosomes are formed, which eventually fuse with lysosomes. In the accomplished autophagolysosome, autophagic cargo is subsequently degraded by lysosomal hydrolases (Image adapted from Zaffagnini & Martens, 2016).

Since oligomers and aggregates are largely resistant against degradation, the autophagy pathway is of high importance in cellular handling of protein aggregates to protect the cell against cytotoxicity (Bence, 2001; Sarkar, 2013). Accordingly, dysfunction of autophagy has been linked to neurodegenerative diseases. As a result, misfolded proteins accumulate and have toxic effects on the cell (Menzies et al., 2011). Furthermore, in a transgenic mouse model for HD, inhibition of mTORC1 results in the activation of the autophagy pathway, leading to amelioration of the disease phenotype (Ravikumar et al., 2004). In PD, overexpression of the disease related protein α-synuclein has been shown to even inhibit autophagosome synthesis (Winslow et al., 2010). Autophagy dysfunction has been reported to play an important role in AD initiation and progression, as AD patients displayed a significantly increased amount of autophagosomes. Most importantly, dysregulation of autophagy showed to influence the accumulation of Aβ and tau protein (Di Meco et al., 2020; Menzies et al., 2017; Nixon et al., 2005). Thus, activation of autophagy signaling might ameliorate disease pathology in several neurodegenerative diseases, showing a high potential for future therapeutic applications.

1.7.3 Crosstalk between autophagy and the proteasome system

The UPS and autophagy seem to be distinct degradation mechanisms. However, evidence suggests a crosstalk between those pathways with Ub as an important interaction partner. Possibly more than half of the proteins degraded via the

autophagy pathway are ubiquitinated (Khaminets et al., 2016). Thus, both machineries use Ub as a signaling molecule to initiate degradation. As p62 binds Ub and is involved autophagic protein degradation, it also plays an important role in the process of protein degradation in general. It has been shown that oligomerization defines the fate of an Ub bound protein. Oligomers can form under stress conditions, caused by high concentrations of free Ub within the cells. This can happen due to a heat shock or prolonged inhibition of the proteasome machinery (Fan et al., 2018; Peng et al., 2017). Using the proteasome inhibitor MG132, reduced cell proliferation accompanied by stimulation of autophagy through an increase in Beclin-1 and LC3 levels, was observed (Ge et al., 2009). In contrast, inhibition of autophagy via mTORC1 showed enhanced degradation of long-lived proteins by autophagy and the UPS (J. Zhao et al., 2015; J. Zhao & Goldberg, 2016). Also, enhanced autophagy activity was induced by proteasome inhibition in retinal pigment epithelial cells and cultured cardiomyocytes (Kyrychenko et al., 2014; Tang et al., 2014). However, in several studies, the accumulation of ubiquitinated proteins was observed upon proteasome inhibition (Hara et al., 2006; Komatsu et al., 2006; Korolchuk et al., 2009). Thus, most studies suggest a compensatory mechanism of autophagy when the UPS is inhibited or defect. However, the UPS is not always capable of maintaining the cellular homeostasis when the autophagy-lysosomal pathway is defect. It possibly depends on the cell type and conditions, whether successful compensation and cellular homeostasis is sustained.

1.8 Aim of the thesis

AD has become the most common cause of dementia and affects over 30 million people worldwide (The Alzheimer's Association, 2020). The connection between AD and the immune system has been described, as inflammatory pathways seem to be highly involved in the pathogenesis of AD (Heneka et al., 2015). Several genes related to inflammatory processes were found to be associated with an increased risk of developing AD, including mutations in TREM2. The TREM2 variant T66M has been shown to be a cause for NHD in homozygous carriers (Le Ber et al., 2014). Some rare TREM2 variants are also associated with an increased risk of developing AD. The R47H variant increases the risk for AD 2-3 fold, comparable to the effect of the apolipoprotein ε4 allele (Guerreiro et al., 2013; Jonsson et al., 2013). The R47H substitution is located in the ligand-binding site within the Ig-like domain. It does not

alter TREM2 translocation to the cell surface or overall structure of the ectodomain. Instead, the R47H variant decreases the interaction with anionic lipids (Kober et al., 2016). Recently, the R47H variant was also shown to impair functions of sTREM2 in microglial survival and inflammatory responses (Zhong et al., 2017). A novel TREM2 G145W variant segregating with early onset dementia in a family appears to cause changes in the protein conformation, thus affecting the function and signaling of TREM2 (Karsak et al., 2020). Additionally, the TREM2 H157Y variant shows association with AD in some cohorts, and leads to enhanced processing of TREM2 by ADAM proteases (Jiang, Tan, et al., 2016; Schlepckow et al., 2017; Thornton et al., 2017).

The main goal of this study is the generation and characterization of a cell culture model for investigation of TREM2 subcellular transport, expression at the cell surface, its degradation, and TREM2-DAP12 receptor complex mediated signaling. In addition, the system should be applied to study effects of physiological ligands of TREM2 and antibodies against the TREM2 ectodomain.

2 Material & Methods

2.1 Biological safety

All work with genetically modified organisms was conducted under biosafety level 1 according to the present guidelines of the German Act on Genetic Engineering. All instruments and materials contaminated with genetically modified organisms were collected and inactivated according to official rules.

2.2 Chemicals

All chemicals used for experiments in this study were purchased from Carl Roth (Karlsruhe, Germany) or Sigma-Aldrich (Steinheim, Germany) as not otherwise stated.

2.3 Molecular biological methods

2.3.1 Polymerase chain reaction (PCR)

For amplification or modification of plasmid DNA, constructs were first amplified by PCR. Primers were purchased from Eurogentec (Seraing, Belgium, Table 1). A mixture of the following components with specific primer pairs was prepared:

Forward Primer	1 µM
Reverse Primer	1 µM
Template DNA	100 ng
5x Taq Master Mix	10 µl
dNTPs	0.2 mM
MgCl2	1.5 mM
PCR buffer	1x
Taq Polymerase	25 U/µl

add $H_2O_{dest.}$ to 50 µL

A PCR program was followed with denaturation of DNA, annealing of respective primers and elongation. This cycle (steps 2-4) was repeated 29 times before the DNA was elongated in a final step.

1. Initial denaturation of DNA	95 °C, 30 s
2. Denaturation of DNA	95 °C, 30 s
3. Annealing of Primers	64,7 °C, 30 s
4. Elongation of Primers	68 °C, 2.5 min
5. Final Elongation	72 °C, 5 min
6. Hold	4 °C, ∞

Table 1: Oligonucleotides

Name	Sequence 5' - 3'	Application
fwd-TREM2-R47H	ACTGGGGGAGGCACAAGGCCTGGTG	Site-directed Mutagenesis
rev-TREM2-R47H	CACCAGGCCTTGTGCCTCCCCCAGT	Site-directed Mutagenesis
fwd-TREM2-T66M	CAGCGTGTGGTCAGCATGCACAACTGTGGC	Site-directed Mutagenesis
rev-TREM2-T66M	GCCACAAGTTGTGCATGCTGACCACACGCTG	Site-directed Mutagenesis
fwd-TREM2-G145W	ATCTCTGGTTCCCCTGGGAGTCTGAGAGC	Site-directed Mutagenesis
rev-TREM2-G145W	GCTCTCAGACTCCCAGGGGAACCAGAGAT	Site-directed Mutagenesis
fwd-TREM2-H157Y	CGAGGATGCCCATGTGGAGTACAGCATCTCC	Site-directed Mutagenesis
rev-TREM2-H157Y	GGAGATGCTGTACTCCACATGGGCATCCTCG	Site-directed Mutagenesis
Fwd-TREM2aa19	TTGCACTTGTCACGAATTCGCACAACACCACAGTGTTC	Gibson Assembly
Rev-TREM2aa112	GGGCATGTGTGAGTTTTGTCGCTCTGGCACTGGTAGAG	Gibson Assembly
Fwd-TREM2aa113	TTGCACTTGTCACGAATTCGCTCCATGGCAGTGAGGCTG	Gibson Assembly
Rev-TREM2aa130	GGGCATGTGTGAGTTTTGTCTGCCAGCACCTCCACCAG	Gibson Assembly

Fwd-TREM2aa131	TTGCACTTGTCACGAATTCGGACCCCCTGGATCACCGG	Gibson Assembly
Rev-TREM2aa148	*GGGCATGTGTGAGTTTTGTCCTCAGACTCCCCGGGGAAC*	Gibson Assembly
Fwd-TREM2aa149	TTGCACTTGTCACGAATTCGAGCTTCGAGGATGCCCATG	Gibson Assembly
Rev-TREM2aa157	GGGCATGTGTGAGTTTTGTCGTGCTCCACATGGGCATC	Gibson Assembly
Fwd-FC2	GACAAAACTCACACATGC	Gibson Assembly
Rev-FC2	CGAATTCGTGACAAGTGC	Gibson Assembly

2.3.2 Agarose gel electrophoresis

1x TBE buffer	9 mM Tris-borate 2 mM EDTA pH 8.0
6x OrangeG loading dye	60 % Glycerin 0.15 % OrangeG 60 mM EDTA 10 mM Tris 1:1.000 GelRed® (Biotium Inc., Fremont, USA) pH 7.6
Agarose	AppliChem, Darmstadt, Germany
1 kbp & 100 bp DNA ladder	Invitrogen, Carlsbad, USA

Agarose gel electrophoresis is used to separate DNA fragments based on their size and conformation. Negatively charged DNA migrates via an electric field through an agarose gel matrix. Smaller DNA fragments migrate more quickly than larger ones. Agarose gels were prepared by boiling 1-1.5 % agarose in 1 x TBE buffer. The solution was poured in an electrophoresis chamber prepared with a comb. After gels were dried, they were covered with 1 x TBE buffer and loaded with the respective samples. The DNA samples were prepared by adding an appropriate amount of

OrangeG loading buffer and were eventually loaded on the gel along with a DNA ladder containing DNA fragments of known sizes. The OrangeG loading buffer is supplemented with GelRed, which intercalates between the DNA's nucleotide bases and makes it possible to detect DNA when exposed to ultraviolet light (UV) via its fluorescent signal. The gel was run at 120 V for 60-90 min and bands were visualized using UV illumination (ChemiDoc™ XRS System, BioRad).

2.3.3 DNA fragment purification from agarose gels

Gel Extraction Kit, peqGOLD	PEQLAB Biotechnologie, Erlangen, Germany

Using an UV transilluminator (Trans UV Illuminator GVM 20, Syngene™), the DNA was visualized and an appropriate DNA band was cut out of the agarose gel. The DNA was extracted from the gel using the Gel Extraction Kit, peqGOLD according to manufacturer's instructions.

2.3.4 Quick change site-directed mutagenesis

QuikChange II Site-Directed Mutagenesis Kit	Agilent Technologies, Santa Clara, USA

Site-directed mutagenesis was performed according to manufacturer's instructions. PCR primers used are depicted in Table 1.

2.3.5 Gibson assembly

5x isothermal (ISO) reaction buffer	25 % PEG-8000 500 mM Tris-HCl, pH 7.5 50 mM $MgCl_2$ 50 mM DTT 1 mM each dGTP, dATP, dTTP, dCTP 5 mM NAD	
Gibson assembly Master Mix	320 µl	5x ISO buffer
	0.64 µl	10 U/µl T5 exonuclease
	20 µl	2 U/µl Phusion polymerase
	160 µl	40 U/µl Taq Ligase
	add $H_2O_{dest.}$ to 1.2 ml	

The Gibson assembly is an easy method for cloning of multiple linear DNA fragments in one reaction (Gibson et al., 2009). DNA fragments were generated by PCR and subsequently separated using agarose gel electrophoresis. The appropriate fragment was purified by gel extraction. 15 µl of the Gibson assembly Master Mix was combined with 5 µl of DNA with equimolar concentrations of DNA fragments and a total amount of 20-200 ng DNA. The mixture was incubated at 50 °C for 60 min and subsequently transformed into *E.coli* XL10-Gold (2.3.7).

2.3.6 Generation of chemically competent *E.coli* XL10-Gold

Transformation Buffer I (TFB I)	100 mM RbCl
	50 mM $MnCl_2$
	30 mM potassium acetate
	10 mM $CaCl_2$
	15 % Glycerol
	pH 5.8
Transformation Buffer II (TFB II)	10 mM MOPS
	10 mM RbCl
	75 mM $CaCl_2$
	15 % Glycerol
	pH 6.8
Lysogeny Broth (LB) medium	2.5 % LB Broth

For generation of chemically competent bacteria, a pipette tip of frozen *E.coli* XL10-Gold was inoculated into 5 ml LB medium and cells were grown over night in a shaker at 37 °C and 200 rpm. The next day, an appropriate amount of the cell suspension was transferred into 200 ml LB medium to reach an optical density at 600 nm (OD_{600}) of 0.1. Bacterial cells were further incubated at 37 °C and 200 rpm until the suspension had an OD_{600} of 0.5. The culture was cooled for 15 min at 4 °C and subsequently centrifuged for 10 min at 4000 x*g* and 4 °C. The supernatant was discarded and cells were resuspended in 80 ml TFB I. After 15 min incubation on ice, cells were centrifuged at the same speed and time, supernatant was discarded and the pellet was resuspended in TFB II. Next, cells were incubated again for 15 min on ice, immediately aliquoted, snap frozen in liquid nitrogen and stored at -80 °C.

2.3.7 Transformation of competent *E.coli* with plasmid DNA

Super optimal broth with catabolite repression (SOC) Medium	0.5 % yeast extract 2 % Tryptone 10 mM NaCl 2.5 mM KCl 20 mM $MgSO_4$ 20 mM Glucose
Low-salt LB medium	1 % Tryprone 0.5 % yeast extract 0.5 % NaCl pH 8.0
LB/Low-salt LB agar plates	Respective Medium + 15 g/l Agar
Selection antibiotics	Ampicillin – 100 µg/ml Zeocin – 25 µg/ml

For transformation of competent bacteria with plasmid DNA, 50-500 ng of respective plasmid was mixed with bacteria and incubated on ice for 30 min. Afterwards a heat shock was performed for 45 s at 42 °C to permeabilize the bacterial membrane. Bacteria were cooled on ice for 2 min before adding 1 ml SOC medium and incubating the mixture for 1 h at 37 °C and 750 rpm. After centrifugation for 2 min at 600 x*g* the supernatant was aspirated and the cell pellet was resuspended in approximately 50 µl SOC medium. Bacteria were plated on agar plates supplemented with appropriate antibiotics and incubated over night at 37 °C. For plasmids with Zeocin resistance, low-salt LB Medium and agar plates were used.

Table 2: Plasmids

Construct	Vector Backbone	Bacterial Resistance
myc-TREM2-wt-FLAG_T2A_DAP12-wt	pcDNA5/FRT	Ampicillin
myc-TREM2-R47H-FLAG_T2A_DAP12-wt	pcDNA5/FRT	Ampicillin
myc-TREM2-T66M-FLAG_T2A_DAP12-wt	pcDNA5/FRT	Ampicillin
myc-TREM2-G145W-FLAG_T2A_DAP12-wt	pcDNA5/FRT	Ampicillin
myc-TREM2-H157Y-FLAG_T2A_DAP12-wt	pcDNA5/FRT	Ampicillin
TREM2aa19-157-Fc	pFUSE-hIgG1-FC2	Zeocin
TREM2aa19-112-Fc	pFUSE-hIgG1-FC2	Zeocin
TREM2aa113-157-Fc	pFUSE-hIgG1-FC2	Zeocin
TREM2aa113-130-Fc	pFUSE-hIgG1-FC2	Zeocin
TREM2aa131-157-Fc	pFUSE-hIgG1-FC2	Zeocin
TREM2aa131-148-Fc	pFUSE-hIgG1-FC2	Zeocin
TREM2aa149-157-Fc	pFUSE-hIgG1-FC2	Zeocin

2.3.8 Cultivation of bacteria and plasmid preparation

NucleoSpin™ Plasmid Kit Macherey-Nagel, Düren, Germany
NucleoBond™ Xtra Midi Kit Macherey-Nagel, Düren, Germany

A single colony of transformed bacteria on agar plates was selected and inoculated in 5 ml LB medium supplemented with respective antibiotics. The liquid culture was incubated in a shaking incubator at 37 °C and 200 rpm over night. The following day plasmid preparation was performed using either the NucleoSpin Plasmid Kit for 5 ml cultures or the NucleobondExtra Midi Kit for 200 ml cultures. Both Kits were performed according to manufacturer's instructions. Briefly, cells were pelleted, resuspended and incubated with a lysis and neutralization buffer. After centrifugation, the clear supernatant was loaded on a DNA binding column. The DNA was washed and eluted. For the NucleobondExtra Midi Kit, DNA was further precipitated with isopropanol and washed with ethanol. The DNA was centrifuged and resuspended in an appropriate amount of DNase-free H_2O. Plasmid DNA concentrations were measured using the NanoPhotometer P-class P330 (Implen, Munich, Germany) and

eventually stored at -20 °C. Sequencing of plasmid DNA was performed by Eurofins Genomics (Ebersberg, Germany).

2.4 Cell biological methods

Cell culture was performed under sterile conditions in a Cell Culture bench Euroflow EF6 (Clean Air, Telstar) with sterile consumables.

Table 3: Cell lines

Cell line	Property	Reference
HEK 293	Human embryonic kidney cells	ATCC CRL-1573
HEK 293 Flp-In	HEK 293 cells with a Flp-In locus	Invitrogen R75007
HEK 293 Flp-In myc-TREM2-FLAG_T2A_DAP12	HEK 293 Flp-In cells stably expressing myc-TREM2-FLAG_T2A_DAP12	Generated in this study
HEK 293 Flp-In myc-TREM2-R47H-FLAG_T2A_DAP12	HEK 293 Flp-In cells stably expressing myc-TREM2-R47H-FLAG_T2A_DAP12	Generated in this study
HEK 293 Flp-In myc-TREM2-T66M-FLAG_T2A_DAP12	HEK 293 Flp-In cells stably expressing myc-TREM2-T66M-FLAG_T2A_DAP12	Generated in this study
HEK 293 Flp-In myc-TREM2-G145W-FLAG_T2A_DAP12	HEK 293 Flp-In cells stably expressing myc-TREM2-G145W-FLAG_T2A_DAP12	Generated in this study
HEK 293 Flp-In myc-TREM2-H157Y-FLAG_T2A_DAP12	HEK 293 Flp-In cells stably expressing myc-TREM2-H157Y-FLAG_T2A_DAP12	Generated in this study
BIONi010-C	iPSC	PHAGO consortia, kindly provided by Life&Brain GmbH, Bonn, Germany

BIONi010-C-7	iPSC with homozygous R47H mutation inserted into the TREM2 locus of BIONi010-C	PHAGO consortia, kindly provided by Life&Brain GmbH, Bonn, Germany
BIONi010-C-8	iPSC with homozygous T66M mutation inserted into the TREM2 locus of BIONi010-C	PHAGO consortia, kindly provided by Life&Brain GmbH, Bonn, Germany
BIONi010-C-17	iPSC with KO of TREM2 exon 1 derived from BIONi010-C	PHAGO consortia, kindly provided by Life&Brain GmbH, Bonn, Germany

2.4.1 Thawing of HEK 293 cells

HEK 293 Culturing Medium	10 % Fetal Calf Serum (FCS, PAN-Biotech, Aidenbach, Germany) 1 % Penicillin/Streptomycin (Gibco, Waltham, USA) in Dulbecco's Modified Eagle Medium (DMEM) + GlutaMAX™ (Gibco, Waltham, USA)

For thawing, cells of the human embryonic kidney cell line HEK293 were quickly thawed at RT and transferred into a 15 ml falcon tube containing fresh, pre warmed culturing medium. Cells were centrifuged for 5 min at 300 x*g* and supernatant was aspirated. Cell pellet was resuspended in fresh medium and transferred into a new 10 cm tissue culture dish followed by incubation at 37 °C in a 5 % CO_2 atmosphere.

2.4.2 Culturing and passaging of HEK 293 cells

PBS	Invitrogen, Carlsbad, USA
Trypsin-EDTA, 0.05 %	PAN-Biotech, Aidenbach, Germany

At a confluency of 80-90 %, cells were split in fresh 10 cm dishes. Therefore, medium was aspirated and cells were washed with PBS. To detach cells, trypsin/EDTA was

added and cells were incubated for 5 min. Proteolysis was stopped by addition of fresh culturing medium. An appropriate amount of cell suspension was transferred into a new 10 cm dish. Medium for HEK 293 Flp-In cells was supplemented with 100 µg/ml Zeocin. Plasmid transfected HEK 293 Flp-In cells were cultured in cell culture medium supplemented with 200 µg/ml Hygromycin B.

2.4.3 Cryoconservation of HEK 293 cells

Freezing Medium	10 % Dimethyl Sulfoxide (DMSO) in FCS

For long-term storage, cells were washed with PBS and incubated with trypsin/EDTA for 5 min. Cells were collected in fresh medium. After centrifugation for 5 min at 300 x*g*, supernatant was aspirated and cells were resuspended in an appropriate amount of freezing medium. Cell suspension was transferred into cryovials and stored at -80 °C over night. Eventually, frozen cells were stored in liquid nitrogen.

2.4.4 Thawing of induced pluripotent stem cells (iPSCs)

Geltrex™	Gibco, Waltham, USA
Basal medium	DMEM/F12 + Hepes (Gibco, Waltham, USA)
iPSC culture medium	StemMACS iPS-Brew XF, human (Miltenyi Biotec, Bergisch Gladbach, Germany)

For iPSC culture, 6-well tissue culture plates were pre-coated with geltrex. Therefore, geltrex stock solution was mixed with cold basal medium in a ratio of 1:100. Tissue culture plates were coated with the geltrex solution and incubated for minimum 1 h at room temperature. Meanwhile, for thawing iPS cells, the cryovial was placed in a 37 °C water bath for 3 min. Cells were subsequently transferred in a 50 ml Falcon tube and 9 ml of basal medium was added dropwise while gently shaking the falcon tube. Cells were centrifuged at 300 x*g* for 3 min and the supernatant was discarded. Cells were resuspended in an appropriate amount of iPSC culture medium containing 5 µM Rock inhibitor. Inhibition of the Rock pathway prevents cell death while iPSCs are single cells. After removing the extra geltrex solution from coated plates, cells were evenly distributed onto wells with 2 ml per well and incubated at 37 °C in a 6 %

CO_2 atmosphere. After 24 h, medium containing Rock inhibitor was replaced with fresh iPSC culture medium.

2.4.5 Culturing and passaging of iPSCs

iPS cells were passaged at a confluency of 70-80 %. A new 6-well tissue culture plate was coated with geltrex as described (2.4.4). Cells were washed once with 500 µM EDTA in PBS and then incubated with the very solution for 5 min at room temperature. EDTA/PBS was removed and cells were collected in iPSC culture medium and after gentle resuspension, evenly distributed onto new geltrex-coated plates in an appropriate dilution (1:4 – 1:6).

2.4.6 Differentiation into induced pluripotent stem cell derived microglia (iPSdMiG)

Differentiation of iPSC into microglia was performed according to EP456-26 and Mathews-Ajendra et al. (in preparation). Briefly, to start a differentiation into iPSdMiG, iPS cells in confluent dishes were detached using 1 mg/ml collagenase. Therefore, cells were incubated with collagenase for approximately 30 min until colonies detach from the dish. The formed colonies were collected and centrifuged at 200 x*g* for 3 min and the medium was discarded. Colonies were gently resuspended in differentiation medium and transferred to a PETG Erlenmeyer flask with vented caps for suspension culture and placed on a rocker at cell culture conditions. The emryoid bodies (EBs) in suspension were cultured for 4 days with daily media change in respective differentiation media according to EP456-26 and Mathews-Ajendra et al. (in preparation). On the 4^{th} day, flow cytometry analysis was performed (2.4.7) with a few EBs using antibodies against CD235a and Brachyury. If a sufficient amount (>10 %) of $CD235a^+$ and $Brachyury^+$ cells (characterizing myeloid precursor cells) was present, remaining EBs were manually inoculated onto a macrocarrier according to EP456-26 and Mathews-Ajendra et al. (in preparation) and placed in a 10 cm petri dish. After adherence of EBs on macrocarriers, they were transferred into non-tissue culture coated T75 flasks to ensure free floating in the medium. Media was changed once a week with media additions twice a week. Expansion of the progenitor cells usually takes 4-6 weeks. Once microglia started being produced and secreted into the medium, the media exchange was performed including a centrifugation step

(400 x*g*, 3 min) and microglia were transferred back into the cell culture flask in fresh media. Microglia cells can be identified as round and shiny cells with an approximate size of 25 µm in suspension. The production of microglia can last up to the 12th week of differentiation.

Microglia were harvested for experiments by collecting the supernatant and centrifuging at 400 x*g* for 3 min. The supernatant was replaced into respective differentiation flask and the microglial cell pellet was resuspended in pre-warmed basal media. The cell suspension was filtered using a 40 µm cell strainer to remove large clumps of debris or detached EBs. The stained cell suspension was counted and seeded according to the required density and plate format for experiments. Of note, remaining microglial cells that were not plated were replaced into the differentiation flask.

2.4.7 Flow cytometry analysis

For flow cytometry of EBs, 5-6 EBs were collected on the 4th day after induction and centrifuged at 200 x*g* for 3 min. The supernatant was discarded and pelleted EBs were resuspended in 1 ml accutase (ThermoFisher Scientific, Waltham, USA) and incubated for 10 min at 37 °C. Once EBs have dissociated into single cells, the suspension was centrifuged again and the media was discarded. For flow cytometry of HEK 293 cells, 1*10^6 cells were used. Pellet of single cells were resuspended in 400 µl PBS and split into two samples. While the secondary-antibody controls were left on ice, primary antibodies (Table 4) were added to the samples at an appropriate dilution and incubated for 60 min on ice. Subsequently, cells were washed 3 times by centrifugation for 3 min at 300 x*g,* the supernatant was removed and both, control and samples were incubated with secondary antibodies for 30 min on ice (Table 5). Cells were washed 3 times with PBS by centrifugation and dissolved in an appropriate amount of PBS for flow cytometry analysis (FACS ACCURI™, BD Biosciences, Franklin Lake, USA). Data analysis was performed using FlowJo (FlowJo LLC, USA).

2.4.8 Transfection of cells

Lipofectamine™ 2000 Transfection Reagent	Invitrogen, Carlsbad, USA
Opti-MEM™ Reduced Serum Media	Gibco, Waltham, USA

For transfection of plasmid DNA, cells were seeded in 6 cm cell culture dishes. The next day, an appropriate amount of plasmid DNA was mixed in 200 µl Opti-MEM, as DNA-Lipofectamine 2000 complexes must be made in serum-free conditions. Lipofectamine 2000 was diluted in Opti-MEM 1:20 in a total volume of 200 µl for each transfection. Lipofectamine and plasmid preparations were mixed and incubated for 20 min at RT. Meanwhile, cells were washed with PBS and cell culture medium without supplements was added. Lipofectamine-plasmid complexes were dropwise added to 6 cm dishes. Cells were incubated at cell culture conditions. For stable transfections in HEK 293 Flp-In cells, a co-transfection of 7.2 µg pOG44 coding for Flp recombinase and 0.8 µg of respective plasmids was performed. Also, 24 h post transfection medium was replaced with culturing medium supplemented with 200 µg/ml Hygromycin B for selection.

2.4.9 Limiting dilution cloning

For generation of homogenous cell populations, limiting dilution cloning was performed. After collection of cells, the cell number was determined and cells were seeded in 96-well plates at a density of one cell per well. Cells were cultivated for at least one week before single cell clones were detected using a microscope. Single clones were further expanded and analyzed for protein expression.

2.4.10 Immunocytochemistry analysis (ICC)

Poly-L-Lysine (PLL)	Sigma-Aldrich, Steinheim, Germany
DAPI	Invitrogen, Carlsbad, USA
Immu-Mount™	ThermoFisher Scientific, Waltham, USA
Leica SP8 Lightning	Leica Microsystems, Wetzlar, Germany

For immunofluorescence analysis cells were plated on PLL coated coverslips or 96-well plates and eventually fixed with 4 % pre-warmed PFA in PBS for 20 min. All following solutions were prepared in PBS. Cells were washed three times and

incubated with 0.25 % Triton X-100 for 2 min at RT for permeabilization of the cellular membrane. Cells were blocked for 1 h with 2.5 % BSA, 0.125 % Triton X-100. Incubation with antibodies was performed in 0.125 % BSA, 0.125 % Triton X-100 for 1 h at RT in a humidified chamber. After incubation with primary antibodies, cells were washed three times with 0.125 % Triton X-100 followed by 1 h incubation at RT with DAPI and the appropriate secondary antibody conjugated with fluorophores. Cells were rinsed three times with 0.125 % Triton X-100, followed by two wash steps with PBS and shortly dipped in $H_2O_{dest.}$ before mounting on microscopic slides using Immu-Mount™. Images were obtained using a Leica SP8 Lightning Confocal microscope and further analyzed by ImageJ software (NIH, USA).

Table 4: Primary antibodies

Antibody	Origin	Specificity	Dilution	Reference
Anti-TREM2 (4B2A3)	Mouse monoclonal	TREM2 aa 131-148	WB 1:1000 ICC 1:300 Flow cytometry 1:400	Genscript, generated by AG Walter
Anti-TREM2 (9D11)	Rat monoclonal	C-terminus of human TREM2	WB 1:1000	Provided by Prof. Haass, DZNE, Munich, Germany
Anti-TREM2 (AF1828)	Goat polyclonal	N-terminus of human TREM2	WB 1:1000 ICC 1:800	R&D Systems, Minneapolis, USA
Anti-TREM2 (17C9)	Rat monoclonal	N-terminus of human TREM2	WB 1:1000	Provided by Prof. Haass, DZNE, Munich, Germany
Anti-DAP12 (ab124834)	Rabbit monoclonal	human DAP12 within aa 50-150	WB 1:1000 ICC 1:300	Abcam, Cambridge, UK
Anti-Calnexin (H-70)	Rabbit polyclonal	N-terminus of human Calnexin	WB 1:1000 ICC 1:200	Santa Cruz Biotechnology, Dallas, USA
Anti-Calnexin (AF18)	Mouse monoclonal		WB 1:1000	Invitrogen, Carlsbad, USA

Anti-TGN46	Rabbit polyclonal	human TGN46 aa 426-437	WB 1:1000 ICC 1:200	Sigma-Aldrich, Steinheim, Germany
Anti-LC3 (PM036)	Rabbit polyclonal	human LC3B aa 1-120	WB 1:1000 ICC 1:200	MBL/Biozol, Eching, Germany
Anti-EEA1 (PM062)	Rabbit polyclonal	early endosome antigen 1	WB 1:1000 ICC 1:200	MBL/Biozol, Eching, Germany
Anti-Lamp2 (H4B4)	Mouse monoclonal	Full length protein	WB 1:1000	Iowa Hybridoma Bank
Anti-Lamp2	Rabbit polyclonal	C-terminus of human Lamp2	ICC 1:200	Abcam, Cambridge, UK
Anti-58K (ab27043)	Mouse monoclonal	58K Golig protein	ICC 1:200	Abcam, Cambridge, UK
Anti-Rab7 (ab137029)	Rabbit monoclonal	C-terminus of human Rab7	WB 1:1000	Abcam, Cambridge, UK
Psmb5	Rabbit polyclonal	Psmb5 aa 243-259	ICC 1:100	Thermo Fisher Scientific, Waltham, USA
82E1	Mouse monoclonal	N-terminus of human Aβ	WB 1:1000	IBL International, Hamburg, Germany
Anti-Fc-HRP	Goat polyclonal	Gamma Immunoglobin Fc region	WB 1:1000	Invitrogen, Carlsbad, USA
Brachyury	Mouse monoclonal	Human Brachyury within aa 375-393	Flow cytometry 1:50	Santa Cruz Biotechnology, Dallas, USA
APC conj. CD235a	Mouse monoclonal		Flow cytometry 1:50	BD Biosciences, Minneapolis, USA

Table 5: Secondary antibodies

Antibody	Origin	Dilution	Reference
Horseradish peroxidase (HRP) conj. anti-mouse IgG	Rabbit	1:10000	Sigma-Aldrich, Steinheim, Germany
HRP conj. anti-rabbit	Goat	1:10000	Sigma-Aldrich, Steinheim, Germany
HRP conj. anti-goat	Rabbit	1:10000	Sigma-Aldrich, Steinheim, Germany
HRP conj. anti-rat	Goat	1:10000	Rockland, Gilbertsville, USA
IRDye® 680RD conj. anti-mouse	Goat	1:10000	Li-COR Biosciences, Bad Homburg, Germany
Alexa Fluor 488-conj. anti-mouse	Donkey	1:1000	Invitrogen, Carlsbad, USA
Alexa Fluor 488-conj. anti-rabbit	Donkey	1:1000	Invitrogen, Carlsbad, USA
Alexa Fluor 488-conj. anti-goat	Donkey	1:1000	Invitrogen, Carlsbad, USA
Alexa Fluor 488-conj. anti-rat	Donkey	1:1000	Invitrogen, Carlsbad, USA
Alexa Fluor 546-conj. anti-mouse	Donkey	1:1000	Invitrogen, Carlsbad, USA
Alexa Fluor 546-conj. anti-rabbit	Donkey	1:1000	Invitrogen, Carlsbad, USA
Alexa Fluor 546-conj. anti-goat	Donkey	1:1000	Invitrogen, Carlsbad, USA
Alexa Fluor 546-conj. anti-rat	Donkey	1:1000	Invitrogen, Carlsbad, USA
APC-conj. anti human CD235a	Mouse	1:50	BD Biosciences, Franklin Lakes, USA
APC-conj. anti-mouse IgG2B	Mouse	1:200	R&D Systems, Minneapolis, USA

2.4.11 Immunocytochemistry of cell surface proteins

For staining of cell surface proteins, cells were seeded on PLL coated coverslips in 24-well plates. At the desired confluency, cells were washed once with warm DMEM medium. Plates were placed on ice and cells were incubated for 1 h with the primary antibody in DMEM (Table 4). After gentle washing with ice-cold DMEM for three times, cells were incubated for 1 h with the corresponding secondary antibody conjugated with fluorophores (Table 5). Prior to fixation with 4 % PFA, another wash step with ice-cold DMEM was performed. Cells were washed three times with PBS and cell membranes were permeabilized with 0.25 % Triton X-100 in PBS for 2 min. Nuclei were stained with DAPI and coverslips were washed three times with PBS and once with $H_2O_{dest.}$. Eventually, cells were mounted on microscopic slides using Immu-Mount™ and analyzed as descried above.

2.5 Protein biochemical methods

2.5.1 Aβ preparation and aggregation

Aβ synthetic peptides were purchased as lyophilized powder from PSL peptides (Heidelberg, Germany). Peptides were dissolved in 10 mM NaOH to achieve a stock concentration of 230 µM. After sonication for 10 min, peptides were snap frozen in liquid nitrogen and stored at -20 °C. To generate oligomeric Aβ, peptides were incubated at 100 µM in PBS for 24 h at 4 °C. As another protocol for oligomerization, peptides were incubated at 37 °C for 3 h. Here, the concentration for oligomerization was 23 µM in PBS. Aggregated Aβ was generated by preparation of peptides in 10 mM HCl to obtain a concentration of 100 µM. The solution was further incubated for 24 h at 37 °C. The different Aβ preparations were analyzed by either SDS-PAGE (2.5.11) or Native PAGE (2.5.12).

2.5.2 Preparation of cell lysates

1x STEN lysis buffer	50 mM Tris-HCl, pH 7.4 150 mM NaCl 2 mM EDTA 1 % Triton X-100 1 % NP-40 (Igepal CA-630)
Protease Inhibitor (cOmplete™, EDTA free)	Roche Diagnostics, Basel, Switzerland

For preparation of whole cell lysates, cells in dishes were washed with ice-cold PBS, scraped using a cell scraper and collected in tubes. Cells were centrifuged and the supernatant was removed. 1x STEN lysis buffer was used for resuspension of the cell pellet followed by incubation for 20 min on ice. Further, cell lysates were centrifuged for 10 min at 16.000 x*g* and 4 °C and the supernatant was stored at -20 °C or directly analyzed by SDS-PAGE (2.5.11).

2.5.3 Membrane preparations

Hypotone Buffer	10 mM Tris 1 mM EGTA 1 mM EDTA pH 7.4

Membrane fractions were obtained by first scraping cells from dishes in an appropriate volume of hypotonic buffer supplemented with protease inhibitor cocktail and collected in tubes. Cells were incubated on ice for 10 min and subsequently lysed using a syringe with a 0.6 mm cannula, drawing 20 times. After centrifugation for 5 min at 1.300 x*g* at 4 °C, the supernatant containing cell membrane and cytosol was transferred into a fresh tube and centrifuged for 1 h at 16.000 x*g* and 4 °C. The supernatant (cytosol) was removed and the remaining pellet was lysed in 1x STEN lysis buffer supplemented with protease inhibitor cocktail. Cell membranes were incubated for another 20 min on ice. The lysate was further centrifuged for 10 min at 16.000 x*g* and 4 °C and the resulting supernatant was transferred into a fresh tube for determination of protein concentrations or SDS-PAGE analysis (2.5.11).

2.5.4 Determination of protein concentrations

Pierce™ BCA™ Protein Assay Kit ThermoFisher Scientific, Waltham, USA

Bicinchoninic acid was used for determination of protein concentrations from cell membrane preparations according to manufacturer's instructions. In presence of proteins, Cu(II) is reduced to Cu(I) directly proportional to the protein concentration. The absorbance was measured at 562 nm and concentrations were calculated according to a BSA standard curve.

2.5.5 Trichloroaceticacid (TCA) precipitation

5x SDS loading buffer	125 mM Tris
	10 % SDS
	100 mM DTT
	50 % Glycerol
	Bromphenol blue

After collection of cell culture medium, the suspension was centrifuged at 16.000 x*g* for 10 min at 4 °C. Supernatant was transferred into a fresh tube and sodiumdeoxycholat (NaDOC) was added to achieve a final concentration of 0.02 %. The solution was inverted and incubated for 15 min at RT. TCA was added to a final concentration of 10 %, again, samples were inverted and incubated for 1 h at RT for precipitation of proteins. Subsequently, the suspension was centrifuged at 16.000 x*g* for 10 min at 4 °C. The supernatant was discarded and samples were centrifuged again. Remaining supernatant was removed and samples were resuspended in an appropriate volume of 50 mM Tris/1 % SDS and SDS loading buffer was added. Samples were boiled at 95 °C for 5 min and separated using SDS-PAGE (2.5.11).

2.5.6 Deglycosylation

For deglycosylation, TCA precipitated conditioned media of TREM2 expressing cells were resuspended in 50 mM Tris. Following endoglycosidases were used: PNGase F, Endo H, Endo D, Endo F2, Endo F3, Neuraminidase and O-glycosidase (New England Biolabs, Ipswich, USA). Preparation of samples was performed according to the respective manufacturer's instructions. Briefly, for PNGase F, Endo H, Endo D and O-glycosidase digestion, samples were denatured for 10 min or

3 min (Endo D) at 100 °C with corresponding buffers and mixed with the respective glycosidase and supplements. Digestion with Endo F2, F3 and Neuraminidase was performed under native conditions without prior boiling. The reactions were incubated at 37 °C for 1 h and stopped by addition of SDS loading buffer (2.5.5). Samples were analyzed by SDS-PAGE (2.5.11).

2.5.7 Antibody fragmentation

Pierce™ Fab Preparation Kit	ThermoFisher Scientific, Waltham, USA
Pierce™ F(ab')$_2$ Preparation Kit	ThermoFisher Scientific, Waltham, USA

To specify whether stimulation of cells with antibodies occurs via crosslinking, fragments of respective antibodies were generated using the Fab and F(ab')$_2$ Preparation Kits. Antibody fragmentation was performed according to manufacturer's instructions. Briefly, antibodies were digested with either Papain (Fab) or Pepsin (F(ab')$_2$) and subsequently purified using Protein A to remove undigested antibodies and Fc fragments. The concentration of Fab and F(ab')$_2$ fragments was determined (2.5.4) and completion of the procedure was confirmed by SDS-PAGE and Coomassie staining (2.5.11).

2.5.8 Biotinylation of cell surface proteins

1x STEN buffer	150 mM NaCl 50 mM Tris 2 mM EDTA 0.2 % NP-40 pH 7.6
EZ-Link™ Sulfo-NHS-Biotin	ThermoFisher Scientific, Waltham, USA
Streptavidin Sepharose	GE Healthcare, Little Chalfont, UK

Cells were cultured in PLL coated 6 cm cell culture dishes to a confluency of 80-90 %. For biotinylation of cell surface proteins, cells were kept on ice and washed twice with ice-cold PBS. Subsequently, cells were incubated with 0.5 mg/ml Sulfo-NHS-biotin in PBS under constant gentle shaking. The biotin solution was removed and cells were washed three times with 20 mM glycine in PBS, incubating the last wash step for 15 min. Cells were washed again with ice-cold PBS prior to cell lysis

for 15 min with 900 µL STEN lysis buffer (2.5.1). Insoluble cell fractions were removed by centrifugation for 10 min, 12.000 x*g* and 4 °C. In parallel, streptavidin-sepharose was washed three times with PBS, followed by one wash step with STEN buffer. Beads were used as 50 % in STEN buffer. 50 µl of washed streptavidin-sepharose was added to cell lysates and incubated over night at 4 °C on an overhead shaker. Streptavidin-sepharose was washed four times for 10 min with STEN buffer and centrifuged for 3 min at 600 x*g* and 4 °C. The supernatant was aspirated and samples were supplemented with 20 µL 2x SDS loading buffer and boiled for 5 min at 95 °C. Further, samples were analyzed by SDS-PAGE (2.5.11).

2.5.9 AlphaLISA immunoassay

AlphaLISA® SureFire® Ultra™ p-SYK (Tyr525/526) Assay Kit	Perkin Elmer, Waltham, USA

Using the AlphaLISA technology, detection of phosphorylated SYK (pSYK) in cell lysates after stimulation of TREM2-DAP12 signaling was performed according to manufacturer's instructions. Briefly, cells were stimulated for indicated time points. Subsequently, cells were lysed with the respective lysis buffer for 10 min. 10 µl of cell lysates were transferred into a 384-well OptiPlate™ and incubated with 5 µl Acceptor Mix for 1 h in the dark. 5 µl Donor Mix was added and the mixture was incubated for another 1 h in the dark. The OptiPlate™ was measured with standard AlphaLISA settings (Envision® 2105 Multimode Plate Reader, Perkin Elmer, Waltham, USA).

2.5.10 Subcellular fractionation by density gradient centrifugation

Hypotone D buffer	10 mM Tris
	10 mM NaCl
	0.1 mM EGTA
	25 mM β-Glycerophosphate
	1 mM DTT
	pH 7.5

OptiPrep™, 60 % Iodixanol	Sigma-Aldrich, Steinheim, Germany
Diluent	0.25 mM Sucrose 6 mM EDTA 60 mM HEPES pH 7.4

Density gradient centrifugation was performed to separate cellular vesicles and organelles according to their density. For preparation of density gradients, 9 solutions with varying densities were prepared using OptiPrep™ and diluent. The following solutions were prepared and a gradient was loaded starting with the highest density: 30 %, 20 %, 17.5 %, 15 %, 12.5 %, 10 %, 7.5 %, 5 %, and 2.5 %.

Cells were seeded in 10 cm dishes and grown until 80-90 % confluent. Cells were washed once with cold PBS and subsequently incubated with 750 µl Hypotone D buffer and incubated 10 min on ice before cells were scraped and transferred into tubes. Lysis was performed using a syringe with a 0.6 mm cannula as described above (2.5.3) and the cell suspension was centrifuged for 5 min at 1300 x*g* and 4 °C. The pellet was discarded and the postnuclear supernatant (PNS) was transferred into a fresh tube. Gradients were loaded with 500 µl PNS and centrifuged at 200.000 xg for 8 h using a SW 41 Ti Swinging-Bucket Rotor and an Optima™ XPN-80 Ultracentrifuge (Beckman Coulter, Brea, USA). Subsequently, 1 ml fractions were collected and proteins were precipitated using TCA (2.5.5). Protein estimation was performed with the remaining PNS, which was further used as a total load, and all samples were analyzed by SDS-PAGE (2.5.11).

2.5.11 Continuous sodium dodecylsulfate – polyacrylamide gel electrophoresis (SDS-PAGE)

Novex™ NuPAGE™ MES SDS Running Buffer (20x) 4-20 % Bis-Tris gels LDS Sample Buffer (4x)	Invitrogen, Carlsbad, USA
Novex™ SeeBlue™ Protein Standard	Invitrogen, Carlsbad, USA
PageRuler™ Prestained Protein Ladder	Invitrogen, Carlsbad, USA

Coomassie staining solution	0.5 % Coomassie brilliant-blue R-250
	45 % Isopropanol
	10 % Acetic acid
Coomassie destaining solution	45 % Methanol
	10 % Acetic acid

SDS-PAGE was used to separate proteins according to their molecular weight. Pre-cast gels were set up in NuPAGE™ running chambers and 1x MES SDS Running Buffer was added. An appropriate amount of protein sample was mixed with SDS loading buffer (2.5.5) or LDS Sample Buffer and boiled for 5 min at 95 °C. Protein samples and 3 µL protein standard were loaded on the gel and gels were run at 120 V until samples were separated. SDS-PAGE gels were further analyzed using western immunoblotting (2.5.13) or directly stained using Coomassie staining solution for 30-45 min with subsequent use of Coomassie destaining solution to remove excess Coomassie dye.

2.5.12 Native PAGE

Novex™ Native PAGE™	Invitrogen, Carlsbad, USA
4-16 % Bis-Tris gels	
Running Buffer (20x)	
Cathode Additive (20x)	
Sample Buffer (4x)	

For investigation of native proteins, especially Aβ, Native PAGE was performed. Therefore, samples were prepared by addition of Sample buffer and loaded on Native PAGE™ gels. Cathode and Anode running buffers were prepared according to manufacturer's instructions. The gel was run for 60-90 min at 120 V and further analyzed by western immunoblotting (2.5.13).

2.5.13 Western immunoblotting

1x Blotting buffer	20 % Methanol 5 mM Tris 200 mM Glycine
10x Ponceau	2 % Ponceau S 30 % TCA
1x TBST	50 mM Tris 150 mM NaCl pH 7.6 1 % Tween20
Blocking buffer	5 % skim milk powder in 1x TBST
Amersham™ ECL™ Prime, Western Blotting Detection Reagent	GE Healthcare, Little Chalfont, UK

To specifically detect proteins in a sample extract, Towbin and coworkers invented the western immunoblotting technique (Burnette, 1981). Proteins are separated according to their size using SDS-PAGE and afterwards blotted on a nitrocellulose membrane. A protein of interest can be bound to a specific primary antibody, which is then bound by a primary-antibody-specific secondary antibody conjugated to HRP. Detection of the desired protein can be achieved using the enhanced chemiluminescence (ECL) method. Thereby, in the presence of H_2O_2, luminol is oxidized by the HRP leading to emission of light.

As previously described, proteins were separated by SDS-PAGE (2.5.11). The western immunoblotting was performed using the wet blot technique. Therefore, nitrocellulose membrane and whatman paper were cut in the size of the gel and pre-equilibrated in blotting buffer. Gel, membrane, whatman paper and pre-wetted sponge pads were packed and placed into the wet blot tank. The chamber was filled with blotting buffer and transfer of proteins from gel to membrane was performed for 105 min at 400 mA. Afterwards, the membrane was blocked in blocking buffer for 1 h and incubated with primary antibodies in TBST over night at 4 °C. To remove unbound antibodies, the membrane was washed three times for 10 min with 1 x TBST. Afterwards, it was incubated with the corresponding secondary HRP-conjugated antibody 1:10.000 in 1x TBST for 1 h at RT and washed again three

times. To detect the protein of interest, membranes were incubated for 1 min with ECL solution and placed in a transilluminator (ChemiDoc™ XRS System, BioRad).

2.6 Statistical analysis

For statistical analysis, at least three independent experiments or samples were analyzed. Data were analyzed using GraphPad Prism 6 (Graph Pad Software, La Jolla, USA). All data were tested for normality and subsequently analyzed by one-way ANOVA followed by *post hoc* Tukey's multiple comparisons test or Student's t-test (unpaired, two-sided) for comparison of two groups. A p-value less than 0.05 was considered as statistically significant (*$p<0.05$; **$p<0.01$; ***$p<0.001$).

3 Results

3.1 Generation and characterization of a TREM2-DAP12 reporter cell system

TREM2 is a receptor mainly expressed on monocyte-derived cell types, including microglia and tissue macrophages (Colonna, 2003b; Colonna & Wang, 2016; Paloneva et al., 2003). It interacts with its co-receptor DAP12 and upon ligand binding induces intracellular signaling leading to phagocytosis, survival or migration (Colonna, 2003a; Jay et al., 2017; J. Walter, 2016). In monocyte-derived cell types, other receptors might interact with DAP12 when TREM2 is absent. Therefore, investigation of TREM2 characteristics of TREM2 common and rare variants might be difficult. In this study, we co-expressed TREM2 and DAP12 in HEK 293 cells that do not express both proteins endogenously. HEK 293 cells show many advantages, as they proliferate and represent a robust reporter system to overcome the possible interaction of DAP12 with other immune-receptors.

In order to allow stable expression of TREM2 and its co-receptor DAP12 in stoichiometric amounts, a bicistronic construct encoding human TREM2 and DAP12 separated by a T2A peptide sequence was cloned into the Flp-In vector (Figure 6A), and used to transfect HEK 293 Flp-In cells with an endogenous Flp recombination target (FRT) site. A plasmid encoding the Flp recombinase was co-transfected. Stable single cell clones were selected and expression of TREM2 and DAP12 was analyzed by western immunoblotting in purified cellular membrane fractions (Figure 6C). In parallel, transiently transfected cells were included for comparison. TREM2 was detected as mainly immature protein of approximately 38 kDa in stably and transiently transfected cells. In addition, TREM2 C-terminal fragments (CTFs) migrating below 15 kDa were observed upon transient and stable transfection, however, in different amounts. Comparison of stable and transient transfection also revealed differences in the relative amounts of DAP12 monomers (12 kDa), dimers (24 kDa) and higher assemblies.

TREM2 can undergo proteolytic cleavage by ADAM proteases, resulting in the secretion of its ectodomain (Kleinberger et al., 2014; Wunderlich et al., 2013). In conditioned media, secreted soluble TREM2 (sTREM2) was detected as diffuse

signals between 35 and 55 kDa rather than as distinct bands (Figure 6D), consistent with complex N-glycosylation within the TREM2 ectodomain (Kleinberger et al., 2014; Park et al., 2015). Interestingly, sTREM2 of transiently transfected cells showed a lower molecular weight signal compared to cells with stable expression, indicating aberrant glycosylation and incomplete maturation of the protein.

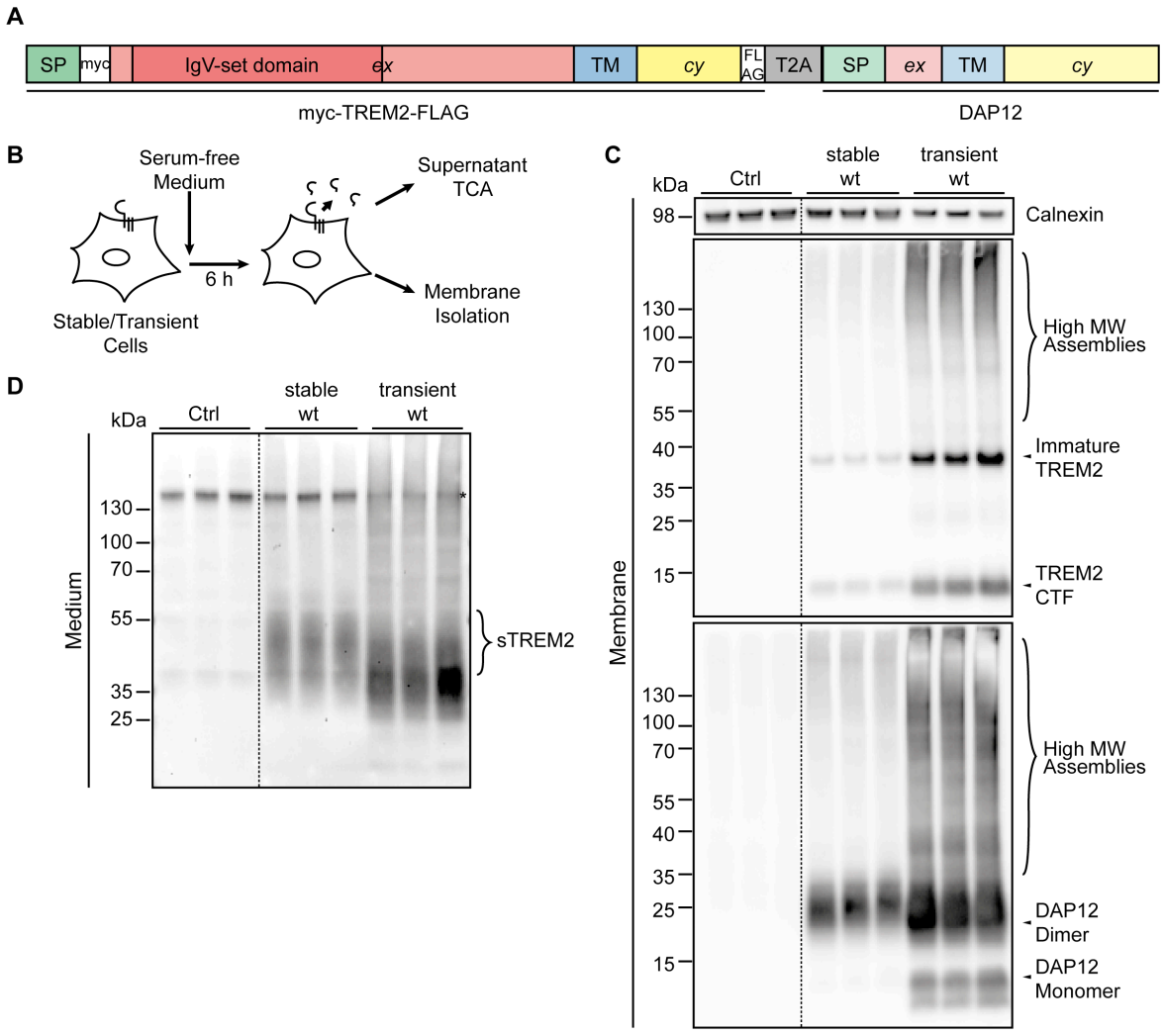

Figure 6: Expression of TREM2 and DAP12 in stably and transiently transfected cells. (A) Illustration of the bicistronic construct of TREM2 and DAP12, including a myc-tag after the signal peptide and a FLAG-tag behind the cytoplasmic region of TREM2. A T2A peptide separates TREM2 and DAP12 allowing equal initial translation of both proteins from one mRNA. SP, signal peptide; *ex*, extracellular domain; TM, trans-membrane domain; *cy*, cytoplasmic domain. (B) Schematic illustration of the experiments. Cell culture medium of stably or transiently transfected cells was replaced with serum-free medium for secretion of sTREM2 for 6 h. Media were collected and precipitated using TCA. Membrane fractions were isolated and both were analyzed via western immunoblotting. (C) Analysis of isolated membrane fractions. For the control, non-transfected HEK 293 Flp-In cells (Ctrl) were used. Anti-TREM2 9D11 antibody recognizing a C-terminal epitope was used for detection of

TREM2. Anti-DAP12 was used for detection of DAP12. Calnexin served as a loading control. (D) Analysis of TCA precipitated conditioned medium of TREM2-DAP12 expressing cells. Anti-TREM2 AF1828 was used to detect sTREM2 in conditioned media.

To test N-glycosylation of TREM2, sTREM2 from conditioned media of stably or transiently transfected cells was subjected to deglycosylation using three different enzymes (Figure 7). PNGase F removes the entire N-glycan right at the Asn linkage, whereas Endo D and Endo H specifically hydrolyze high-mannose and/or hybrid structures that are typically located in the ER or early Golgi compartments (Freeze & Kranz, 2010; Plummer et al., 1984; Tarentino et al., 1989). In stable and transient samples, treatment with PNGase F resulted in the disappearance of the diffuse signal and formation of a ~17 kDa polypeptide, representing deglycosylated sTREM2. In contrast, the higher molecular weight smear was largely resistant against Endo D and Endo H in supernatants of stably expressing cells. However, in transiently transfected samples, a minor 17 kDa peptide was generated by deglycosylation with Endo D and Endo H. Together these results indicate that sTREM2 from stably expressing cells mainly contains mature mannose-poor, complex glycostructures whereas transiently expressing cells partly secrete immature TREM2 and mainly mature TREM2 with less complex glycostructures due to aberrant glycosylation.

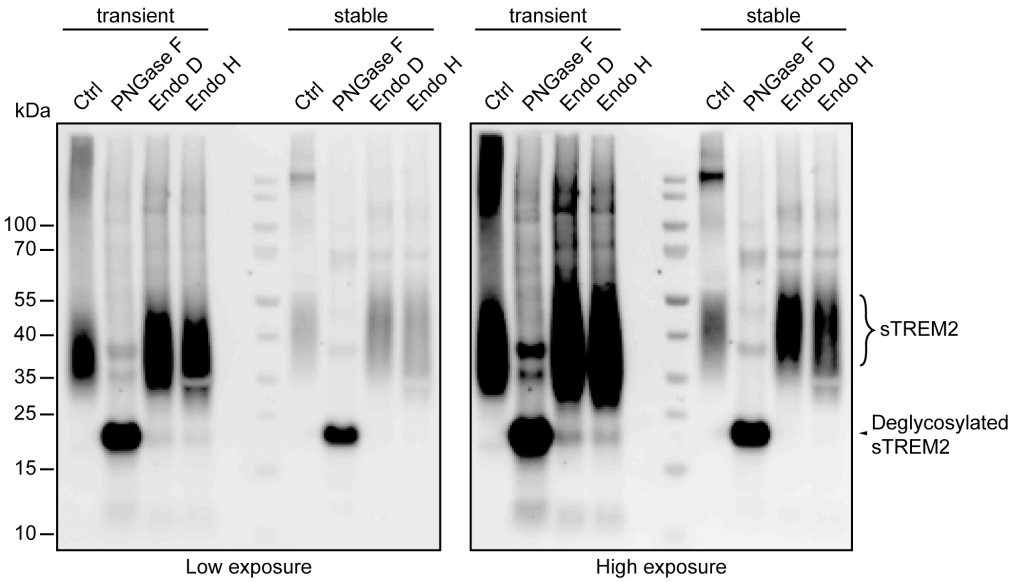

Figure 7: Differential glycosylation of TREM2 in transiently and stably transfected cells. Conditioned medium from transiently and stably transfected TREM2-DAP12 expressing cells was subjected to deglycosylation with PNGase F, Endo D and Endo H. Samples were incubated with respective glycosidases at 37°C for 1 h and subsequently analyzed by western immunoblotting. sTREM2 was detected by anti-TREM2 AF1828.

Mature TREM2 is transported to the cell surface to function in a receptor complex with DAP12. Specific labeling of cell surface proteins by biotinylation (Figure 8) showed formation of high molecular weight forms for both, TREM2 and DAP12 in transiently transfected cells, further suggesting aberrant maturation and assembly upon transient overexpression of these proteins (Figure 8B). DAP12 is mainly migrating at ~24 kDa, indicating formation of characteristic stable dimers at the plasma membrane. A ~38 kDa TREM2, likely representing immature TREM2, was also biotin-labeled in transiently transfected cells, indicating aberrant transport of immature TREM2 to the cell surface. In contrast, biotin-labeled TREM2 in stably expressing cells is exclusively presented as a smear, indicating that TREM2 undergoes complex maturation before it is exposed at the cellular surface. Thus, only cell lines stably co-expressing TREM2 and DAP12 were used for further experiments, as they represent a better system for studying TREM2 characteristics.

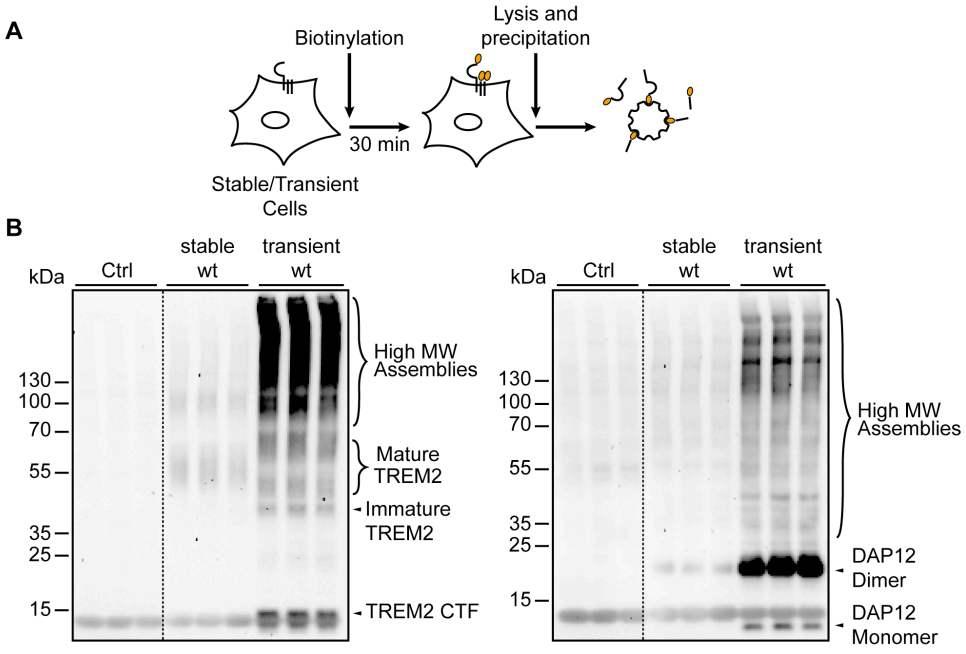

Figure 8: Expression of immature TREM2 at the cell surface of transiently transfected cells. (A) Schematic illustration of the experiment. Stably or transiently transfected cells were labeled with Sulfo-NHS-biotin, lysed and biotin-labeled proteins were precipitated using streptavidin-sepharose. (B) Western immunoblotting of biotinylated cell surface proteins of stably and transiently transfected cells. Anti-TREM2 AF1828 was used for detection of TREM2 (left panel), anti-DAP12 was used for detection of DAP12 (right panel).

3.2 Epitope characterization of anti-TREM2 antibodies

In this study, different anti-TREM2 antibodies were used for experiments. The rat monoclonal antibody 17C9, kindly provided by the DZNE Munich, was raised against the ectodomain of human TREM2. Additionally, we developed a mouse monoclonal antibody (4B2A3) against human TREM2 using the complete ectodomain of human TREM2 for immunization. The commercially available polyclonal goat antibody AF1828, raised against the human TREM2 ectodomain, was used as well.

To investigate the epitopes of respective antibodies, TREM2 fusion proteins of different length were generated (Figure 9A). The TREM2 sequence was fused to the human Fc for easier purification and detection of the respective peptides. After generation of the different TREM2 constructs, cells were transiently transfected and the supernatant was collected for precipitation of fusion proteins (Figure 9B). Western immunoblotting revealed that antibody 17C9 mainly recognized the fusion protein containing the complete sTREM2 sequence (aa 19-157), and weakly other fusion proteins, whereas 4B2A3 does not bind to the Ig-like domain (aa 29-112), but

selectively recognized an epitope within the stalk region of TREM2 (aa 131-148). Thus, 17C9 possibly recognizes either an epitope around aa 112-113 that might not be present in the other fusion proteins or it detects a conformational epitope of TREM2. The same pattern of recognition as for the 4B2A3 antibody could be observed for the AF1828 antibody, even though it is a polyclonal antibody. Here, the main epitope lies within aa 131-148. However, it also weakly recognizes aa 149-157.

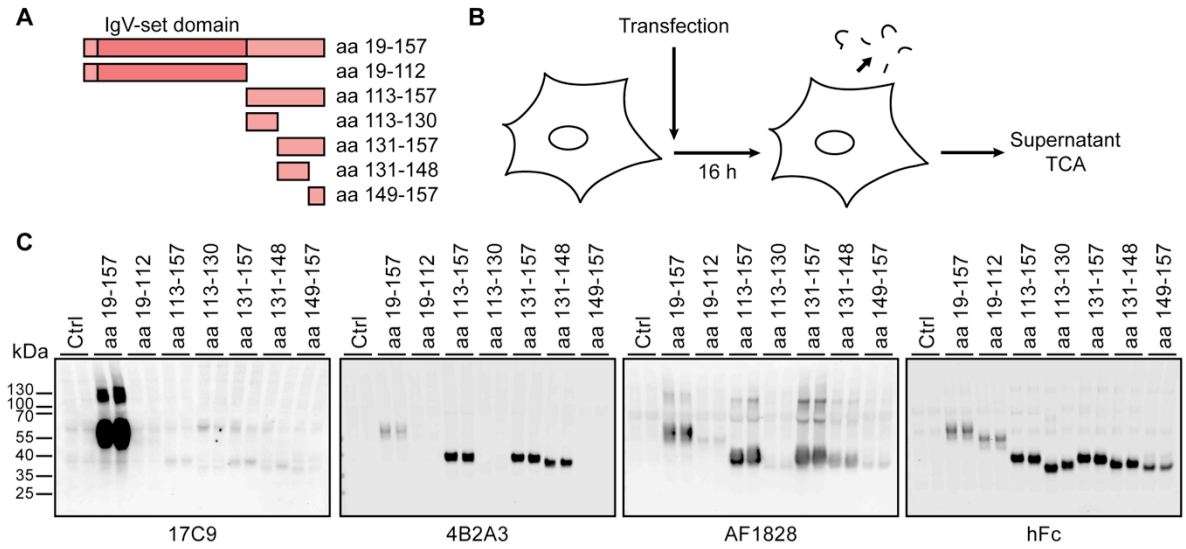

Figure 9: Epitopes of TREM2 specific antibodies. (A) Illustration of TREM2 fragments that were generated for investigation of TREM2 antibody binding. The sequences were C-terminally fused to human Fc. (B) Schematic illustration of the experiment. Cells were transfected with respective constructs and after 16 h incubation, the supernatant with secreted fragments was collected and precipitated using TCA. (C) Western immunoblotting of precipitated cell culture supernatants. Antibodies 17C9, 4B2A3 and AF1828 were used for detection of TREM2 fragments. Anti-human Fc (hFc) was used as a control for successful transfection of fusion proteins.

Though all antibodies were generated against the TREM2 ectodomain, they still show differences in the recognition of the different fusion proteins. Antibodies 4B2A3 and AF1828 appear to detect similar epitopes within the sequence of aa 131-148 however, AF1828 shows a stronger and more diffuse signal. The characterization of the available antibodies was important for the analysis of selective TREM2 variants in the following experiments.

3.3 Differential effects of TREM2 variants on subcellular transport, proteolytic processing, and secretion

Several TREM2 variants have been linked to neurodegenerative diseases. After the validation of the HEK 293 Flp-In cell system to stably co-express TREM2 and DAP12, we generated additional cell models for disease-associated variants of TREM2 together with DAP12. Beside the common (wt) TREM2 variant, we also used the R47H variant associated with an increased risk for AD (Guerreiro & Hardy, 2013; Jonsson et al., 2013) and the H157Y variant that also showed association with AD in some cohorts (Jiang, Tan, et al., 2016). In addition, we used the T66M variant associated with frontotemporal dementias (Le Ber et al., 2014), and a novel G145W variant that has been shown to segregate with a familial form of dementia (Karsak et al., 2020).

To investigate the processing and secretion of the different TREM2 variants, levels of sTREM2 in cell supernatants, and those of full length TREM2 and CTFs in cellular membranes were analyzed (Figure 10A). As compared to the TREM2 wt variant, the AD-associated R47H variant showed decreased levels of sTREM2 normalized to the amount of immature TREM2 in the respective cell models. Additionally, higher expression of immature TREM2 and DAP12 was shown in cells expressing disease-associated TREM2 R47H, whereas no changes could be detected in the ratio of TREM2 CTF over immature TREM2 levels. sTREM2 and CTFs were hardly detectable in media and membrane fractions of TREM2 T66M expressing cells, consistent with efficient retention of TREM2 T66M in ER and Golgi compartments, thereby preventing proteolytic processing by ADAM proteases. In addition, a higher band of ~70 kDa could be observed for this variant, possibly indicating accumulation of dimeric TREM2 T66M. In line with the absence of CTFs, DAP12 could barely be detected in TREM2 T66M expressing cells. As TREM2 is not transported to the cell surface and cannot function properly, DAP12 is not needed and thus possibly cleared from the cell.

It could be observed that sTREM2 for variants G145W and H157Y was detected differently by the antibodies 17C9 and AF1828. As described before, the AF1828 antibody binds mainly within the stalk region of TREM2. The G145W mutation is located within this region, and might contribute to the weaker detection by the

AF1828 antibody compared to the 17C9 antibody that recognizes other epitopes. In contrast, the 17C9 antibody shows a weaker detection of sTREM2 H157Y. The exact epitope for this antibody could not be determined as it presumably binds to a conformational epitope within the ectodomain of TREM2. However, as analyzed with both antibodies, shedding of the novel TREM2 G145W mutant was significantly decreased, as well as the amount of CTFs compared to the wt protein.

The AD-associated variant H157Y has not been extensively studied so far. This variant has been shown to result in increased shedding resulting in lower levels of mature TREM2 at the cell surface (Schlepckow et al., 2017; Thornton et al., 2017). Here, the amount of sTREM2 in conditioned media of cells expressing TREM2 H157Y was rather decreased, when detected by the anti-TREM2 antibody 17C9, whereas detection with anti-TREM2 AF1828 did not reveal decreased shedding. Hence, this mutation could affect binding of antibody 17C9. Interestingly, an increase of DAP12 over immature TREM2 and CTFs could be observed. This cannot be observed in all other variants, suggesting an effect of the TREM2 H157Y variant on DAP12 stability or complex formation.

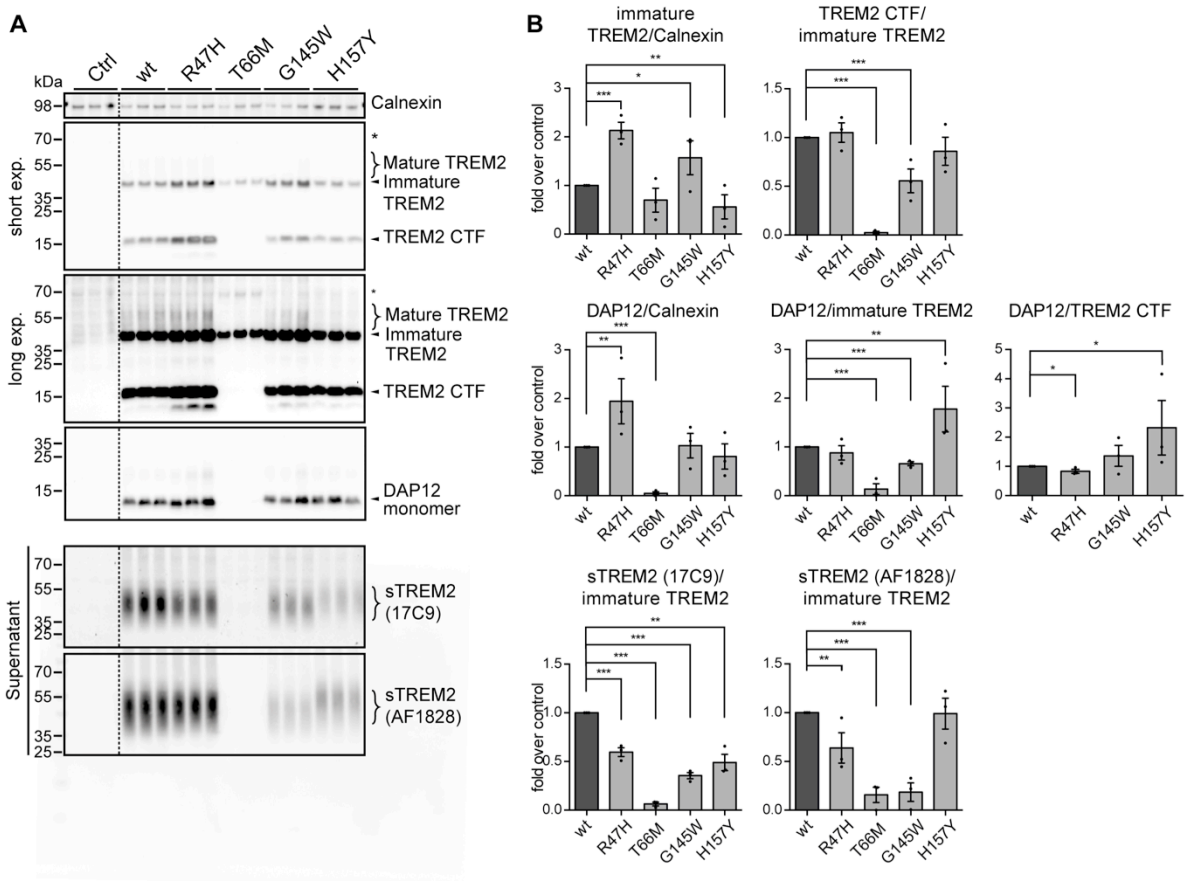

Figure 10: Comparative characterization of the common and disease-associated TREM2 variants. (A) Monoclonal cell lines stably expressing TREM2 wt, R47H, T66M, G145W and H157Y together with DAP12 were incubated with serum-free medium for secretion of sTREM2. Media were collected and precipitated using TCA. Membranes were isolated and both here analyzed via western immunoblotting. Anti-TREM2 9D11 antibody was used for detection of C-terminal TREM2 in membrane fractions. Anti-DAP12 was used for detection of DAP12. Anti-TREM2 17C9 and AF1828 antibodies were used to detect sTREM2 in conditioned media. Calnexin served as a loading control for membrane fractions. * Shows accumulation of TREM2 in T66M variant expressing cells. (B) Quantitation of western immunoblotting as shown in A. Data represent the mean ± SEM of three independent experiments with triplicates each (n=3). Student's t-test (unpaired, two-tailed), *p<0.05; **p<0.01, ***p<0.001.

For further analysis of TREM2 variants, immunocytochemical stainings of TREM2 and DAP12 were performed (Figure 11). The obtained results correspond to the expression levels of western immunoblotting for all TREM2 variant expressing cell lines. TREM2 R47H expressing cells show a high expression of TREM2 and DAP12, whereas for the T66M variant, DAP12 was barely detectable and TREM2 was exclusively detected intracellularly. For TREM2 H157Y, a stronger intensity of DAP12 was detected compared to the other variants, which is in line with previous results (Figure 10). In general, TREM2 was mainly localized at the plasma membrane and in

vesicular structures inside the cell. A detailed analysis of subcellular localization of TREM2 common and rare variants will be addressed in further experiments in this study.

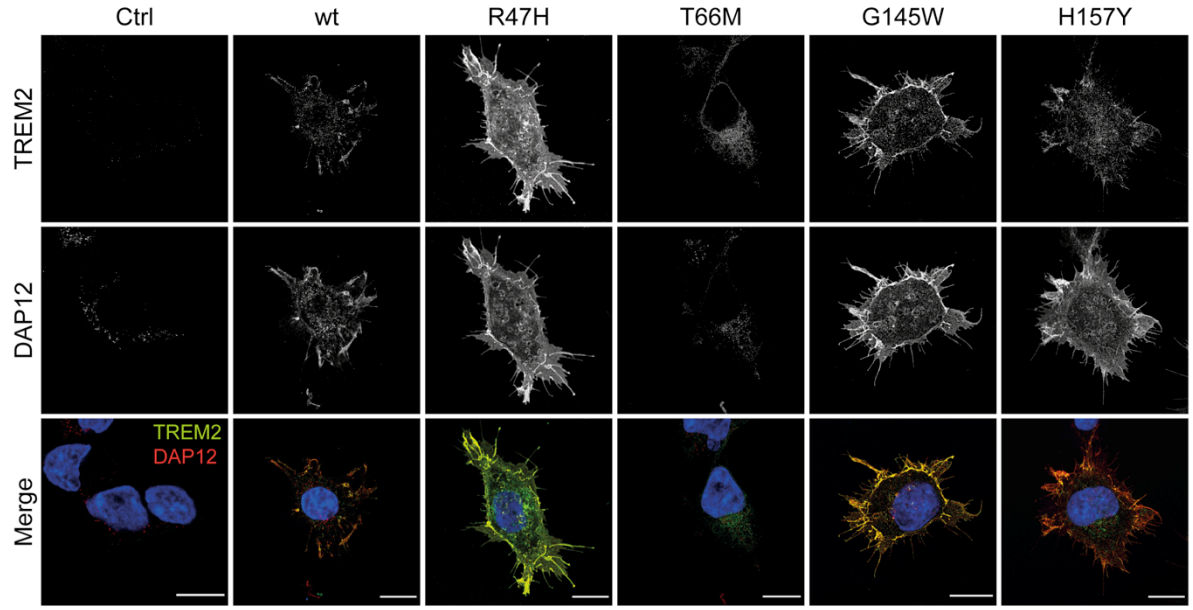

Figure 11: Immunocytochemical detection of TREM2 common and rare variants. Representative images of TREM2-DAP12 expressing cells for different variants of TREM2 are shown. TREM2 is shown in green and DAP12 in red. TREM2 was labeled with the 4B2A3 anti-TREM2 antibody and images are depicted with the same intensities for TREM2 and DAP12 in all variants. Nuclei were counterstained with DAPI. Scale bar = 10 µm.

Furthermore, biotinylation of surface proteins and staining of TREM2 in non-permeabilized cells was performed to investigate the surface expression of the protein variants (Figure 12). Levels of surface TREM2 analyzed over the amount of immature TREM2 from previous experiments (Figure 10) revealed that all variants had a significantly lower expression of TREM2 at the surface compared to the common variant (Figure 12B, surface TREM2/ immature TREM2). However, absolute values of surface TREM2 revealed similar levels of TREM2 R47H or even increased levels over the common variant (Figure 12B, surface TREM2, detected with 17C9 and AF1828, respectively). Hence, elevated expression levels of TREM2 R47H result in an increased amount of surface TREM2 compared to the common variant, even though ratios of surface TREM2 over immature TREM2 were decreased. A reason for the enhanced expression levels of TREM2 R47H could be a higher stability or aberrant transport of the R47H variant compared to the common variant. Levels of DAP12 in TREM2 R47H expressing cells were also increased.

In previous experiments (Figure 10), lack of TREM2 T66M at the cell surface was assumed due to the aberrant transport of the protein to the cell surface, confirmed by the lack of TREM2 CTFs and sTREM2 in membrane fractions and cellular supernatants, respectively. Biotinylation and cell surface staining could further confirm this result, as strongly decreased expression at the cell surface was observed (Figure 12A and D). The same could be observed for DAP12 levels, as those were strongly decreased in biotinylated membrane fractions of TREM2 T66M expressing cells as well. In all variants, biotin-labeled DAP12 predominantly presented as a band of ~23 kDa, possibly representing SDS-resistant DAP12 dimers.

Levels of mature TREM2 G145W were differently detected with anti-TREM2 17C9 and AF1828 antibodies. AF1828 mainly detects an epitope including amino acid 145, indicating that the G→W substitution could affect AF1828 binding. Even though the amount of TREM2 at the cell surface of TREM2 H157Y expressing cells was decreased, sTREM2 levels in conditioned media were not increased, but rather decreased compared to that of the TREM2 common variant (Figure 10).

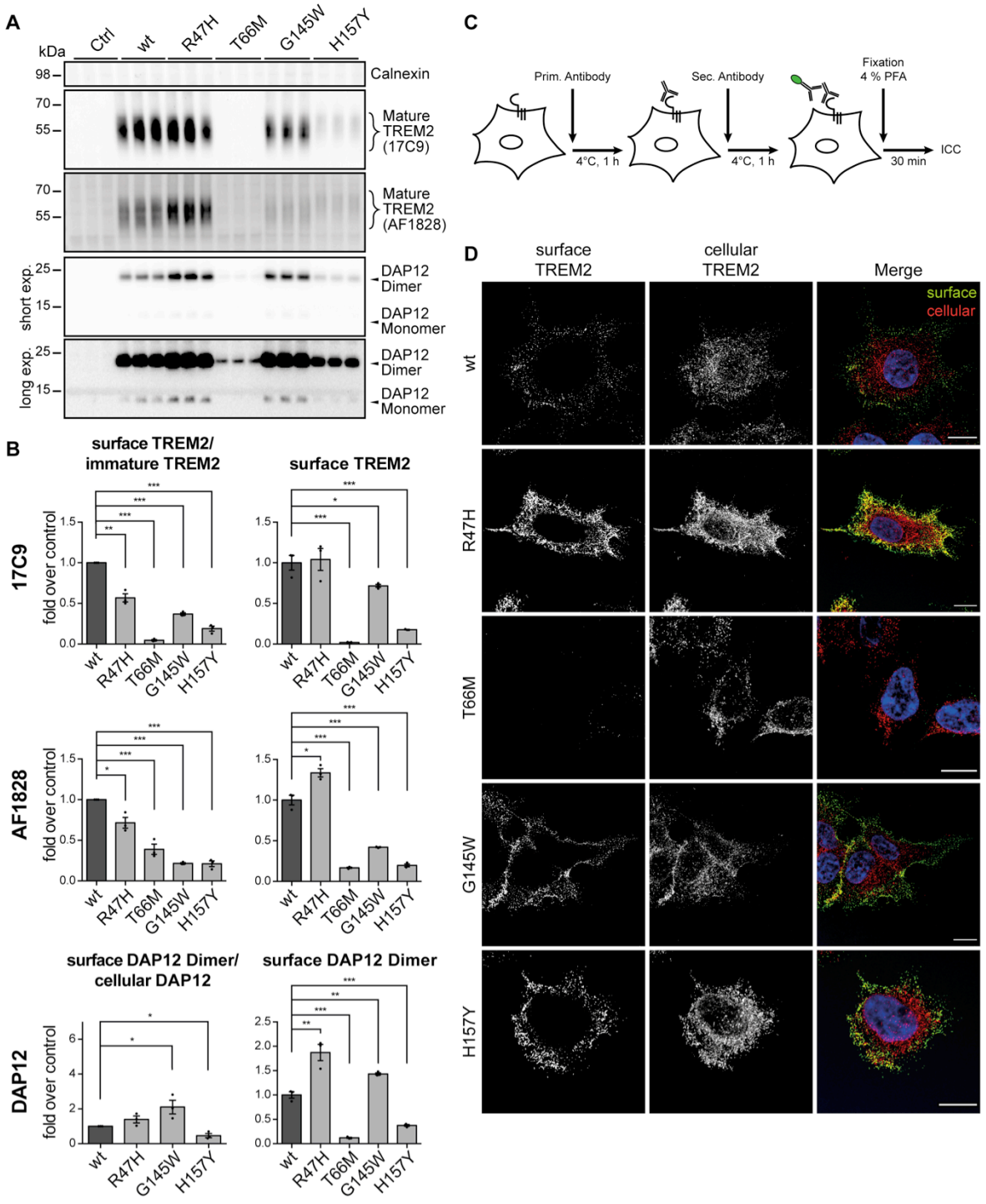

Figure 12: Cell surface expression of TREM2 common and rare variants. (A) Western immunoblotting of biotinylated cell surface proteins using Sulfo-NHS-biotin and Streptavidin-sepharose precipitation. Mature TREM2 was detected with 17C9 and AF1828 antibodies. DAP12 was detected using anti-DAP12 antibody. Calnexin served as a negative control for plasma membrane specific fractions. (B) Quantification of western immunoblotting as shown in A. Data represent the mean ± SEM of three independent experiments with triplicates each (n=3). Student's t-test (unpaired, two-tailed), *p<0.05; **p<0.01; ***p<0.001. (C) Schematic illustration of cell surface immunocytochemistry. Living cells were incubated with primary antibodies. Secondary antibody incubation was followed by fixation with 4 % PFA. Subsequently, cells were analyzed by immunocytochemistry. (D) Representative images of

TREM2-DAP12 expressing cells for different variants of TREM2 are shown. Surface TREM2 was stained using 4B2A3 antibody (green). Cellular TREM2 was stained using AF1828 (red). Nuclei were counterstained with DAPI (blue). Scale bar = 10 µm.

Using an additional method to determine the surface expression of TREM2 common and rare variants in the HEK 293 reporter cell system, we have subjected the cells to flow cytometry analysis (Figure 13). This technique gives information about the mean fluorescence intensity for each sample, as well as the relative cell count that was positive for surface TREM2 (Figure 13B left and right, respectively).

Remarkably, the relative cell count obtained in flow cytometry analysis revealed that most cells are expressing TREM2 at the cell surface with 82.7 % (TREM2 wt), 93.8 % (R47H), 89.4 % (G145W) and 71.9 % (H157Y). For TREM2 wt and H157Y two peaks could be detected, indicating that, even though monoclonal cell lines were used, distinct fractions of cells expressing higher and lower levels of these TREM2 variants were identified (Figure 13A). In contrast, TREM2 R47H and G145W expressing cells have a minor population with lower expression and the majority of cells with higher expression of TREM2 and thus probably more TREM2 protein at the cellular surface of a single cell. It is interesting to note that even TREM2 T66M showed surface expression of TREM2 in 10.9 % of all cells. However, as there is barely a fluorescence signal detectable, the amount of cell surface TREM2 is supposedly very low in each positive cell. Interestingly, the fluorescence intensity for the TREM2 variants showed a higher expression of TREM2 G145W compared to the biotinylation (Figure 12).

Taken together, this reporter cell system revealed differential effects of distinct TREM2 variants on proteolytic processing, thereby partially confirming and extending previous results (Kober et al., 2016; Schlepckow et al., 2017; Thornton et al., 2017). Particularly, all variants, except the T66M, were detected at plasma membrane, albeit at different amounts. All tested variants, including the recently identified TREM2 G145W variant showed a lower expression at the cell surface over the amount of immature TREM2, analyzed by western immunoblotting of biotinylated cell surface proteins and the amount of TREM2 in isolated membrane fractions. However, most cells for TREM2 common and rare variants R47H, G145W and H157Y were positive for TREM2 at the cellular surface, as assessed by flow cytometry analysis.

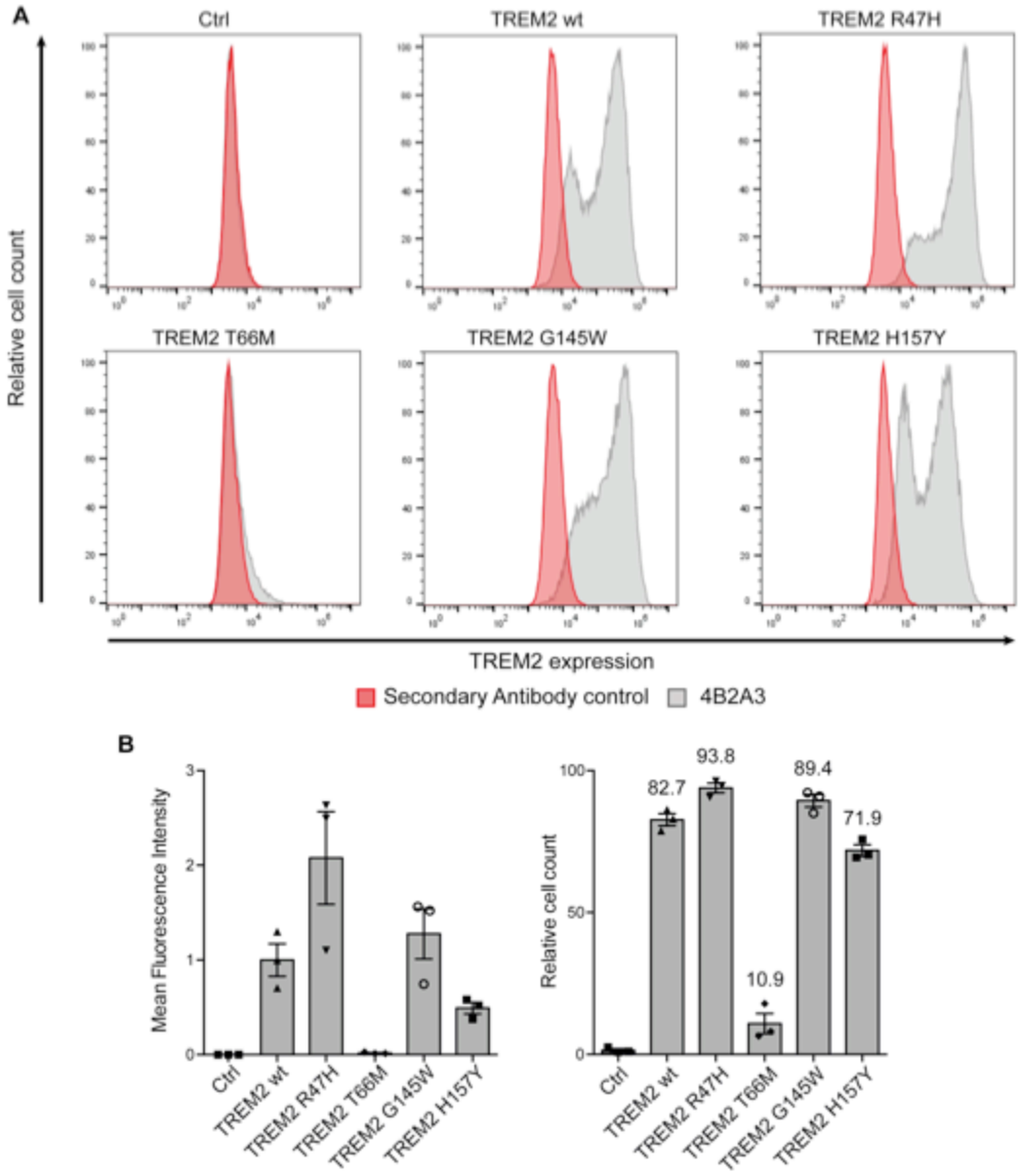

Figure 13: Surface expression of TREM2 common and disease-associated variants assessed by flow cytometry. (A) Relative cell count of TREM2 expressing cells detected by anti-TREM2 4B2A3 antibody. Representative flow cytometry histogram plot shown for Control cells, TREM2 wt, R47H, T66M, G145W and H157Y expressing cells. (B) Quantification of flow cytometry as shown in A. The mean fluorescence intensity was determined and normalized to TREM2 wt expressing cells. Relative numbers of cells with TREM2 expression at the cell surface were depicted as percentage of positive cells. Data represent the mean ± SD of three independent experiments (n=3).

3.4 TREM2 variant H157Y is differentially glycosylated

In previous experiments, it could be observed that sTREM2 of TREM2 H157Y had a slightly different migration in western immunoblotting of TCA precipitated cell culture supernatants compared to the common TREM2 variant (Figure 10). The higher apparent molecular mass could suggest a more complex glycosylation of the protein. TREM2 is glycosylated at two amino acids within the ectodomain, Asn 20 (N20) and Asn 79 (N79) (Kober et al., 2016; Sudom et al., 2018). For investigation of the TREM2 glycosylation, different glycosidases were used (Figure 14A). PNGase F cleaves glycoproteins right at the N residue and thus removes the entire N-linked glycan, whereas Endo D and Endo H specifically hydrolyze high-mannose and/or hybrid structures (Freeze & Kranz, 2010; Plummer et al., 1984; Tarentino et al., 1989). Proteins with high-mannose and hybrid residues are located in the ER and early Golgi compartments, as they further mature in the *medial*- and *trans*-Golgi. Both, wt and H157Y sTREM2 were resistant to Endo D and Endo H hydrolysis, suggesting a proper maturation of both proteins followed by translocation and secretion into the supernatants of TREM2 expressing cells (Figure 14B). Incubation with PNGase F generates a ~17 kDa band, representing deglycosylated sTREM2. Notably, the deglycosylated TREM2 H157Y shows an oppositional shift compared to the glycosylated form of this variant, as is migrates faster than the common variant. Endo F2 and Endo F3 both hydrolyze complex glycan types. Whereas Endo F2 mainly hydrolyses biantennary glycans, Endo F3 has a higher affinity for triantennary glycans but also shows hydrolysis of biantennary glycan substituted with a core fucose (Tarentino & Plummer, 1994). Upon incubation of precipitated supernatants with both enzymes, a band representing deglycosylated sTREM2 could be detected. For Endo F3, a stronger band was detected for TREM2 wt compared to H157Y samples. Additionally, both variants still showed a smear representing glycosylated sTREM2. Neuraminidase, catalyzing the hydrolysis of neuraminic acid residues, did not show an effect on the glycosylated sTREM2 of the common and H157Y variant. Furthermore, O-linked glycosylation was investigated. In TREM2, O-linked glycosylation has not been observed (Sirkis et al., 2017), which could be confirmed using O-glycosidase incubation of precipitated supernatants from TREM2 common and H157Y variants (Figure 14C). For both samples, no difference could be observed compared to the control conditions.

These results suggest that sTREM2 is mainly glycosylated with complex glycans. Interestingly, the TREM2 H157Y variant shows a higher migration of glycosylated sTREM2 and decreased deglycosylation with Endo F3 suggests less triantennary glycans compared to the common variant. Therefore, we assume that TREM2 is mainly glycosylated by complex tetraantennary glycans and TREM2 H157Y has supposedly even more complex glycostructures.

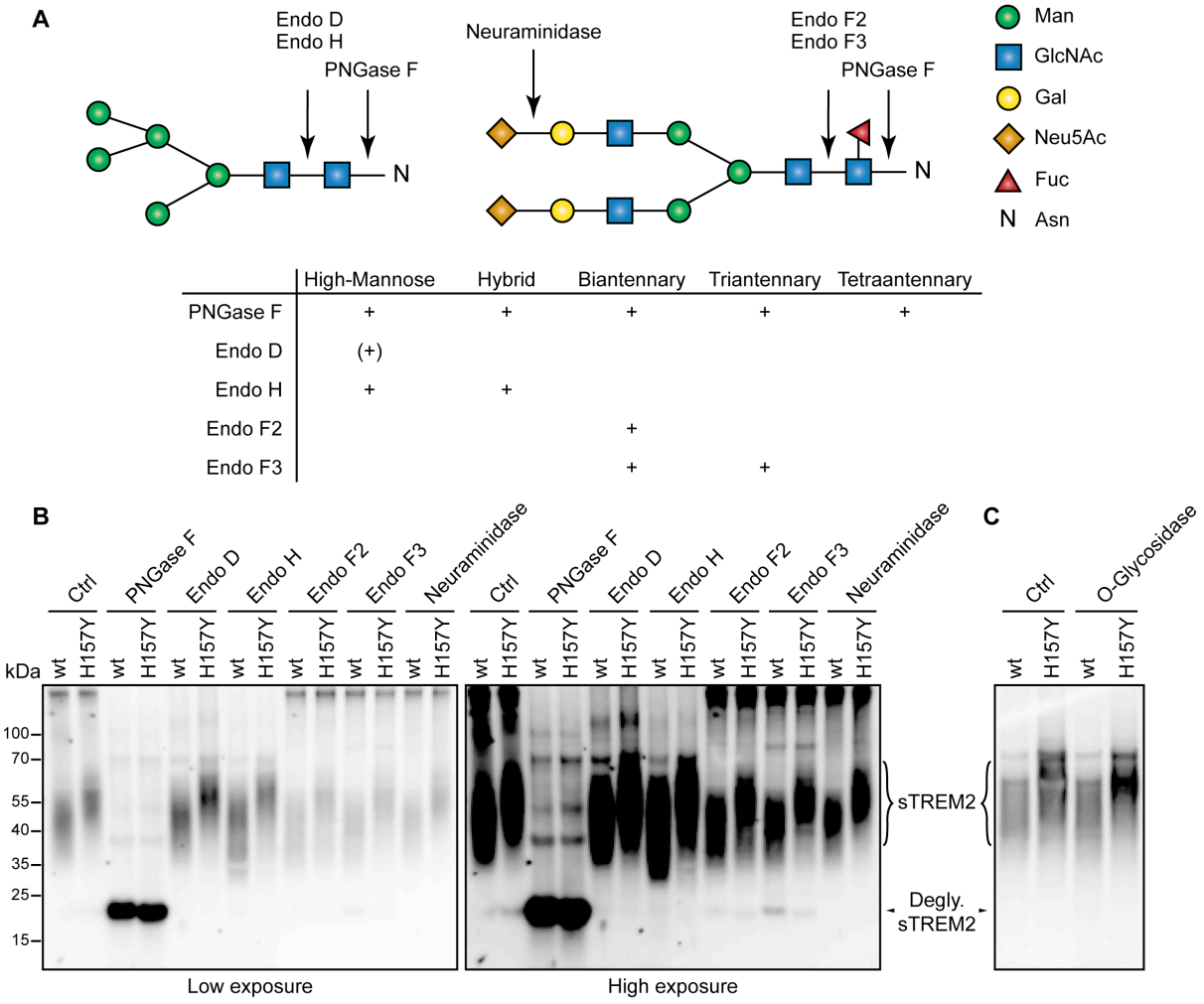

Figure 14: Deglycosylation of TREM2 common and H157Y variant. (A) Illustration of PNGase F and endoglycosidase cleavage sites in N-linked glycans. PNGase F cleaves the entire glycostructure between Asn and GlcNAc of high-mannose, hybrid and complex (bi-, tri- and tetraantennary) glycans. Endoglycosidases (D, H, F2, F3) hydrolyze the bond between the first two GlcNAc, leaving one GlcNAc bound to the protein. Endo D recognizes one specific high-mannose structure. Endo H has a specificity to high-mannose and hybrid structures. Endo F2 specifically cleaves only biantennary, whereas Endo F3 additionally recognizes triantennary structures. Neuraminidase releases Neu5Ac from complex glycans. (B-C) Deglycosylation of TCA precipitated cell culture supernatants from TREM2 wt and H157Y expressing cells. Precipitated proteins were incubated with respective enzymes for 1 h at RT in appropriate buffers. Samples were analyzed by western immunoblotting and

sTREM2 was detected with anti-TREM2 AF1828. Representative blots for 3 independently performed experiments are shown.

3.5 Subcellular localization of TREM2 variants

The expression levels of TREM2 common and rare variants were characterized in previous experiments in this study. It has been reported that some disease-associated mutations alter the intracellular trafficking and thus the localization of TREM2 (Kleinberger et al., 2014; Park et al., 2015; Y. Zhao et al., 2017). We showed that all variants except for T66M localized to the plasma membrane (Figure 12 and 13). To further investigate the intracellular localization of TREM2, a sucrose density gradient was performed (Figure 15). Immature TREM2 mainly localized to the high-density fractions (8-10) for all variants. In these fractions, Calnexin, 58K and Rab7 were mainly localized, defining the ER, Golgi compartments and endosomal or lysosomal fractions. Lamp2, a marker for lysosomes, also localizes to fractions 7-9. The same localization could be seen for DAP12 monomers and dimers that are mainly present in fractions 9-10 with minor presence in middle fractions as well (6-8). Here, TREM2 CTFs can also be detected, suggesting a colocalization of TREM2 CTFs and DAP12.

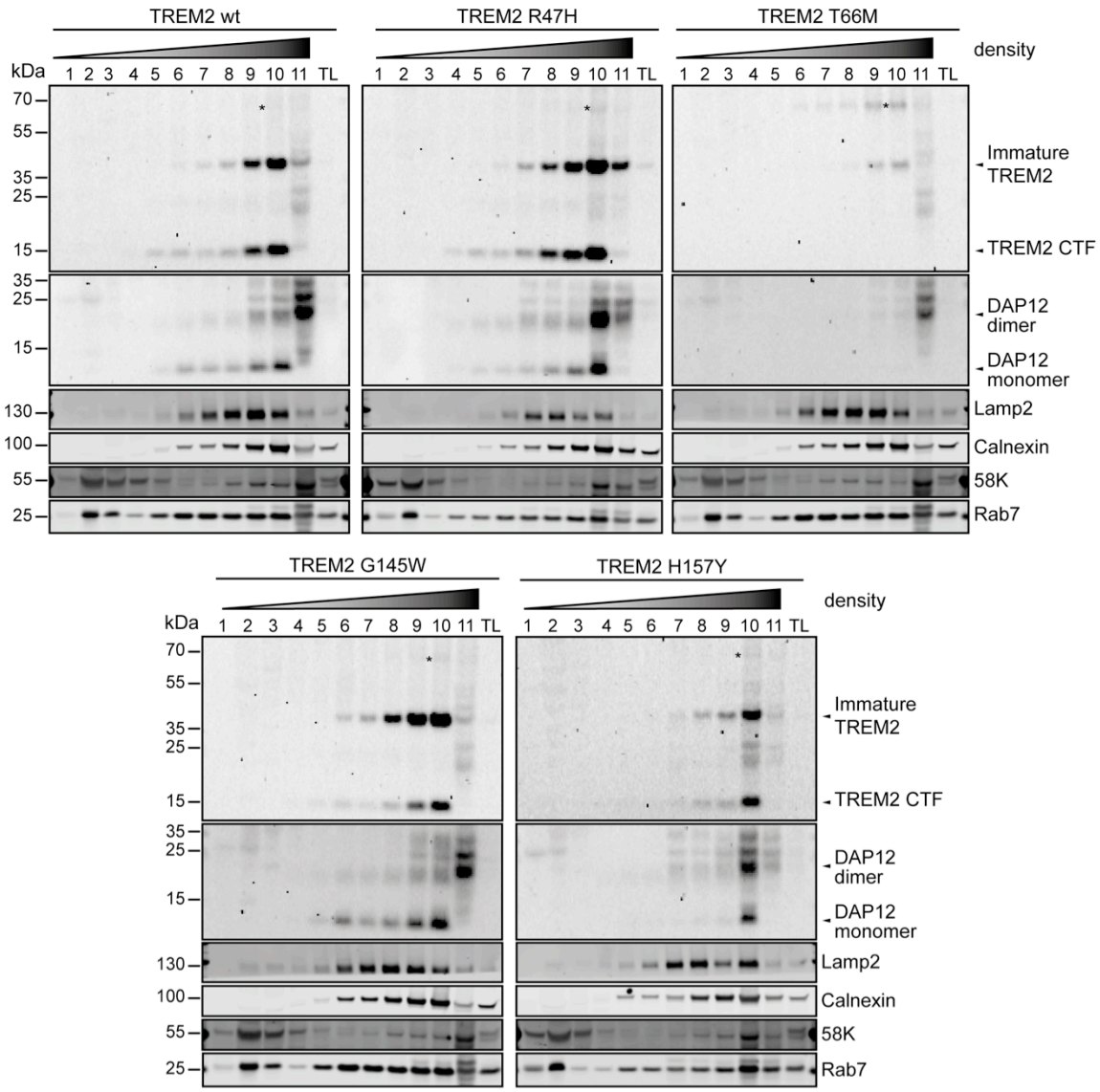

Figure 15: Subcellular distribution of TREM2 and DAP12 by density gradient centrifugation. Post-nuclear supernatants of cell lines stably expressing TREM2 wt, R47H, T66M, G145W and H157Y were subjected to density gradient centrifugation to separate intracellular vesicles and organelles. 11 fractions were collected and proteins were precipitated using TCA and analyzed by western immunoblotting. Specific marker proteins were used to determine lysosomal (Lamp2), ER (Calnexin), Golgi (58K) and late endosomal/lysosomal (Rab7) fractions. Anti-TREM2 9D11 and anti-DAP12 antibodies were used for detection of TREM2 and DAP12, respectively. TL = total load. * Shows accumulation of TREM2.

Besides the different expression levels of TREM2 variants, a similar co-fractionation in density gradients of TREM2 and DAP12 with organelle markers could be seen for all variants. For further validation of TREM2 localization, immunocytochemistry analysis was performed (Figures 16-18). Co-staining with the ER marker Calnexin revealed that all variants partly localize to the ER (Figure 16, white arrows). Whereas

all TREM2 variants additionally localized to *trans*-Golgi compartments (Figure 17), TREM2 T66M mainly co-localized with Calnexin, further supporting efficient retention of this variant in the ER. In addition, TREM2 T66M is more reticular and spread throughout the cytosol compared to the other variants.

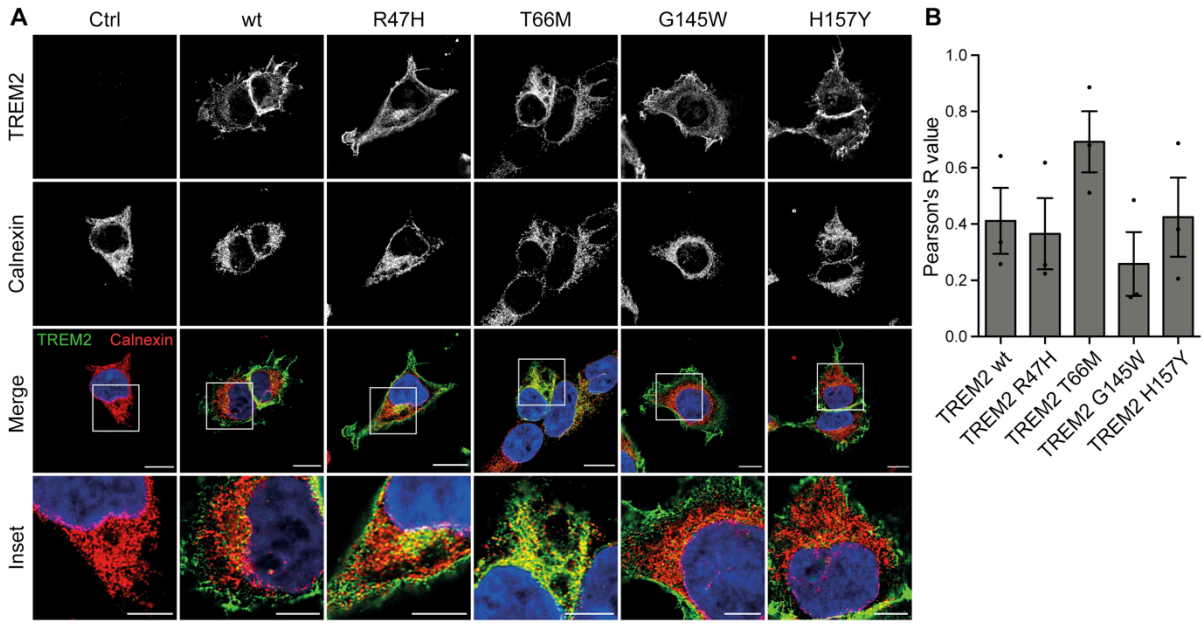

Figure 16: Colocalization of TREM2 common and rare variants with ER. (A) Representative images of TREM2-DAP12 expressing cells for different variants of TREM2 are shown. TREM2 was stained using 4B2A3 antibody (green). ER was stained using anti-Calnexin (red). Nuclei were stained with DAPI (blue). Scale bar = 10 µm; Inset scale bar = 5 µm. (B) Pearson's R value calculation of colocalization for TREM2 and Calnexin as shown in A. Data represent the mean ± SEM of images obtained in two independently performed experiments (n=2). Student's t-test (unpaired, two-tailed).

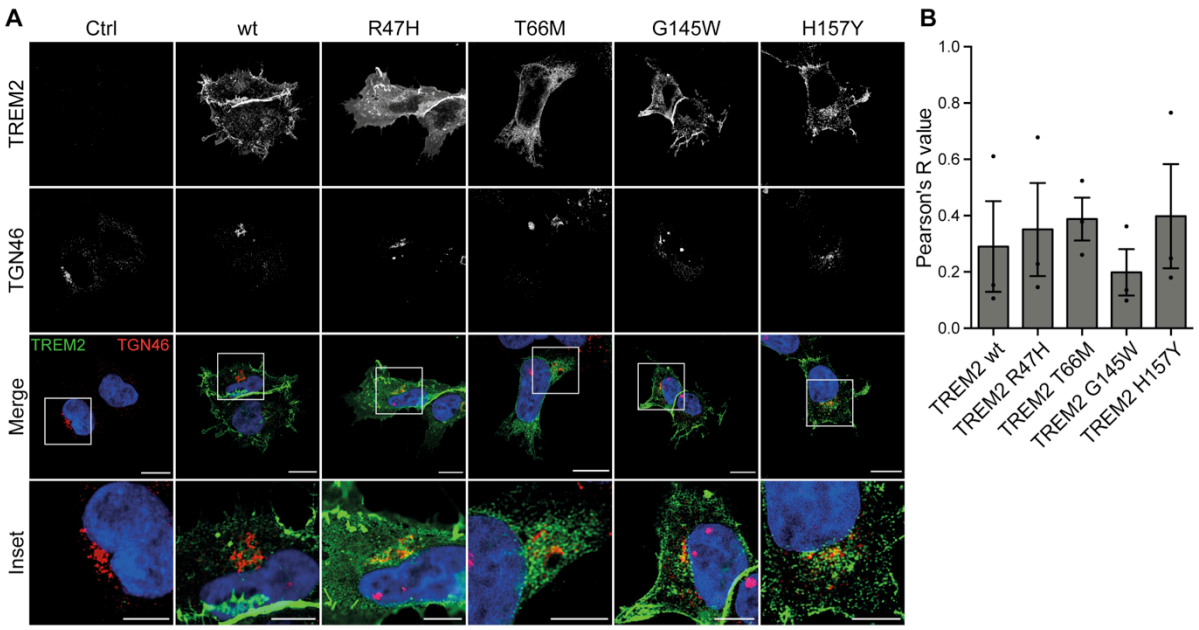

Figure 17: Colocalization of TREM2 common and rare variants with Golgi compartments. (A) Representative images of TREM2-DAP12 expressing cells for different variants of TREM2 are shown. TREM2 was stained using 4B2A3 antibody (green). Cis-Golgi and trans-Golgi were stained using anti-Giantin (A) and anti-TGN46 (B), respectively. Nuclei were counterstained with DAPI (blue). Scale bar = 10 µm; Inset scale bar = 5 µm. (B) Pearson's R value calculation of colocalization for TREM2 and TGN46 as shown in A. Data represent the mean ± SEM of images obtained in two independently performed experiments (n=2). Student's t-test (unpaired, two-tailed).

Staining for EEA-1 and TREM2 revealed a costaining of most variants with early endosomes (Figure 18, white arrows). TREM2 variant T66M only showed minor localization to endosomes, whereas all other variants had many colocalizing puncta, especially in close proximity to the plasma membrane. Little if any TREM2 T66M is present at the plasma membrane or in early endosomes, further confirming ER retention of this variant (Kleinberger et al., 2017; Park et al., 2015).

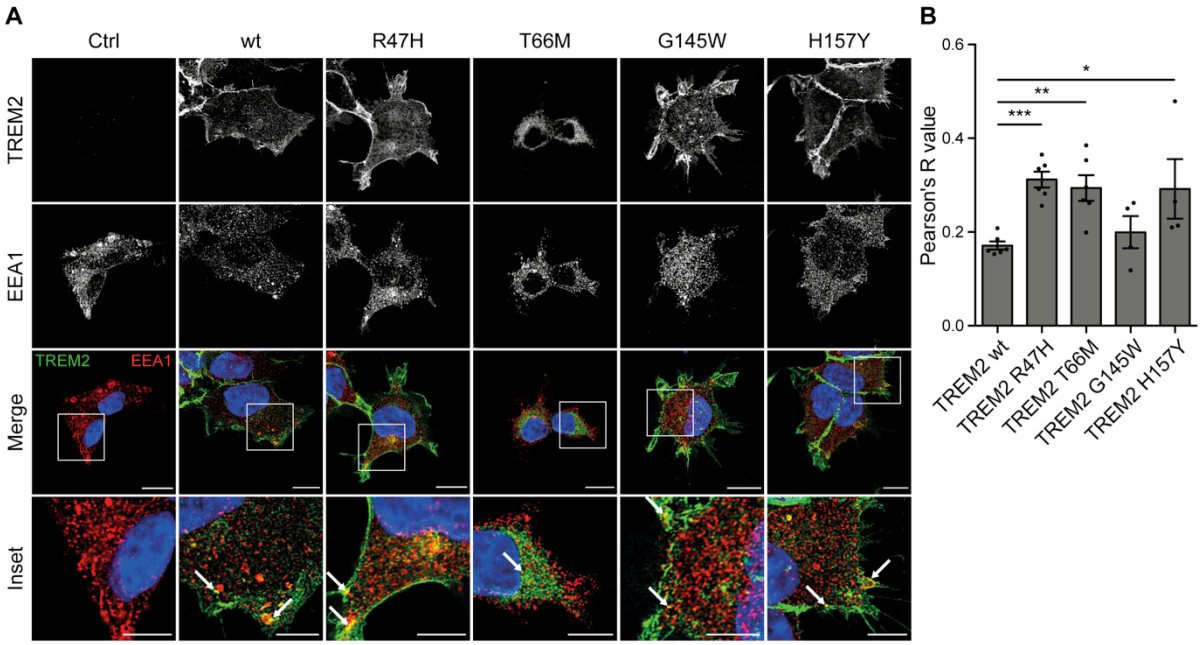

Figure 18: Colocalization of TREM2 common and rare variants with early endosomal compartments. (A) Representative images of TREM2-DAP12 expressing cells for different variants of TREM2 are shown. TREM2 was stained using 4B2A3 antibody (green). Early endosomes were stained using anti-EEA1 (red). Nuclei were counterstained with DAPI (blue). Scale bar = 10 µm; Inset scale bar = 5 µm. Arrows mark TREM2 positive early endosomes. (B) Pearson's R value calculation of colocalization for TREM2 and EEA1 as shown in A. Data represent the mean ± SEM of images obtained in two independently performed experiments (n=2). Student's t-test (unpaired, two-tailed), *p<0.05; **p<0.01; ***p<0.001.

Taken together, the intracellular localization of TREM2 common and variants R47H and T66M highly correlates to previous publications (Kleinberger et al., 2014; Park et al., 2015; Y. Zhao et al., 2017). The TREM2 variants G145W and H157Y showed a similar distribution compared to the wt protein. Thus, both amino acid substitutions do not appear to have strong effects on subcellular localization. Moreover, TREM2 is internalized via endocytosis, confirmed by colocalization of all variants, except for TREM2 T66M, with early endosome markers.

3.6 TREM2 is mainly degraded by the autophagy-lysosomal pathway

Proteolytic degradation is an important mechanism for regulation of cellular functions. Turnover of proteins provides new amino acids to obtain protein homeostasis and prevents abnormal protein accumulation. Degradation pathways are controlled by complex regulatory mechanisms to adopt protein levels to the respective metabolic state of a cell and to maintain cellular functions (Lecker et al., 2006). The ubiquitin-proteasome system (UPS) and the autophagy-lysosomal pathway are two major pathways for proteolytic degradation. The UPS degrades most short-lived proteins and soluble misfolded proteins. However, entire organelles and aggregates are more likely to be fragmented by the autophagy-lysosomal pathway (Kraft et al., 2009).

As only little is known about degradation pathways of TREM2, common and rare variant expressing cell lines were analyzed by immunocytochemistry. TREM2 cell lines were stained for autophagosomal and proteasomal markers LC3 and PSMB5, respectively. Under basal conditions, LC3 I is located in the cytosol and upon conjugation with PE, LC3 II is formed, which localizes to autophagosomal membranes and serves as a specific marker for autophagy and autophagy-related processes (Sarkar, 2013). Immunocytochemistry showed few TREM2 positive LC3 puncta (Figure 19A). In contrast, staining of PSMB5, a subunit of the proteasome 20S subunit (Coux et al., 1996), showed enhanced colocalization with TREM2 R47H and T66M (Figure 19C and D).

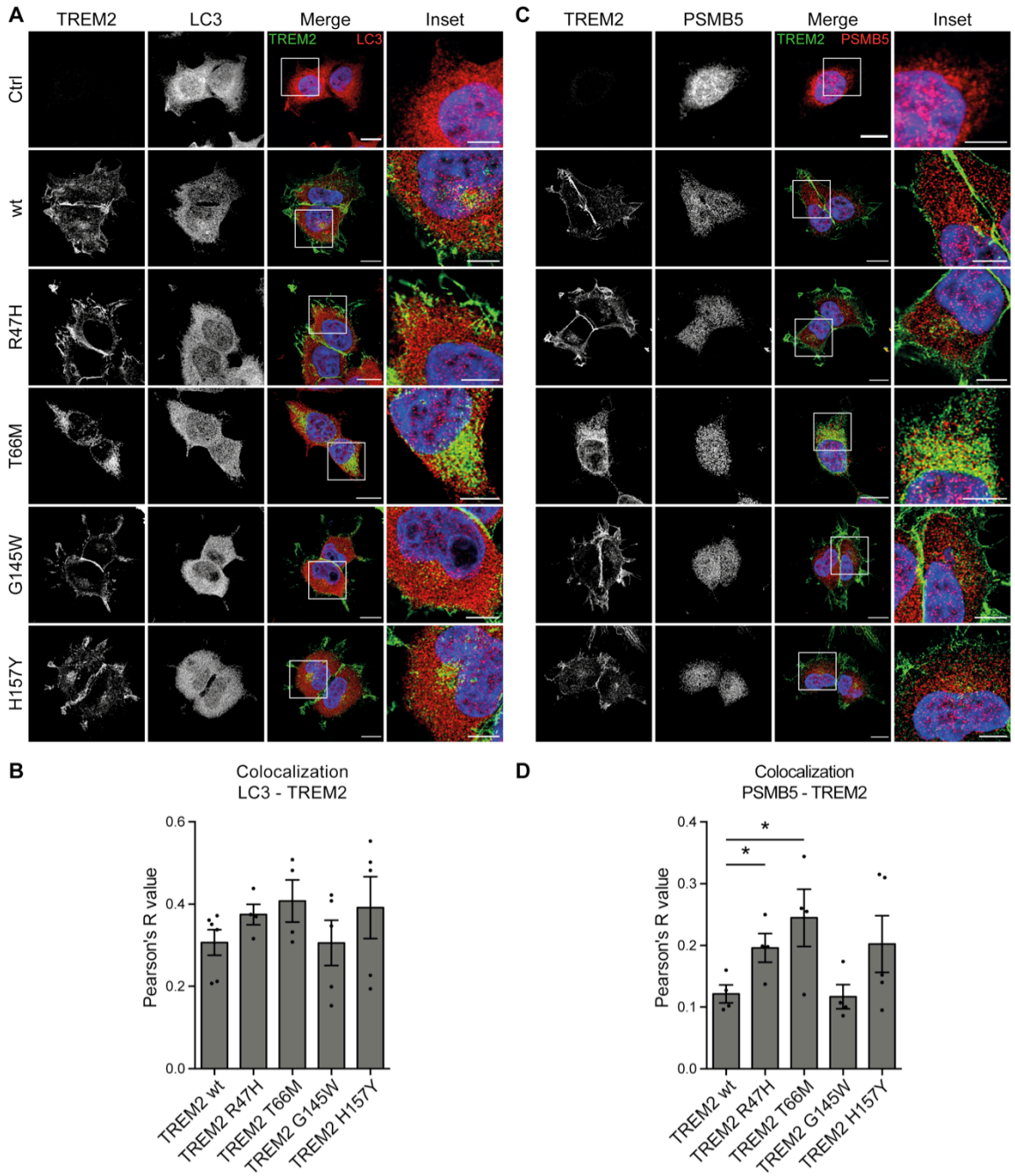

Figure 19: Localization of TREM2 common and rare variants to autophagosomes and proteasomes. (A, C) Representative images of TREM2-DAP12 expressing cells for different variants of TREM2 are shown. TREM2 was stained using 4B2A3 antibody (green). Autophagic vesicles were stained with LC3 (A, red). Proteasome was stained with anti-PSMB5 (C, red). Nuclei were counterstained with DAPI (blue). Scale bar = 10 µm; Inset scale bar = 5 µm. (B, D) Pearson's R value calculation of colocalization for TREM2 and LC3 (B) and PSMB5 (D) as shown in A and C, respectively. Data represent the mean ± SEM of images obtained in two independently performed experiments (n=2). Student's t-test (unpaired, two-tailed), *p<0.05.

However, as these experiments were performed in steady state conditions, further analysis was done with inhibitors of both degradation pathways. Therefore, cells were treated with either Chloroquine or MG132 for inhibition of the autophagy-lysosomal pathway or the proteasome system, respectively. MG132 inhibits the proteolytic activity of the 26S proteasome by covalent binding to the 20S subunit (D. H. Lee & Goldberg, 1998) and can also inhibit calpains (Tsubuki et al., 1996). Chloroquine accumulates in lysosomes, changes the lysosomal pH and inhibits enzymes needed for degradation of proteins in the autophagy-lysosomal pathway but also impairs autophagosome-lysosome fusion (Mauthe et al., 2018; Pasquier, 2016). TREM2-DAP12 expressing cells were treated with Chloroquine for 4 h and subsequently, membrane fractions were analyzed by western immunoblotting (Figure 20A). TREM2 full-length, CTFs and DAP12 were detected in membrane fractions. APP and APP CTFs were also analyzed, as mature APP and APP CTFs are known to be degraded by the autophagy-lysosomal pathway (Jaeger et al., 2010). Treatment with Chloroquine significantly increased levels of immature TREM2 for all variants (Figure 20B). In comparison to the common TREM2 variant that accumulated ~3 fold, this effect was attenuated by variants T66M and G145W that accumulated less than 1.5 fold. TREM2 CTF and DAP12 levels were also increased about 1.5 – 2 fold upon Chloroquine treatment in cell lines expressing TREM2 wt, R47H, G145W and H157Y. For TREM2 variant T66M, both TREM2 CTFs and DAP12 could be barely detected, which is why they were not further quantified.

To further test the effect of Chloroquine on TREM2 degradation, immunocytochemistry was performed. Cells were fixed and stained for TREM2 and LC3 or PSMB5 (Figure 21A and C, respectively). Staining with LC3 shows LC3-positive large puncta likely representing autophagosomes and autophagolysosomes. Due to inhibition of lysosomal enzymes by Chloroquine, those vesicles are enriched and show colocalization with TREM2 for all TREM2 variants (Figure 21A, white arrows). Interestingly, costaining with PSMB5 showed stronger colocalization with TREM2 T66M compared to the other TREM2 variants (Figure 21C and D).

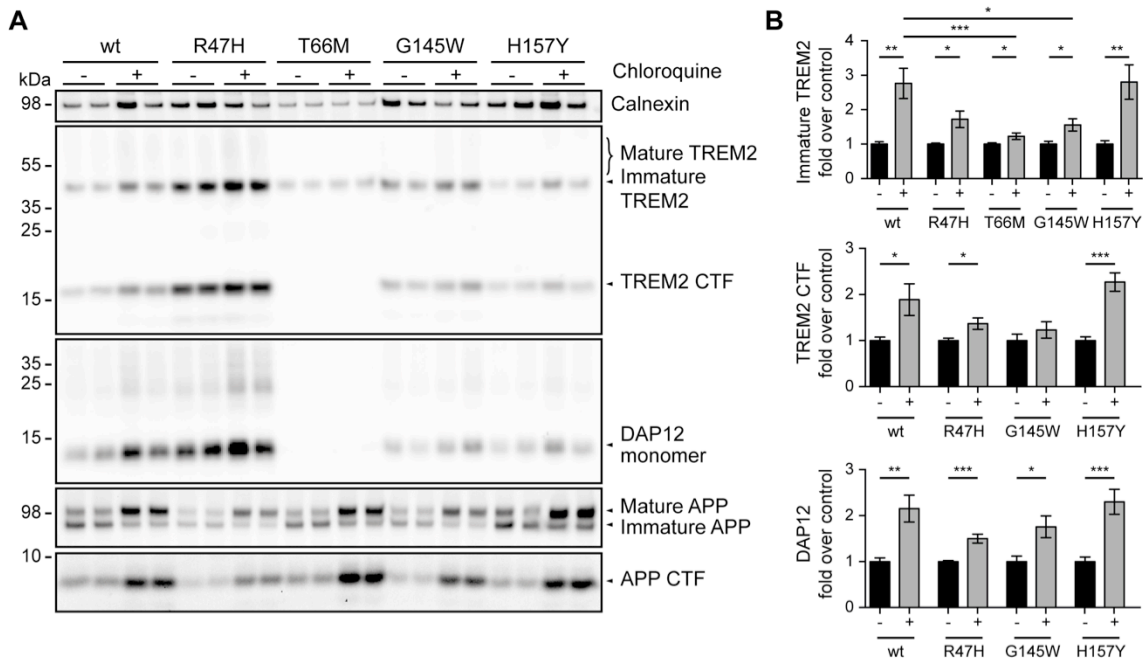

Figure 20: TREM2 expression is increased upon inhibition of autophagolysosomal formation. (A) Cell lines stably expressing TREM2 wt, R47H, T66M, G145W and H157Y were treated with 50 µM Chloroquine for 4 h or left untreated as a control. Membrane fractions were isolated and analyzed by western immunoblotting. Anti-TREM2 9D11 antibody was used for detection of C-terminal TREM2. Anti-DAP12 was used for detection of DAP12. Calnexin served as a control for membrane specific fractions. APP and APP-CTFs were detected using 6E10 antibody. (B) Quantification of western immunoblotting as shown in A. Data represent the mean ± SEM of two independently performed experiments in duplicates or triplicates each (n=2). Student's t-test (unpaired, two-tailed), *p<0.05; **p<0.01; ***p<0.001.

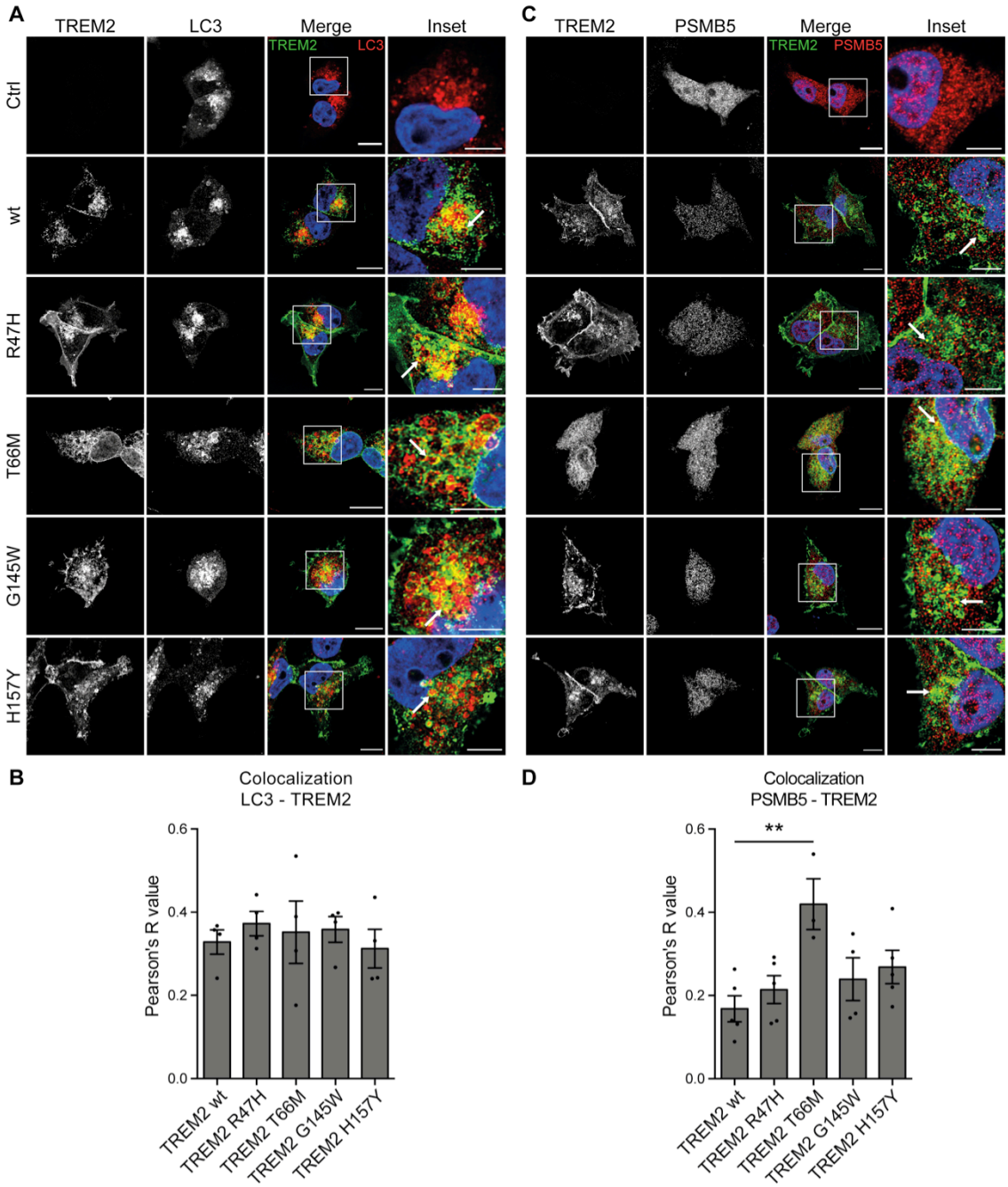

Figure 21: TREM2 localizes to autophagosomes upon inhibition of autophagolysosomal formation. Cell lines stably expressing TREM2 wt, R47H, T66M, G145W and H157Y were treated with 50 µM Chloroquine for 4 h or left untreated as a control. (A, C) Representative images of cells treated with Chloroquine are shown. TREM2 was stained using 4B2A3 antibody (green). Autophagic vesicles were stained with LC3 (A, red). Proteasome was stained with PSMB5 (C, red). Nuclei were counterstained with DAPI (blue). Scale bar = 10 µm; Inset scale bar = 5 µm. Arrows mark TREM2 positive autophagosomes (A) or proteasomes (C). (B, D) Pearson's R value calculation of colocalization for TREM2 and LC3 (B) and PSMB5 (D) as shown in A and C, respectively. Data represent the mean ± SEM of images obtained in two independently performed experiments. Student's t-test (unpaired, two-tailed), **p<0.01.

Furthermore, similar experiments were performed with inhibition of the proteasome by MG132 (Figure 22 and 23). In western immunoblotting of isolated membrane fractions, a significant decrease of TREM2 expression could be observed for all TREM2 variant expressing cell lines. In addition, it has been shown that APP degradation was induced upon inhibition of the proteasome machinery (F. Zhou et al., 2011). Therefore, detection of APP and APP CTFs served as a control in these experiments. In contrast to decreased immature TREM2, levels of TREM2 CTFs and DAP12 show a slight increase, with the only significant difference being detected in TREM2 H157Y expressing cells. (Figure 22B). In immunocytochemistry stainings of MG132 treated cells, TREM2 T66M showed significantly increased colocalization with both, LC3 and PSMB5, as compared to the common TREM2 variant (Figure 23). Both, levels of TREM2 CTFs and DAP12 in western immunoblotting were accumulated up to 1.5 fold upon MG132 treatment (Figure 22). TREM2 H157Y expressing cells showed the strongest accumulation of TREM2 CTF levels that were significantly increased more than 1.5 fold.

Degradation of TREM2 and DAP12 has barely been investigated so far. Here, immunocytochemistry and western immunoblotting of TREM2 common and rare variant expressing cells revealed that immature TREM2 is mainly degraded by the autophagy-lysosomal pathway, whereas TREM2 CTFs and DAP12 are supposedly also degraded by the proteasome machinery.

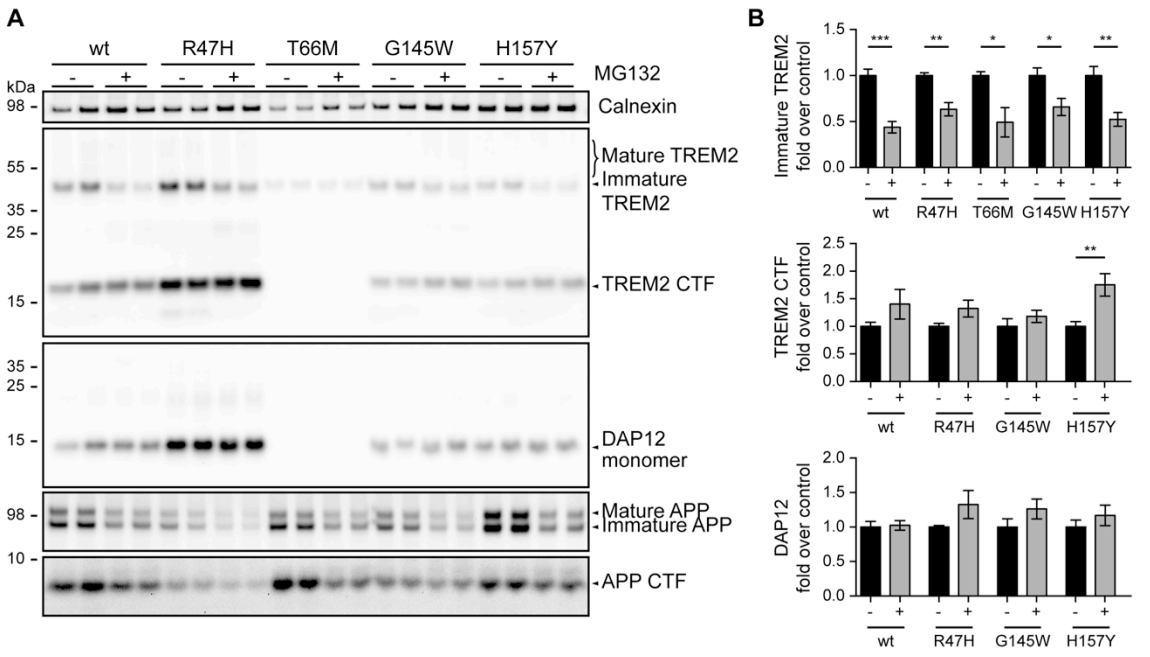

Figure 22: TREM2 expression is decreased upon inhibition of proteasomal proteases. (A) Cell lines stably expressing TREM2 wt, R47H, T66M, G145W and H157Y were treated with 10 µM MG132 for 4 h or left untreated as a control. Membrane fractions were isolated and analyzed by western immunoblotting. Anti-TREM2 9D11 antibody was used for detection of C-terminal TREM2. Anti-DAP12 was used for detection of DAP12. Calnexin served as a control for membrane specific fractions. APP and APP-CTFs were detected using 6E10 antibody. (B) Quantification of western immunoblotting as shown in A. Data represent the mean ± SEM of two independently performed experiments in duplicates or triplicates each (n=2). Student's t-test (unpaired, two-tailed), *p<0.05; **p<0.01; ***p<0.001.

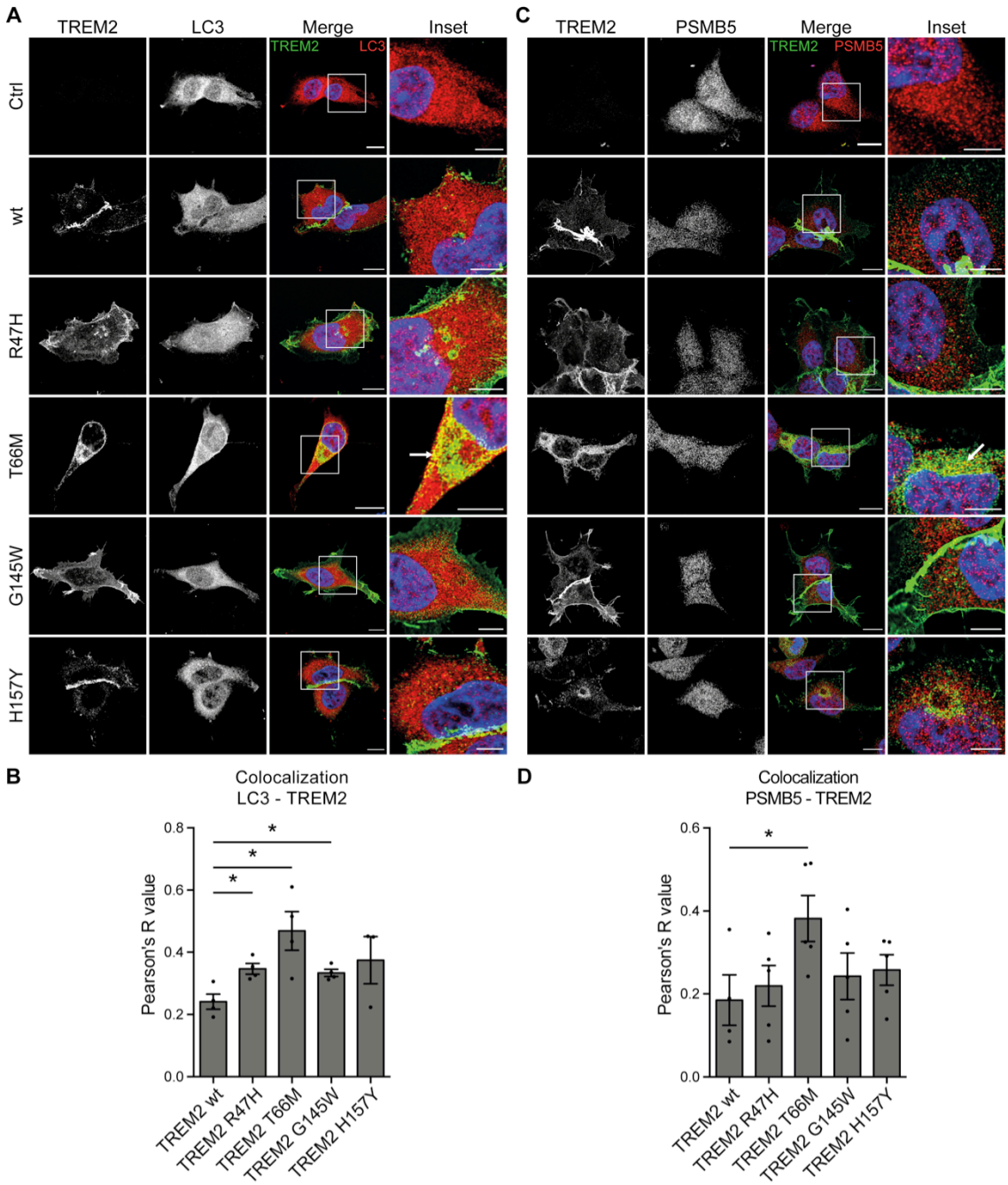

Figure 23: TREM2 does not localize to proteasomes upon inhibition of proteasomal proteases. Cell lines stably expressing TREM2 wt, R47H, T66M, G145W and H157Y were treated with 10 µM MG132 for 4 h or left untreated as a control. (A, C) Representative images of cells treated with MG132 are shown. TREM2 was stained using 4B2A3 antibody (green). Autophagic vesicles were stained with LC3 (A, red). Proteasome was stained with PSMB5 (C, red). Nuclei were counterstained with DAPI (blue). Scale bar = 10 µm; Inset scale bar = 5 µm. Arrows mark TREM2 positive autophagosomes (A) or proteasomes (C). (B, D) Pearson's R value calculation of colocalization for TREM2 and LC3 (B) and PSMB5 (D) as shown in A and C, respectively. Data represent the mean ± SEM of images obtained in two independently performed experiments. Student's t-test (unpaired, two-tailed), *p<0.05.

3.7 Disease-associated TREM2 variants impair the production of reactive oxygen species

Increased oxidative stress has been described in the aging brain and possibly plays an important role in initiation and progression of AD (Kim et al., 2015; Singh et al., 2019; X. Wang et al., 2014), A recent study indicates that TREM2 might regulate genes involved in the oxidative stress response (Linnartz‐Gerlach et al., 2019). To investigate the oxidative stress response in cells expressing different TREM2 variants, the production of reactive oxygen species (ROS) after exposure to necrotic neural debris was analyzed (Figure 24A). Upon treatment of cells with debris alone or in combination with superoxide dismutase 1 (SOD1) or trolox, cells were incubated with dihydroethidium (DHE), which reacts with superoxide radicals and forms a highly fluorescent dye dihydroxyethidium (OH-E+). Incubation of TREM2 wt expressing cells with necrotic neural debris resulted in increased production of ROS (Figure 24B). Here, the addition of SOD1 completely prevented the oxidative stress response induced by debris. Cells expressing the TREM2 H157Y variant also showed an increased oxidative stress response after stimulation with debris. However, addition of SOD1 could not prevent the production of ROS. Interestingly, the other tested TREM2 variants did not evoke an up-regulation of ROS production upon exposure to neural debris, indicating a loss-of-function in detection of cell damage and/or signal transduction.

In summary, a lower oxidative stress of TREM2 mutant cells hints towards a reduced oxidative stress response in most TREM2 variants. The different response in ROS production to simultaneous treatment of debris with SOD1 in TREM2 wt and H157Y expressing cells hints towards the production of a different type of oxygen species upon stimulation of TREM2 H157Y. However, this needs to be further elucidated.

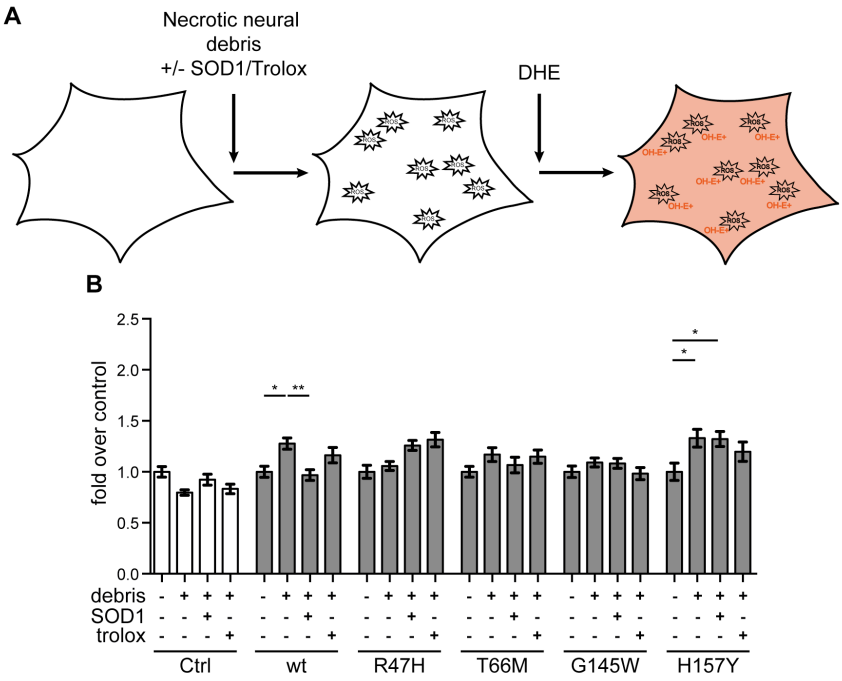

Figure 24: Production of reactive oxygen species in TREM2 expressing cell lines. (A) Schematic illustration of the experiment. Cells were treated with either necrotic neural debris alone or supplemented with superoxide scavengers SOD1 or trolox. ROS were detected by addition of DHE. DHE reacts with ROS and forms OH-E+. Cells were fixed and images were analyzed by confocal microscopy (Assay performed by Bettina Linnartz-Gerlach). (B) Analysis of oxidative stress response in cells expressing myc-TREM2-FLAG_T2A_DAP12 with TREM2 wt, R47H, T66M, G145W and H157Y. Quantitative analysis of relative DHE intensity per cell number. Data represent the mean intensity ± SEM of three independently performed experiments with 5 images each. One-way ANOVA, Tukey's *post hoc* test for multiple comparison, separate for each genotype, *p<0.05; **p<0.01.

3.8 Monoclonal anti-TREM2 antibody 4B2A3 stimulates TREM2 signaling via cross-linking

Just recently, anti-TREM2 antibodies with agonistic activities have been described (Price et al., 2020; Schlepckow et al., 2020; S. Wang et al., 2020). Hence, our approach was to investigate if and how the anti-TREM2 4B2A3 antibody stimulates TREM2 expressing cells. Therefore, Fab, F(ab')$_2$, and Fc fragments of the 4B2A3 antibody were produced using Papain and Pepsin resin, respectively (Figure 25A). Papain cleaves the whole IgG N-terminal from the hinge region, creating two separate Fab fragments and one Fc fragment (Leslie et al., 1971). In contrast, Pepsin digests the Fc part of the antibody and thus produces F(ab')$_2$ fragments that are still connected by two disulfide bonds. Using Protein A resin, Fc fragments and undigested antibodies can be removed from the generated Fab and F(ab')$_2$

fragments of both reactions. To verify the generated fragments, SDS-PAGE was performed under reducing and non-reducing conditions with subsequent analysis by Coomassie staining (Figure 25B (Fab) and C ($F(ab')_2$)). Under non-reducing conditions, the 4B2A3 antibody is detected with an approximate molecular mass of 150 kDa. Reducing the antibody, heavy and light chains are separated with ~50 kDa and ~25 kDa size, respectively. After digestion and Protein A purification, Fab and $F(ab')_2$ are separated from undigested antibody or large Fc fragments. Non-reduced Fab has a molecular mass of ~50 kDa and $F(ab')_2$ of ~110 kDa. Upon elution of Protein A resin, Fc fragments were kept for further experiments (Figure 25B).

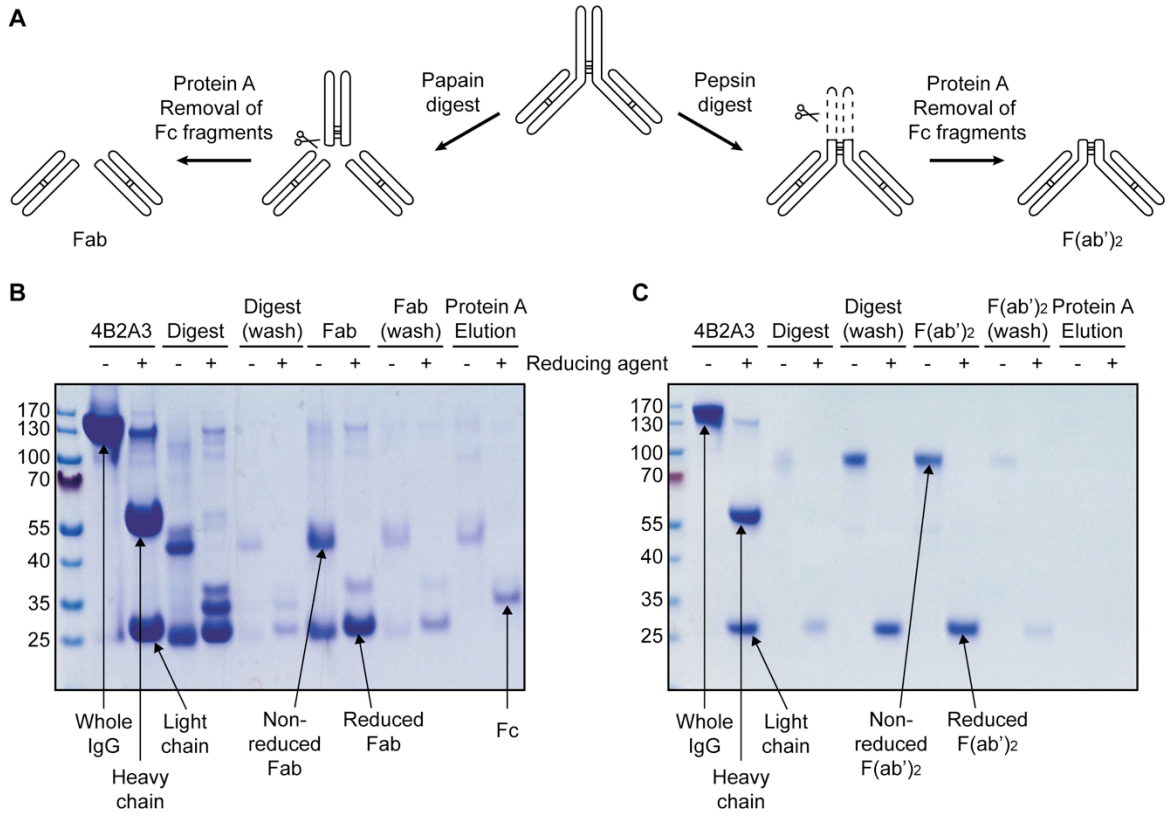

Figure 25: Generation of anti-TREM2 4B2A3 Fab and $F(ab')_2$ fragments. (A) Fab and $F(ab')_2$ fragments were generated by digestion of 4B2A3 antibody with Papain or Pepsin, respectively. Papain cleaves above the hinge region, creating two separate Fab fragments and one Fc fragment. Pepsin digests the Fc and generates one $F(ab')_2$ fragment. In both approaches, Protein A was used to remove undigested 4B2A3 antibodies and Fc fragments. (B, C) Coomassie gel of digested Fab (B) and $F(ab')_2$ (C) fragments. Samples were prepared with and without reducing agent.

For investigation of the stimulating ability of the anti-TREM2 4B2A3 antibody and its separate fragments, an AlphaLISA technology was used (Figure 26A) to detect the phosphorylation of spleen tyrosine kinase (SYK), a kinase directly recruited to the TREM2 co-receptor DAP12. Control cells that were treated with 67 µM of either the whole IgG, F(ab')$_2$, Fab or Fc fragments did not show an increase in pSYK levels in comparison to unstimulated cells, whereas TREM2-DAP12 expressing cells could be stimulated by both, the whole IgG and F(ab')$_2$. Therefore, these data demonstrate that the 4B2A3 antibody has an agonistic activity and stimulates TREM2-DAP12 signaling through receptor cross-linking. Interestingly, F(ab')$_2$ fragments even showed a two-fold increase in pSYK levels compared to the whole IgG.

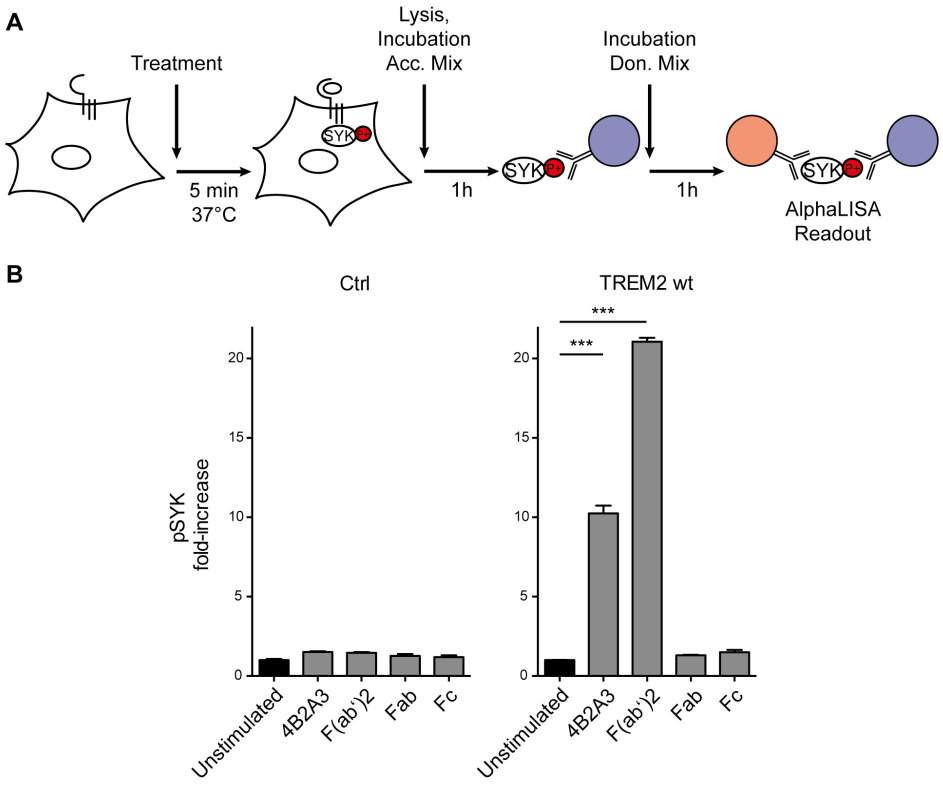

Figure 26: 4B2A3 antibody stimulates TREM2 expressing cells via cross-linking. (A) Schematic illustration of the AlphaLISA experiments. Cells were plated on 96-well plates and treated for 5 min. Cells were lysed and lysates were incubated with acceptor beads (Acc. Mix) and subsequently with donor beads (Don. Mix) for 1 h, respectively. For detection of pSYK levels, samples were measured with a plate reader using standard AlphaLISA settings. (B) TREM2-DAP12 expressing cells as well as empty cells (Ctrl) were treated for 5 min with 67 µM ectodomain-specific antibody or antibody fragments F(ab')$_2$, Fab and Fc against TREM2 (4B2A3) or left untreated as a control (Unstimulated). Cells were lysed and lysates were analyzed for pSYK using AlphaLISA technologies. Data represent the mean ± SD of

one experiment in triplicates. One-way ANOVA, Tukey's post hoc test for multiple comparison, ***p<0.001.

Taken together, anti-TREM2 4B2A3 antibody stimulates TREM2-DAP12 signaling in the HEK 293 Flp-In reporter cell system. Using papain and pepsin digestion, it could be shown that TREM2 stimulation occurs through receptor cross-linking, as single Fab fragments were not able to induce a TREM2-dependent increase in pSYK levels.

3.9 Most disease-associated TREM2 variants are stimulated by the anti-TREM2 antibody 4B2A3

In further experiments, stimulation of SYK phosphorylation by the 4B2A3 anti-TREM2 antibody was compared with TREM2 wt, R47H, T66M, G145W and H157Y expressing cells (Figure 27). Control cells without expression of TREM2 and DAP12 did not respond to the exposure with anti-TREM2-antibody, whereas TREM2 wt expressing cells showed an approximate 11-fold increase in pSYK levels upon stimulation (Figure 27A). The TREM2 T66M variant was not stimulated, consistent with the lack of full-length TREM2 T66M at the cell surface (see Figures 12 and 13). Cells expressing variants R47H, G145W and H157Y showed a reduced phosphorylation of SYK compared to cells expressing the common variant. In western immunoblotting, ratios of pSYK over total SYK showed the same trend as for pSYK levels alone (Figure 27B-H), while the amount of total SYK was unchanged upon stimulation with the anti-TREM2 antibody. Furthermore, pSYK levels from AlphaLISA experiments were normalized to the amount of surface TREM2 from biotinylation and flow cytometry analyses (Figure 27I and J, respectively). For both analyses, similar results could be observed, as TREM2 R47H showed a decreased and TREM2 H157Y an increased stimulation by the 4B2A3 antibody. Varying results were obtained for TREM2 G145W. Here, normalization of pSYK levels over surface TREM2 in flow cytometry was decreased compared to TREM2 wt, whereas quantification with biotinylated surface TREM2 showed the same level of stimulation for TREM2 G145W and TREM2 wt. In addition, pSYK levels were analyzed to the relative cell count obtained in FACS analyses (Figure 27K). Here, all variants showed a partial or total loss-of-function compared to the common TREM2 variant.

In summary, analysis of pSYK levels obtained in AlphaLISA experiments that were normalized to the intensity and the relative cell count expressing TREM2 at the cell

surface show different results. As the amount of TREM2 on each cell might vary, the number of cells responding to the antibody treatment represents a measure for the response of cells expressing TREM2 common and rare variants.

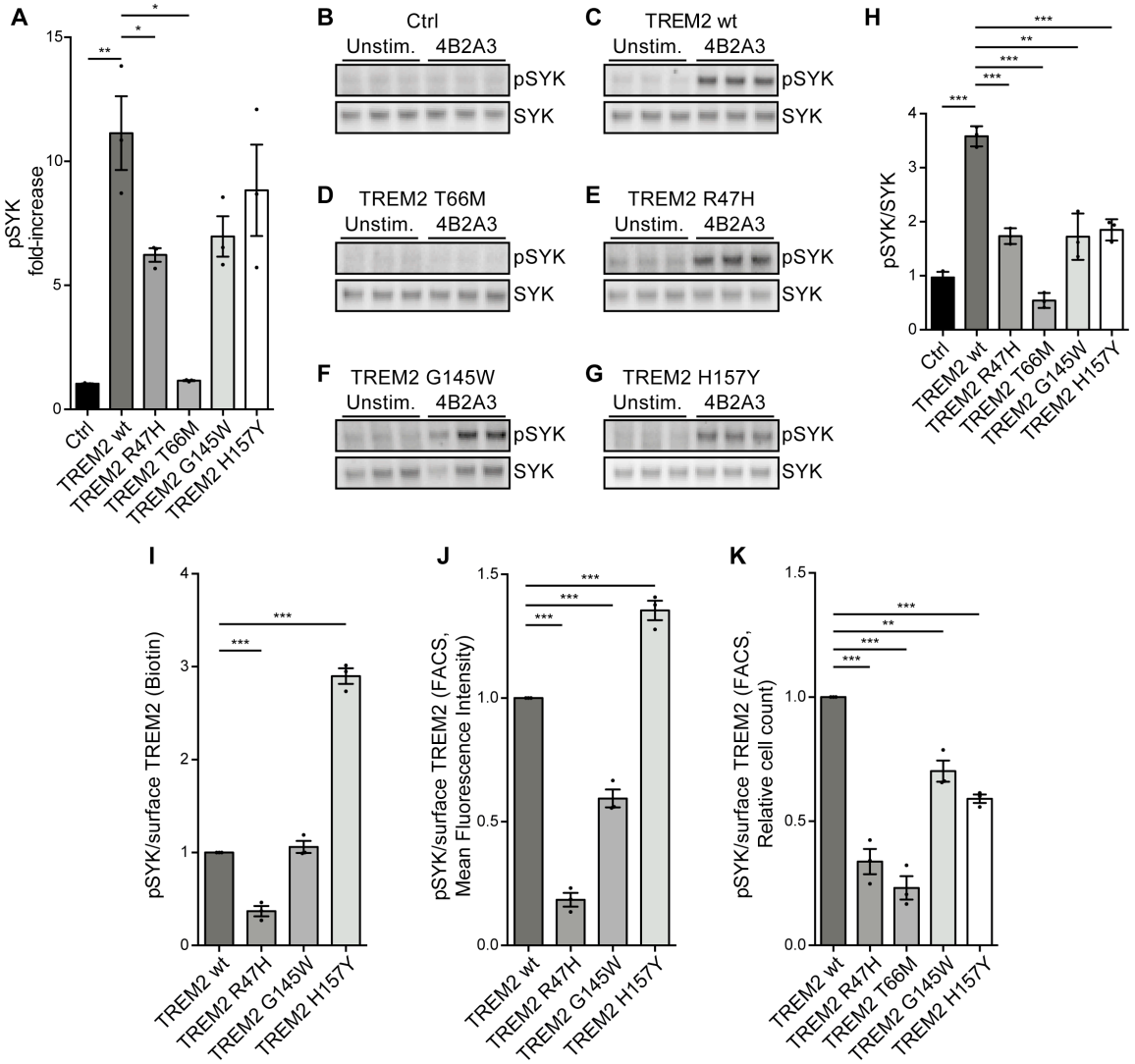

Figure 27: Differential activation of TREM2 disease-associated variants by agonistic anti-TREM2 antibody 4B2A3. (A) TREM2-DAP12 expressing cells with TREM2 variants R47H, T66M, G145W and H157Y as well as control cells were plated on 96-well plates and treated for 5 min with 10 µg/ml ectodomain-specific antibody against TREM2 (4B2A3) or left untreated as control (Unstimulated). Cells were lysed and lysates were analyzed for pSYK levels using AlphaLISA technology. Data represent the mean ± SEM of three independent experiments in triplicates each (n=3). Student's t-test (unpaired, two-tailed), *p<0.05; **p<0.01. (B-G) Western immunoblotting of cell lysates from AlphaLISA experiments. Antibodies were used for detection of pSYK and SYK in 4B2A3 treated and untreated cells. (H) Quantification of western immunoblotting as shown in B-G. Data represent the mean ± SD of one experiment in triplicates. Student's t-test (unpaired, two-tailed), **p<0.01; ***p<0.001. (I) pSYK levels were analyzed over surface TREM2 expression obtained by biotinylation and western immunoblotting (see Figure 7). Data represent the mean ± SEM of

three independent experiments in triplicates each (n=3). Student's t-test (unpaired, two-tailed), ***p<0.001. (J) pSYK levels were analyzed over surface TREM2 expression from flow cytometry analysis (see Figure 8). Data represent the mean ± SEM of three independent experiments in triplicates each (n=3). Student's t-test (unpaired, two-tailed), ***p<0.001. (K) pSYK levels were analyzed over relative cell numbers expressing TREM2 at the plasma membrane from flow cytometry analysis (see Figure 8). Data represent the mean ± SEM of three independent experiments in triplicates each (n=3). Student's t-test (unpaired, two-tailed), **p<0.01; ***p<0.001.

3.10 Most disease-associated TREM2 variants show a loss-of-function upon stimulation with phosphatidylserine

To investigate TREM2-DAP12 signaling using a more physiological ligand, the anionic phospholipid phosphatidylserine (PtdS) was used. PtdS has been described as a natural ligand for TREM2 that activates the TREM2 signaling pathway (Hsieh et al., 2009; Y. Wang et al., 2015). The experiments were performed as described above and levels of pSYK were analyzed using the AlphaLISA technology. Control cells did not respond to PtdS stimulation, whereas TREM2 wt showed an approximately 4-fold increase in pSYK levels (Figure 28A). Stimulation of TREM2 R47H and T66M was significantly reduced compared to the common TREM2 variant. As mentioned before, TREM2 T66M lacks mature TREM2 at the cell surface likely explaining the low pSYK levels. Quantification of representative western immunoblotting of pSYK and total SYK showed the same trend as observed for the pSYK levels measured in AlphaLISA experiments (Figure 28B-H). PtdS did not affect levels of total SYK and the analysis of pSYK levels in relation to surface TREM2 of biotinylation and flow cytometry experiments were comparable to those of the antibody stimulated cells (Figure 28I and J). Stimulation of TREM2 R47H was decreased compared to wt TREM2, whereas TREM2 H157Y appeared to result in stronger membrane-proximal signaling. However, as it was shown for the 4B2A3 anti-TREM2 antibody, all TREM2 rare variants showed a partial loss-of-function due to pSYK levels normalized to the relative cell count that was positive for surface TREM2 in PtdS treated cells (Figure 28K). Thus, using the physiological TREM2 ligand PtdS, a partial or total loss-of-function could be detected for the investigated TREM2 variants.

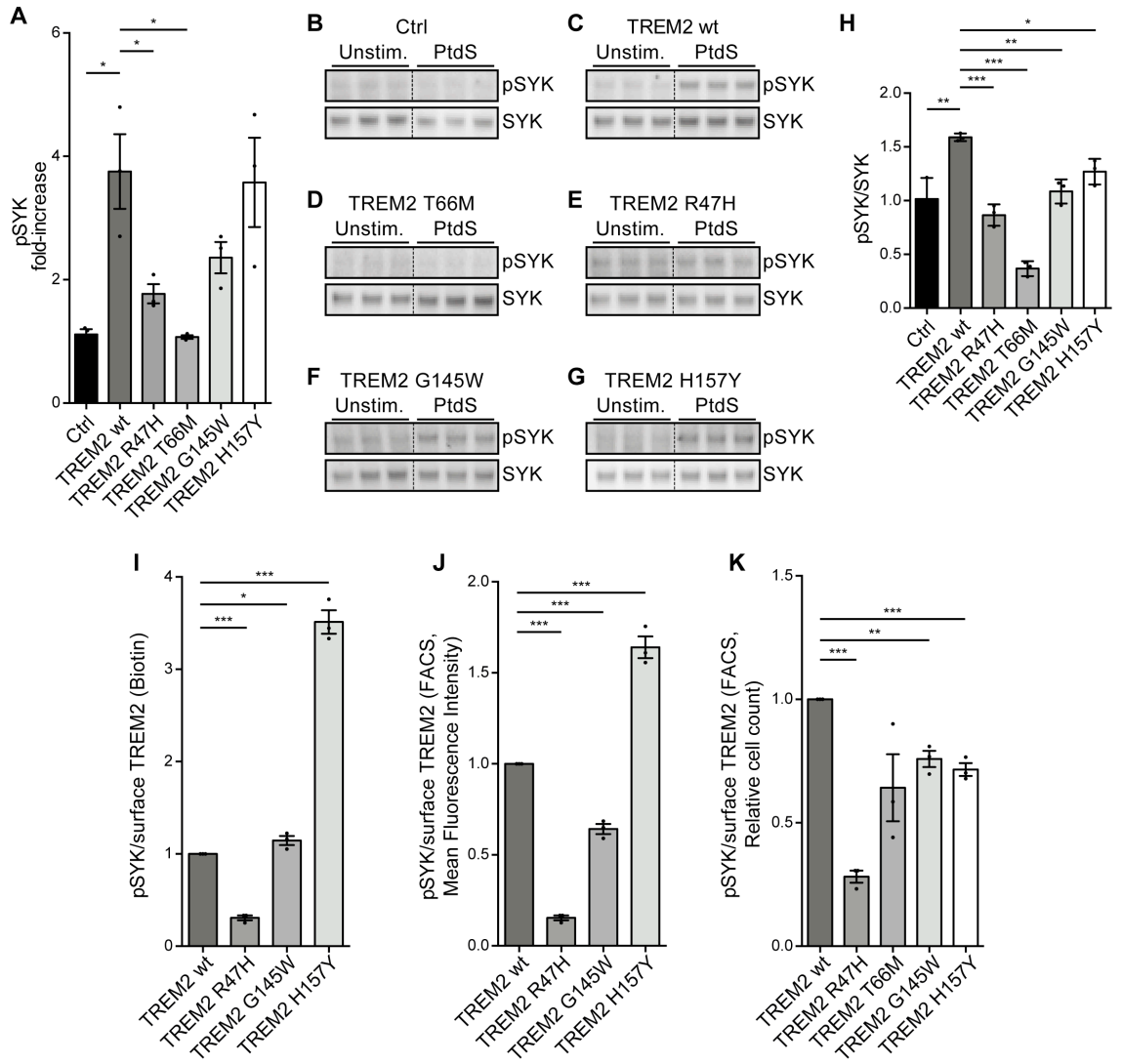

Figure 28: Differential activation of TREM2 disease-associated variants by phosphatidylserine. (A) TREM2-DAP12 expressing cells with TREM2 variants R47H, T66M, G145W and H157Y as well as control cells were plated on 96-well plates and treated for 5 min with 50 µM phosphatidylserine (PtdS) or left untreated as a control (Unstimulated). Cells were lysed and lysates were analyzed for pSYK levels using AlphaLISA technology. Data represent the mean ± SEM of three independent experiments in triplicates each (n=3). Student's t-test (unpaired, two-tailed), *p<0.05. (B-G) Western immunoblotting of cell lysates from AlphaLISA experiments. Antibodies were used for detection of pSYK and SYK in PtdS treated and untreated cells. (H) Quantification of western immunoblotting as shown in B-G. Data represent the mean ± SD of one experiment in triplicates. Student's t-test (unpaired, two-tailed), *p<0.05; **p<0.01; ***p<0.001. (I) pSYK levels were analyzed over surface TREM2 expression obtained by biotinylation and western immunoblotting (see Figure 7). Data represent the mean ± SEM of three independent experiments in triplicates each (n=3). Student's t-test (unpaired, two-tailed), *p<0.05; **p<0.01; ***p<0.001. (J) pSYK levels were analyzed over surface TREM2 expression from flow cytometry analysis (see Figure 8). Data represent the mean ± SEM of three independent experiments in triplicates each (n=3). Student's t-test (unpaired, two-tailed), *p<0.05; ***p<0.001. (K) pSYK levels were analyzed over relative cell numbers expressing TREM2 at the plasma membrane from flow cytometry

analysis (see Figure 8). Data represent the mean ± SEM of three independent experiments in triplicates each (n=3). Student's t-test (unpaired, two-tailed), **p<0.01; ***p<0.001.

3.11 Aβ does not stimulate TREM2 signaling via pSYK in TREM2-DAP12 reporter cells

Recently, the interaction of TREM2 and oligomeric Aβ has been shown. In primary mouse microglia, an increase in pSYK could be detected upon treatment with oligomeric Aβ1-42 (Y. Zhao et al., 2018; Zhong et al., 2018). To further investigate the role of Aβ as a ligand for TREM2, different forms of Aβ were prepared (Figure 29A). The generated Aβ preparations were analyzed by SDS-PAGE and Native PAGE (Figure 29B). Incubation for 24 h at 4°C generated mainly small oligomers that were SDS-sensitive whereas a 3 h incubation at 37°C produced medium molecular weight assemblies that were partly resistant to SDS as they can still be detected in western immunoblotting after separation by SDS-PAGE. Aβ that was incubated at 37°C for 24 h showed high molecular weight assemblies.

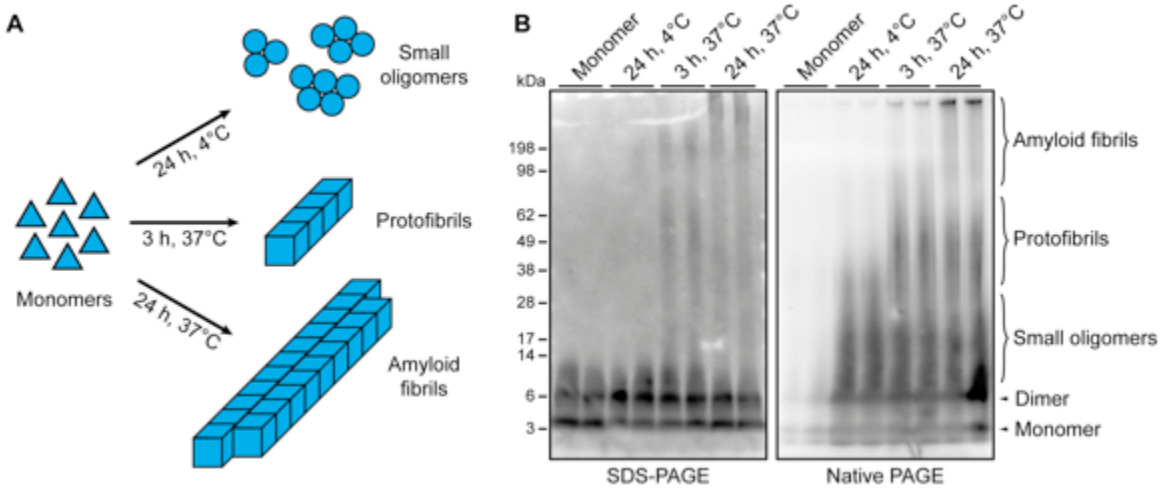

Figure 29: Preparation of Aβ oligomers and fibrils. (A) Schematic illustration of Aβ forms that are generated by incubation at different conditions. Aβ monomers form small oligomers after incubation for 24 h at 4°C. Protofibrils and amyloid fibrils are formed by incubation of Aβ at 37°C for 3 h or 24 h, respectively. (B) Characterization of generated Aβ forms by SDS-PAGE and Native PAGE. Aβ was detected using 82E1 antibody.

To investigate the effect of the different Aβ preparations, TREM2-DAP12 expressing cells were treated with Aβ for different time periods and analyzed using the AlphaLISA technology (Figure 30). Anti-TREM2 antibody 4B2A3 was used as a positive control for performed experiments. Neither of the described Aβ forms could

stimulate the phosphorylation of SYK in the reporter cell system for all tested time points. Interestingly, the control antibody showed its strongest stimulation after 30 min that diminished after 1 h of treatment.

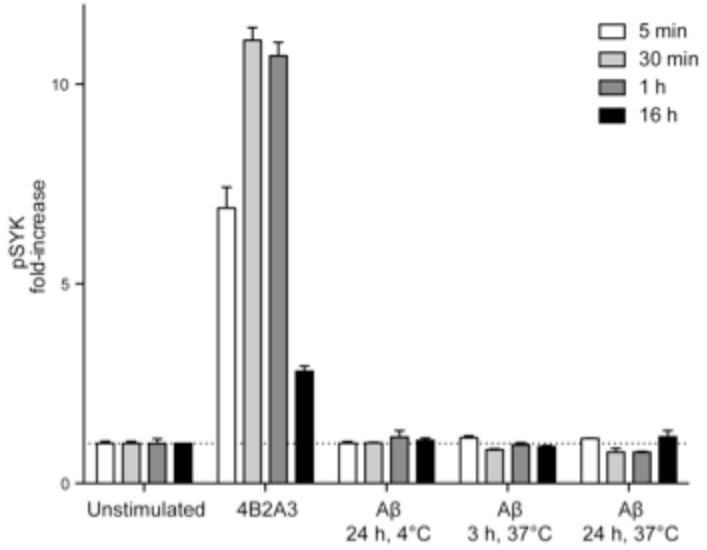

Figure 30: Aβ oligomers and fibrils do not stimulate TREM2 signaling via pSYK. TREM2-DAP12 expressing cells were plated on 96-well plates and treated for 5 min, 30 min, 1 h or 16 h with 10 µg/ml 4B2A3 antibody, 1 µM Aβ forms or not treated as a control (Unstimulated). Cells were lysed and lysates were analyzed for pSYK levels using the AlphaLISA technology.

Aβ can undergo post-translational modifications (PTMs). Among others, phosphorylation at serine 8 and serine 26 (Kumar et al., 2011, 2013; Milton, 2001), nitration (Kummer et al., 2011) and pyroglutamylation (Mori et al., 1992) but also N-terminal truncation can occur (Güntert et al., 2006; Schieb et al., 2011). Previously, it has been shown by our group that some Aβ species bind differently to TREM2 *in vitro* (Joshi et al., manuscript in revision). Thus, different modified variants of Aβ42 were tested for their stimulatory effect on TREM2-DAP12 expressing cells (Figure 31A). For these experiments, non-modified truncated Aβ42 (3-42), phosphorylated at serine 8 (3-42 p8), serine 26 (3-42 p26) and pyroglutamylated (3-42 pE) were prepared. Additionally, non-modified Aβ1-42, phosphorylated at serine 8 (1-42 p8) and nitrated (1-42 Nitrate) species were used. The different Aβ species were oligomerized for 3h at 37°C and subsequently analyzed by SDS-PAGE and Native PAGE (Figure 31B). Most species showed medium and/or high molecular weight assemblies that were mainly SDS-resistant. However, in the TREM2-DAP12 reporter system, neither of these species increased pSYK levels (Figure 31C).

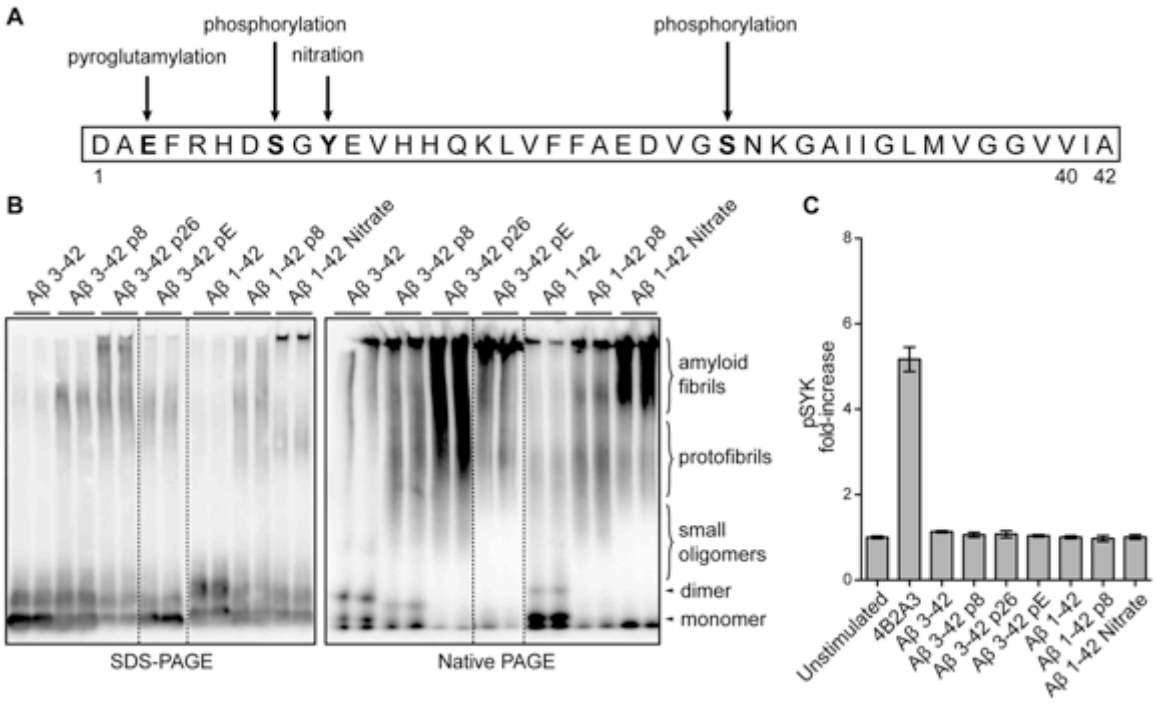

Figure 31: Fibrillar Aβ species do not increase pSYK levels in TREM2 expressing cells. (A) PTMs in the Aβ sequence that were used for experiments. Aβ can undergo pyroglutamylation, phosphorylation and nitration. (B) Characterization of fibrillar Aβ species generated by incubation for 3 h at 37°C. Following Aβ species were used: truncated Aβ 3-42, with additional phosphorylation at Ser8 or Ser26 (p8 and p26, respectively) or pyroglutamylation (pE), Aβ 1-42, with additional p8 or nitration. Aβ species were analyzed by SDS-PAGE and Native PAGE. Aβ was detected using 82E1 antibody. (C) TREM2-DAP12 expressing cells were plated on 96-well plates and treated for 5 min, with 10 µg/ml 4B2A3 antibody, 1 µM fibrillar Aβ species or not treated as a control (Unstimulated). Cells were lysed and lysates were analyzed for pSYK levels using AlphaLISA technology. Data represent the mean ± SEM of three independent experiments in duplicates each (n=3).

In further experiments, oligomeric Aβ species with and without PTMs were prepared by incubation for 24 h at 4°C and used for treatment of TREM2-DAP12 expressing cells. Western immunoblotting showed that the generated oligomers were of smaller size as compared to oligomers prepared by incubation for 3 h at 37°C and thus still SDS-sensitive (Figure 32A). However, some species were already more prone to develop high molecular weight assemblies under these conditions. Especially the truncated Aβ 3-42 p26 and Aβ 1-42 Nitrate showed accumulation of high molecular weight assemblies. The generated Aβ oligomer species were tested for stimulation of control cells and TREM2-DAP12 expressing cells (Figure 32B and C, respectively). However, as it has been shown before with oligomers generated by incubation for 3 h at 37°C, neither of these species increased pSYK levels.

In conclusion, the different Aβ preparations tested here did not stimulate TREM2 membrane-proximal signaling in the TREM2-DAP12 reporter cell system.

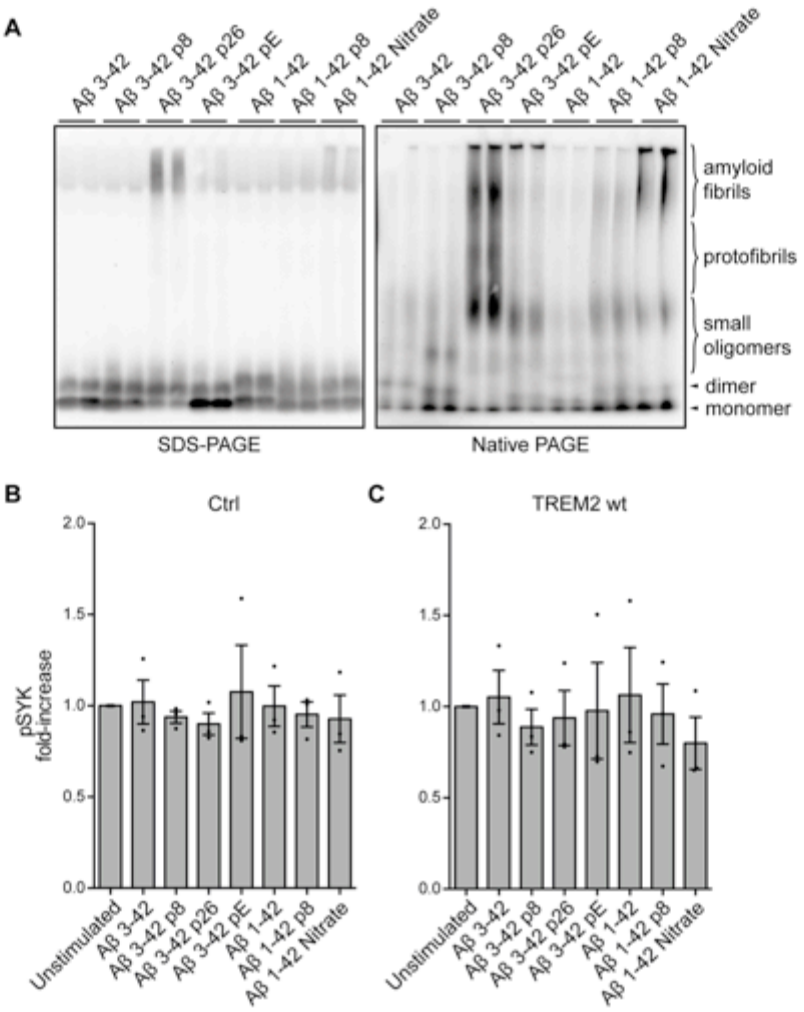

Figure 32: Oligomeric Aβ species do not increase pSYK levels in TREM2 expressing cells. (A) Characterization of oligomeric Aβ species generated by incubation for 24 h at 4°C. Following Aβ species were used: truncated Aβ 3-42, with additional phosphorylation at Ser8 or Ser26 (p8 and p26, respectively) or pyroglutamylation (pE), Aβ 1-42, with additional p8 or nitration. Aβ species were analyzed by SDS-PAGE and Native PAGE. Aβ was detected using 82E1 antibody. (B) TREM2-DAP12 expressing cells were plated on 96-well plates and treated for 5 min, with 10 µg/ml 4B2A3 antibodies, 1 µM oligomeric Aβ species or left untreated as a control (Unstimulated). Cells were lysed and lysates were analyzed for pSYK levels using AlphaLISA technology. Data represent the mean ± SEM of three independent experiments in triplicates each (n=3).

3.12 Stimulation of TREM2 wt and variant expressing iPSdMiG by antibody 4B2A3 and physiological ligand PtdS

All experiments in this study were performed with HEK 293 TREM2-DAP12 reporter cell lines. To validate the obtained results in a model for human microglia, induced pluripotent stemcell-derived microglia cells (iPSdMiG) were used. Cells were differentiated and prepared by M. Mathews-Ajendra, Life&Brain according to a newly established protocol (Mathews-Ajendra et al., in preparation). All cells used had an isogenic background.

First, TREM2 KO and wt iPSdMiG were treated with anti-TREM2 4B2A3 antibody and respective antibody fragments F(ab')$_2$, Fab and Fc (Figure 33). The whole IgG led to stimulation of TREM2 wt expressing cells, whereas TREM2 KO cells showed only a weak increase in pSYK levels that were considerably lower than the increase of pSYK in the HEK 293 reporter system expressing the common TREM2 variant. Interestingly, TREM2 wt iPSdMiG were stimulated by F(ab')$_2$ fragments of the antibody but did not show an increase in pSYK levels with the Fc fragment. Thus, iPSdMiG could be stimulated with anti-TREM2 4B2A3 antibodies via cross-linking.

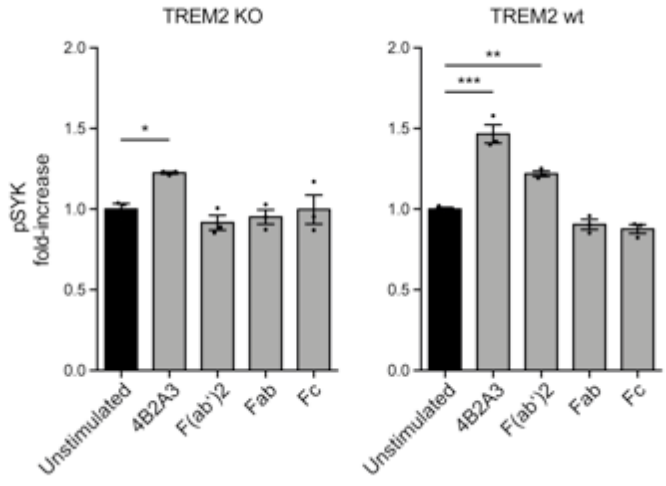

Figure 33: 4B2A3 antibody stimulates iPSdMiG in a TREM2-dependent manner. TREM2 KO and TREM2 wt iPSdMiG were treated for 5 min with 67 µM ectodomain-specific antibody or antibody fragments F(ab')$_2$, Fab and Fc against TREM2 (4B2A3) or not treated as a control (Unstimulated). Cells were lysed and lysates were analyzed for pSYK levels using

AlphaLISA technology. Data represent the mean ± SD of one experiment in triplicates. One-way ANOVA, Tukey's *post hoc* test for multiple comparison, *p<0.05; **p<0.01; ***p<0.001.

Next, pSYK levels of TREM2 wt, R47H and T66M expressing iPSdMiG were measured upon stimulation with 4B2A3 antibody, PtdS containing liposomes and oligomerized Aβ (Figure 34). As seen in HEK 293 cells (Figure 27 and 28), 4B2A3 antibody and PtdS increased pSYK levels in TREM2 wt and R47H expressing iPSdMiG, but not in TREM2 KO or T66M expressing iPSdMiG. Incubation with PtdS also increased levels of pSYK in TREM2 wt and R47H expressing iPSdMiG with similar potency (Figure 34B). In contrast, TREM2 T66M expressing iPSdMiG showed only a minor stimulation compared to TREM2 KO cells. Interestingly, oligomeric Aβ 1-42 did not increase pSYK levels in neither of the tested iPSdMiG.

In summary, obtained results of TREM2 common and variant expressing iPSdMiG highly correlated to HEK 293 reporter cells. The anti-TREM2 antibody 4B2A3 and physiological ligand PtdS activated iPSdMiG in a TREM2-dependent manner and showed the same trend of reduced stimulation in TREM2 R47H and T66M compared to the common variant expressing cells.

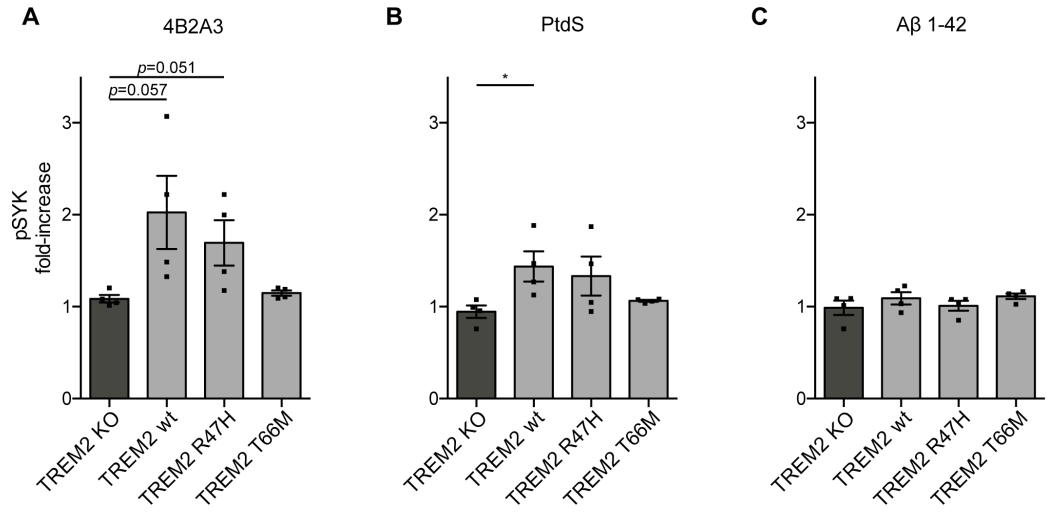

Figure 34: Differential stimulation of iPSdMiG expressing TREM2 common and rare variants. TREM2 KO, wt, R47H an T66M expressing iPSdMiG were treated with 10 µg/ml 4B2A3 antibody (A), 250 µg/ml PtdS containing liposomes (B) or Aβ 1-42 (C, 24 h, 4°C oligomerization) for 5 min and lysates were analyzed for pSYK levels using AlphaLISA technology. Data represent the mean ± SEM of four experiments in triplicates each (n=4). Student's t-test (unpaired, two-tailed), *p<0.05.

4 Discussion

TREM2 mutations have been linked to several neurodegenerative diseases, including NHD, FTD and AD (Hakola et al., 2009; Humphrey et al., 2015; Nasu et al., 1973; Yeh et al., 2017). Evidence suggests that most mutations result in a loss-of-function of TREM2 (Kleinberger et al., 2014, 2017; Mazaheri et al., 2017; Schlepckow et al., 2017; Song et al., 2018), however, the exact molecular mechanisms underlying the effects of disease-associated mutations still remain unclear. Here, we sought to establish a robust cellular model system stably expressing TREM2 and its adaptor protein DAP12 in stoichiometric amounts. Results showed that transient transfection of TREM2 and DAP12 resulted in aberrant maturation and transport of immature proteins to the cell surface (Figure 6 and 8). Due to these observations, a reporter cell system with stable co-expression of TREM2 and DAP12 was established using a HEK 293 Flp-In system (Thermo Fisher Scientific). With help of the Flp recombinase, the gene of interest is specifically inserted into a defined locus of the host cell line, thereby generating isogenic cell lines including a strong promoter for protein expression and a hygromycin antibiotic resistance for selection of TREM2 and DAP12 expressing cells (Lu et al., 2011; O'Gorman et al., 1991). This system allowed studying characteristics of TREM2 common and rare variants and TREM2-DAP12 receptor complex mediated signaling upon ligand binding. Application of this system revealed differential effects of the distinct TREM2 variants on subcellular localization and transport, cell surface exposure, degradation, receptor proximal downstream signaling, cellular response and allowed the identification and characterization of TREM2 ligands.

4.1 HEK 293 TREM2-DAP12 reporter cells represent a suitable model system for studying TREM2 characteristics

In microglia and other monocyte-derived cell types, intracellular signaling of TREM2 and DAP12 is involved in phagocytosis, survival and migration (Colonna, 2003b; Jay et al., 2017; J. Walter, 2016). For investigation of the TREM2 characteristics and signaling, a stable reporter cell system in HEK 293 cells was generated that allows robust protein expression and easy culture of cells due to high proliferation, but also represents a model system without endogenous expression of other immune receptors that might interact with DAP12. Direct comparison of transiently and stably

transfected cells showed an accumulation of high-molecular weight assemblies for TREM2 and DAP12 in transient transfections (Figure 6 and 8). Additionally, deglycosylation of sTREM2 revealed the presence of partly immature mannose-rich glycans in transiently transfected cells (Figure 7). Indeed, it has been shown that high overexpression of proteins could saturate retention and quality control systems in the ER and thus allow export of misfolded or immature proteins (Barlowe & Helenius, 2016; Hammond & Helenius, 1994). To prevent aberrant transport and secretion of immature TREM2 and to better understand the characteristics, trafficking and processing of TREM2 common and disease-associated variants, stably transfected HEK 293 cells co-expressing TREM2 and DAP12 were used for further experiments in this study.

Selected TREM2 variants associated with neurodegenerative diseases were investigated in this study. Variant TREM2 R47H has been associated with an increased risk for AD (Guerreiro et al., 2013; Jonsson et al., 2013), and the H157Y variant also showed association with AD in some cohorts (Jiang, Tan, et al., 2016). TREM2 G145W was linked to a familial form of dementia (Karsak et al., 2020), and TREM2 T66M showed association with frontotemporal dementias (Le Ber et al., 2014). TREM2 R47H and T66M are the most studied TREM2 variants so far. In the established reporter cell system, known characteristics of these variants could be confirmed. It has been previously described that *in vitro* and *in vivo* a decrease in sTREM2 levels for both variants is related to altered transport or maturation (Kleinberger et al., 2014; Song et al., 2018; Sudom et al., 2018). sTREM2 was barely detectable in media of TREM2 T66M expressing cells, consistent with retention of this variant in the ER and Golgi, thus preventing proteolytic cleavage by ADAM proteases (Schlepckow et al., 2017; Thornton et al., 2017). Results showed a broad band between 35 and 55 kDa rather than a distinct band for sTREM2 in all variant cell lines except for TREM2 T66M, which is consistent with complex N-glycosylation within the TREM2 ectodomain (Kleinberger et al., 2014; Park et al., 2015). Furthermore, disease-associated TREM2 variants showed decreased levels of mature TREM2 at the cell surface as compared to the common variant (Figure 12 and 13), which could be due to impaired transport of the protein. Indeed, it has been previously shown that TREM2 T66M is retained in the ER due to misfolding, and the R47H substitution resulted in a lower stability of the TREM2 receptor (Kleinberger et

al., 2014; Song et al., 2017; Sudom et al., 2018). Interestingly, CTF levels of TREM2 R47H were comparable to those of the common TREM2 variant (Figure 10), indicating similar processing of both variants. The R→H substitution thus might effect maturation and transport of TREM2 to the cell surface. In addition, degradation of mature TREM2 R47H could be enhanced, resulting in a decreased amount of mature TREM2 at the plasma membrane and thus lower levels of sTREM2 and CTFs in supernatants and remaining in the cell membrane, respectively. Another reason for lower amounts of sTREM2 R47H in supernatants whereas levels of CTFs over immature TREM2 remain comparable to common TREM2 could be that sTREM2 R47H might be degraded more efficiently upon processing and release into the conditioned medium of TREM2 expressing cells.

As compared to the common TREM2 variant, the TREM2 T66M variant highly localized to the ER (Figure 16), and was barely detected at the cellular surface (Figures 12 and 13). It has already been reported that this mutation impairs N-glycosylation and trafficking to the plasma membrane (Kleinberger et al., 2014; Park et al., 2015). The reporter cell system also revealed a distinct localization of TREM2 T66M as compared to the other TREM2 variants investigated. In addition, TREM2 T66M is more reticular and spread throughout the cytosol compared to the other variants (Figure 16), highly similar to previous results (Kleinberger et al., 2014; Park et al., 2015; Y. Zhao et al., 2017). Interestingly, in T66M expressing cells only a small amount of DAP12 was detected at the plasma membrane. As TREM2 T66M does not reach the cell surface, DAP12 possibly gets retained in the ER as well and cannot be transported to the cell surface without simultaneous receptor trafficking. In contrast to natural killer cells where DAP12 could associate with other immune receptors, HEK 293 cells do not express a compensating receptor (Mulrooney et al., 2013). Furthermore, due to insufficient transport of DAP12, the protein might be degraded in the absence of TREM2.

The present data support and extent previous findings showing retention of TREM2 T66M in the ER and/or decreased maturation by glycosylation (Kleinberger et al., 2014; Park et al., 2015; Sirkis et al., 2017). Thus, results obtained with the TREM2-DAP12 reporter cell system are reliable for the additional TREM2 mutants investigated in this study.

4.2 TREM2 G145W possibly affects cleavage by ADAM proteases

TREM2 variant G145W has been identified in a family with possible familial AD-type dementia. This variant has been shown to result in structural changes of an intrinsically disordered region (IDR) of the TREM2 ectodomain (Karsak et al., 2020). In the reporter cell system, this variant showed increased expression levels of immature TREM2 compared to the common variant (Figure 10). However, the amount of mature surface TREM2 showed high variations in biotinylation and flow cytometry analyses (Figures 12 and 13, respectively). Antibodies AF1828 and 4B2A3 both mainly recognize an epitope within the stalk region of TREM2, containing G145 (Figure 9). Thus, the G145W substitution might affect recognition by both antibodies, as it has been shown for AF1828 before (Karsak et al., 2020). However, in biotinylation experiments with subsequent western immunoblotting, mature TREM2 was detected with AF1828 and revealed a lower expression of the G145W variant at the cell surface compared to the common variant. Interestingly, detection with antibody 17C9 showed a slightly higher level of mature TREM2 at the cell surface and sTREM2 in conditioned medium of TREM2 G145W expressing cells as compared to detection with the AF1828 antibody. Antibody 4B2A3 was used for flow cytometry and immunocytochemistry analysis that was performed with living cells and proteins likely being in their native conformation. Although antibodies often bind preferentially to denatured proteins (Brown et al., 2011; Forsström et al., 2015), flow cytometry analysis with antibody 4B2A3 revealed a comparable amount of mature TREM2 common and G145W variants at the cellular surface. Thus, TREM2 G145W strongly influences the detection by TREM2 specific antibodies.

The G145W substitution shortens the IDR of TREM2 from aa 145-168 to aa 154-168 (Karsak et al., 2020). Within the IDR, TREM2 is processed by ADAM proteases (Feuerbach et al., 2017; Schlepckow et al., 2017; Thornton et al., 2017). Thus, the amino acid substitution might interfere with efficient cleavage by ADAM proteases. Levels of TREM2 CTFs were also decreased for TREM2 G145W in comparison to the common variant (Figure 10), further supporting this notion.

4.3 TREM2 H157Y shows a more complex glycosylation

The H157Y mutation of TREM2 is located right at the cleavage site for ADAM proteases (Feuerbach et al., 2017; Schlepckow et al., 2017; Thornton et al., 2017). It has been shown that mature TREM2 at the cell surface is decreased due to the H157Y mutation, as shedding is enhanced. One study reported increased levels of sTREM2 in supernatants of transfected HEK 293 cells (Thornton et al., 2017). However, our data suggest rather unchanged or even decreased levels of sTREM2 in the reporter cell system (Figure 10, antibody 17C9 and AF1828, respectively). It should be noted that both cellular systems were established in HEK 293 cells, however, in our study cells were stably transfected whereas Thornton et al. (2017) used a transient transfection system. Therefore, divergent results could be due to different experimental systems. We showed that TREM2 CTF levels of TREM2 H157Y expressing cells remained comparable to those of TREM2 wt cells (Figure 10). Previously, DAP12 was shown to enhance the half-life of TREM2 CTF by reducing its turnover rate (Zhong et al., 2015). In line with this, Schlepckow et al. (2017) showed reduced levels of TREM2 CTFs in TREM2 H157Y expressing cells in absence of DAP12, whereas simultaneous expression of DAP12 increased CTF levels to that detected in TREM2 common variant expressing cells. DAP12 is known to stabilize other associated receptors as well (Mulrooney et al., 2013). The interaction of DAP12 with immune receptors could occur early during transport, possibly already in the ER as shown for killer Ig-like receptor (KIR) on natural killer cells (Mulrooney et al., 2013). Interestingly, the ratio of DAP12 over immature TREM2 and respective CTFs of H157Y were significantly increased as compared to the common TREM2 variant, possibly indicating the formation of DAP12 trimers and/or a TREM2-DAP12 receptor complex consisting of more than two DAP12 units in TREM2 H157Y expressing cells. Indeed, formation of trimeric DAP12 complexes has been described before (Knoblich et al., 2015). However, the structure of DAP12 complexes needs to be further investigated using for example immunoprecipitation and subsequent non-reducing SDS-PAGE analysis or cluster analysis of cell surface complexes by immunocytochemistry. Thereby, the exact constitution of TREM2-DAP12 complexes could be determined and differences of the H157Y variant in this context could be elucidated.

Soluble proteins destined for secretion of transmembrane proteins are usually transported through the ER and Golgi network and finally reach the plasma membrane or are secreted into the extracellular space (Kelly, 1985; Palade, 1975; Viotti, 2016). During this transport process, proteins undergo PTMs with glycosylation being the most common one (Spiro, 2002). In previous studies, TREM2 has been described to be glycosylated at Asn 20 (N20) and Asn 79 (N79) (Kober et al., 2016; Sudom et al., 2018). Glycosylation is known to have several effects on protein function and metabolism, including protection against proteolytic degradation and affecting its solubility (Rudd & Dwek, 1997; Spiro, 2002). Furthermore, it acts as a quality control mechanism in the ER for proper folding of proteins before they are further transported to Golgi compartments. Also, glycostructures can affect the activity and function of the protein through acting as a ligand for cell surface receptors (Spiro, 2002; Wormald et al., 2002). Complex glycosylation of TREM2 common and disease-associated R47H, G145W and H157Y variants could be confirmed using different glycosidases (Figure 14). Resistance to Endo D and Endo H cleavage confirmed proper maturation of respective variants in the HEK 293 reporter cell system. Interestingly, the TREM2 H157Y variant shows a shift in migration of sTREM2 in SDS-PAGE and western immunoblotting, and deglycosylation with Endo F3 suggests less triantennary glycans compared to the common variant (Figure 14). However, the main broad band of glycosylated sTREM2 for TREM2 common and H157Y variant is still detectable upon incubation with Endo F3, indicating mainly complex tetraantennary glycostructures for both proteins. The shift in TREM2 H157Y thus might be due to enhanced poly-N-acetyllactosamine (PNL) glycosylation. PNLs are glycans with multiple repeats of N-acetyllactosamine ($Gal\beta_{1-4}$ and $GlcNAc\beta_{1-3}$) (Fukuda et al., 1984; D. Zhou, 2003), that are preferentially attached to a β_{1-6}GlcNAc on complex N-linked glycans (Nabi & Dennis, 1998). Results indicate that TREM2 H157Y has more complex tetraantennary glycostructures containing PNLs compared to the common TREM2 variant. Interestingly, for LAMP2 it has been shown that polylactosamine glycosylation is increased due to longer residence time in the Golgi (Nabi & Dennis, 1998). Hence, TREM2 H157Y might be present in the Golgi for a longer time due to possible conformational alterations, which could lead to differences in protein glycosylation. Nevertheless, mass spectrometry analysis could reveal the exact glycostructure of the protein for further confirmation. Additional experiments to specifically assess the

transport and stability using a pulse chase approach and protease inhibition could provide further insight into the specific characteristics of this disease-associated variant.

4.4 TREM2 is mainly degraded by the autophagy-lysosomal pathway

Degradation pathways of TREM2 have barely been investigated so far. Internalization and receptor recycling of TREM2 through clathrin-mediated endocytosis and retromers, respectively, has previously been described (Yin et al., 2016). Receptor endocytosis results in the formation of early endosomes. Subsequently, receptors are either recycled back to the plasma membrane via retromer transport from early endosomes to the TGN or destined for degradation and transported to the lysosome (Jovic et al., 2010; Mukherjee et al., 1997). Colocalization of TREM2 with early endosomes could be detected in close proximity to the plasma membrane for all variants except TREM2 T66M (Figure 18). This strongly indicates endocytosis of TREM2 either for another round of delivery to Golgi compartments and further to the plasma membrane or for degradation upon transport to lysosomal compartments (Prada et al., 2006; Yin et al., 2016). The lacking colocalization with early endosomes of TREM2 T66M in close proximity to the plasma membrane is in line with the absence this variant on the cell surface (Kleinberger et al., 2017; Park et al., 2015).

Several amino acid sequence motifs are involved in clathrin-mediated endocytosis of cell surface receptors (Owen & Evans, 1998; Traub, 2009). Interestingly, the TREM2 cytoplasmic domain does not contain one of the classical motifs, whereas DAP12 contains one YQEL and one YSDL motif, known to facilitate endocytosis by clathrin-coated vesicles (Owen & Evans, 1998). Hence, internalization of TREM2 possibly depends on DAP12 interaction for receptor recycling and shuttling back to the plasma membrane (Grant & Donaldson, 2009; Steinman et al., 1983). A TREM2 expressing reporter cell line lacking DAP12 could be used for further verification. Receptor-mediated endocytosis is often stimulated upon ligand binding, but can also occur without ligand binding (Hopkins et al., 1985; Mettlen et al., 2018).

In eukaryotic cells, lysosome-associated degradation and the UPS are major pathways for proteolytic degradation. In this study, Chloroquine was used for

inhibition of the autophagy-lysosomal pathway. It is known to accumulate in lysosomes, where it changes the lysosomal pH and inhibits enzymes needed for degradation of proteins but also impairs autophagosome-lysosome fusion (Mauthe et al., 2018; Pasquier, 2016). Interestingly, for all investigated TREM2 variants, an increase in full-length TREM2 could be observed upon inhibition of the autophagy-lysosomal pathway, whereas a decrease was detected upon proteasomal inhibition (Figures 20 and 22, respectively). In several studies, proteasome inhibition resulted in enhanced autophagic activity (Ge et al., 2009; Kyrychenko et al., 2014; Tang et al., 2014). Thus, the decreased amounts of TREM2 in MG132 treated cells could indicate degradation of TREM2 by the autophagy-lysosomal pathway. It has already been shown for APP that the autophagy-lysosomal pathway degrades mature APP and APP CTFs (Jaeger et al., 2010). Moreover, APP degradation was induced by inhibition of the proteasome (F. Zhou et al., 2011), which could also be confirmed by treatment of cells with MG132, as lower levels for APP and respective CTFs were detected as compared to untreated controls (Figure 22). Degradation of TREM2 and its CTFs by lysosome-associated pathways is further supported by the finding that Chloroquine treatment enriched TREM2 CTF levels. Another reason for enriched levels of TREM2 CTFs upon Chloroquine treatment could be due to increased full-length TREM2 levels, that are constantly processed by ADAM proteases (Feuerbach et al., 2017; Schlepckow et al., 2017; Thornton et al., 2017). Both, APP CTFs and TREM2 CTFs can be proteolytically processed by γ-secretase (Haass et al., 1993; Wunderlich et al., 2013). Hence, both protein fragments presumably share common pathways for degradation. Interestingly, DAP12 levels were also increased in Chloroquine treated cells, suggesting likewise degradation of DAP12 by the autophagy-lysosomal pathway. In previous studies, DAP12 showed to stabilize TREM2 CTFs (Zhong et al., 2015), possibly explaining the correlating levels of DAP12 and TREM2 CTFs.

Inhibition of lysosomal activity and thus also of protein clearance by autophagy with Chloroquine in TREM2 T66M and G145W expressing cells resulted in a significantly diminished enhancement of full-length TREM2 compared to the common TREM2 variant (Figure 20). Especially, TREM2 T66M showed stronger colocalization with PSMB5, probably indicating additional involvement of the proteasome. Usually, luminal and membrane proteins in the ER that are misfolded due to mutations can be

translocated from the ER to the cytoplasm and are subsequently degraded by the proteasome (Brodsky, 2012; Vembar & Brodsky, 2008). Indeed, TREM2 T66M constantly cycles between ER and ERGIC, thus this variant is supposedly degraded via the ER-associated degradation (ERAD) pathway (Sirkis et al., 2017; Werner et al., 1996). However, MG132 treatment did not result in an increase of TREM2 T66M levels, whereas Chloroquine treatment did, suggesting its main degradation by the autophagy-lysosomal pathway. Thus, TREM2 T66M could still reach the *trans*-Golgi, leading to degradation after transport to lysosomes. This process has been described for other mutant proteins previously (Coughlan et al., 2004; Kruse et al., 2006). TREM2 variant G145W has barely been studied so far, however, it is known that it causes structural changes by shortening an intrinsically disordered region around the cleavage site of TREM2 (Karsak et al., 2020). Taken together, both mutations, TREM2 T66M and G145W, possibly lead to an additional route for degradation by the proteasome, suggested by the results obtained from inhibition of the autophagy-lysosomal pathway.

4.5 Partial and total loss-of-function in AD- and FTD-associated TREM2 variants

The results of both functional assays, ROS production and SYK phosphorylation upon stimulation of TREM2, suggest a partial loss-of-function for the mutants R47H, T66M, G145W and H157Y (Figure 24, 27 and 28). It has been shown previously that activation of TREM2 increases the production of ROS (Charles et al., 2008; Zhu et al., 2014). Another study revealed that TREM2 KO microglia showed less oxidative stress and thus were retained in a less activated state compared to microglia expressing TREM2 upon exposure to necrotic neural debris or inactivated bacteria (Linnartz‐Gerlach et al., 2019). In addition, iPSdMiG expressing TREM2 variants R47H and T66M were examined for their effect on metabolic function, and both variants induced metabolic deficits and impaired a metabolic switch towards glycolysis (Piers et al., 2020). Hence, the inability of TREM2 rare variants to produce ROS in the reporter cell system correlates to previous results described for TREM2 R47H and T66M. Still, levels of ROS upon stimulation of cells expressing the common variant of TREM2 were very low. The obtained results could be further verified using additional assays for the determination of oxidative stress. ROS production by mitochondria is a byproduct of adenosine triphosphate (ATP)

generation, wherefore determination of mitochondrial ATP could present an additional measure for mitochondrial stress conditions (Brookes et al., 2004).

PtdS is a phospholipid, integrated into the plasma membrane lipid bilayer. Under physiological conditions, PtdS is restricted to the inner leaflet, however, during apoptosis and cell damage PtdS is translocated to the external leaflet of the plasma membrane (Fadok et al., 1992). Recent studies have shown that TREM2 binds PtdS and thus recognizes apoptotic cells (Hsieh et al., 2009; Y. Wang et al., 2015). Here, PtdS was used to stimulate TREM2 signaling. PtdS efficiently stimulated the phosphorylation of SYK in cells expressing the common variant of TREM2, but all disease associated variants showed decreased activation of TREM2 signaling. Analysis of pSYK in relation to expression levels obtained from biotinylation or flow cytometry gives information about the response of the receptor to a stimulus, whereas pSYK in relation to the relative cell number positive for surface TREM2 provides information about the intensity of the cellular response. Thus, all TREM2 variants except for TREM2 T66M were still capable to promote SYK phosphorylation. TREM2 R47H showed a reduced response to PtdS stimulation, consistent with previous literature, as TREM2 R47H has been described to impair ligand binding of TREM2 (Atagi et al., 2015; Kober et al., 2016; Yeh et al., 2016). It has been shown that alterations in the amino acid sequence within the v-set Ig domain could interfere with ligand binding (Sudom et al., 2018; Y. Wang et al., 2015). Consistent with an almost complete lack of T66M on the cell surface, PtdS did not evoke cellular stimulation of TREM2 T66M expressing cells. Thus, the present data support and extent previous findings showing a total loss-of-function of TREM2 T66M due to retention in the ER and/or decreased maturation by glycosylation (Kleinberger et al., 2014; Park et al., 2015; Sirkis et al., 2017) and a partial loss-of-function of TREM2 R47H due to decreased interaction with TREM2 ligands (Kober et al., 2016).

Due to a shortened IDR, TREM2 variant G145W results in conformational changes, leading to impaired signaling activity and morphological response (Karsak et al., 2020). In this study, TREM2 G145W was still capable to promote SYK phosphorylation, albeit with a lower potency. Consequently, the change in conformation leads to a decreased receptor activation and cellular response. Since G145 is localized outside of the ligand-binding domain, it appears unlikely that the disease-associated substitution directly interferes with ligand interaction. However,

IDRs are known to be highly dynamic and rapidly change their conformation (Wright & Dyson, 2015). Due to the shortened IDR in TREM2 G145W, the protein is more defined and inflexible compared to the wt protein. Thus, the TREM2 mutation might affect ligand-induced conformational changes resulting in reduced stimulation of the variant.

Interestingly, TREM2 H157Y expressing cells showed significantly increased ROS production upon incubation with debris as compared to unstimulated cells. However, simultaneous treatment with SOD1 could not prevent the oxidative response, unlike to what was observed in TREM2 wt cells. SOD1 can scavenge superoxide radicals, whereas the vitamin E analog trolox reacts with peroxyl radicals (Lúcio et al., 2009; Rosen et al., 1993). This indicates that cells expressing TREM2 wt produce superoxide radicals, whereas the nature of radicals produced by TREM2 H157Y is unknown. Notably, the response of TREM2 H157Y expressing cells in pSYK experiments showed an increased receptor response, analyzed by the pSYK levels in relation to TREM2 surface intensities (Figure 28I and J). N-glycans are an important part in binding of ligands to their receptors as it has been described for corticosteroid-binding globulin (CBG) that showed a significantly increased interaction with its receptor upon N-glycan removal from CBG (Sumer-Bayraktar et al., 2011). The H157Y variant of TREM2 showed differential glycosylation indicated by an increased apparent molecular mass in SDS-PAGE analysis and different susceptibility to deglycosylation with Endo F3 (Figure 14). It seems reasonable that ligand binding is modulated by the H157Y mutation due to the demonstrated more complex glycosylation compared to the common TREM2 variant. Thus, the difference in glycosylation of TREM2 H157Y appears to have a positive effect on ligand binding as compared to the common TREM2 variant, whereas the cellular response appears to be decreased. Due to the enhanced shedding of TREM2, leading to a reduced presence of full-length TREM2 at the cell surface, the cellular response to PtdS treatment is reduced. It has recently been shown that TREM2 CTFs generated by proteolytic shedding of the ectodomain could be stabilized by its adaptor protein DAP12 (Zhong et al., 2015). The TREM2 CTF-DAP12 complexes could alter downstream signaling pathways by trapping DAP12, thereby preventing its interaction with full-length TREM2 (Glebov et al., 2016; Yao et al., 2019). Thus, the changes in the relative levels of DAP12 and TREM2 CTFs could also contribute to

the observed impairment of TREM2-DAP12 signaling in TREM2 H157Y expressing cells.

4.6 Aβ does not stimulate TREM2-DAP12 signaling in the reporter cell line

Several studies indicate an important role of TREM2 in the pathogenesis of AD, through microglial activation and amyloid plaque clearance, as TREM2 deficiency has been shown to impair the phagocytic activity of microglia cells (Kleinberger et al., 2014; C. Y. D. Lee & Landreth, 2010). Oligomeric Aβ showed the strongest interaction with TREM2, whilst monomeric Aβ just showed weak binding (Lessard et al., 2018; Y. Zhao et al., 2018). While other groups have reported increased pSYK levels due to activation of TREM2 signaling by Aβ (Y. Zhao et al., 2018; Zhong et al., 2018), we could not stimulate TREM2-DAP12 signaling in HEK 293 or iPSdMiG (Figures 30-32 and 34). However, in both studies, primary mouse microglia were exposed to Aβ for at least 30 min before pSYK levels were analyzed. The divergent results from Y. Zhao et al. (2018) and Zhong et al. (2018) as compared to our results could thus be either due to the difference in mouse and human TREM2 response to Aβ or the different treatment timepoints, as we have treated iPSdMiG for 5 min instead of 30 min.

Interestingly, expression of human TREM2 R47H in a transgenic mouse model showed impaired activation of microglia compared to mice expressing the common human TREM2 variant (Song et al., 2018). Furthermore, in TREM2 deficient AD mouse models, clustering of microglia around amyloid plaques was impaired, leading to a decrease of amyloid plaque compaction and enhanced damage of adjacent axons and dendrites (Y. Wang et al., 2016; Yuan et al., 2016). Thus, the interaction of TREM2 with Aβ hints towards an important interplay between amyloid plaques and microglia. TREM2 disease-associated variants showed impaired binding to other physiological ligands, including phospholipids and apolipoproteins (Atagi et al., 2015; Bailey et al., 2015; Y. Wang et al., 2015; Yeh et al., 2016). However, the binding affinity of Aβ to TREM2 R47H was not decreased compared to the common TREM2 variant (Lessard et al., 2018). Contrary, another study showed reduced binding of TREM2 R47H to oligomeric Aβ42 (Zhong et al., 2018). Thus, the role of Aβ in TREM2 activation and signaling needs to be further examined and it remains to be

investigated whether disease-associated TREM2 variants exhibit deficits in binding to Aβ.

Besides binding, activation of TREM2-DAP12 signaling by Aβ treatment was confirmed by using an NFAT reporter system (Lessard et al., 2018). This system is based on the activation of transcription factor NFAT due to calcium mobilization upon stimulation of TREM2. Exposure to Aβ42 oligomers resulted in stimulation of NFAT signaling in TREM2 wt expressing cells, whereas control cells without expression of TREM2 barely responded (Lessard et al., 2018). The AD-associated TREM2 variants R47H and R62H showed a reduced activation of NFAT signaling and further confirmed the partial loss-of-function of both variants (Lessard et al., 2018). Additionally, enhanced levels of pSYK were detected in primary mouse microglia upon stimulation with 1 µM oligomeric Aβ42 for 16 h (Y. Zhao et al., 2018). However, binding of Aβ to TREM2 and subsequent stimulation of pSYK levels was ambiguous, as Y. Zhao et al. (2018) also stated the possibility of alternative, indirect pathways leading to a TREM2-dependent microglial response to Aβ exposure. Indeed, TREM2 deficiency negatively modulated the K^+ membrane inward current upon Aβ exposure and resulted in a reduced excitability of microglia as compared to TREM2 wt microglia (Y. Zhao et al., 2018). This might be explained by the previously described downregulation of K^+ channels in TREM2-deficient microglia (Ulland et al., 2017; Y. Wang et al., 2015; Y. Zhao et al., 2018). Binding of Aβ was shown to be unaltered by the deletion of TREM2 in primary mouse microglia, similarly to its phagocytic uptake, possibly due to other surface receptors expressed on microglia cells (Doens & Fernández, 2014; Y. Zhao et al., 2018). In this study, TREM2 expressing HEK 293 and iPSdMiG cells were mainly treated with Aβ for 5-30 min, which did not lead to induction of TREM2-DAP12 signaling via stimulation of pSYK levels. However, we have also treated HEK 293 cells for longer time points, supporting the results that Aβ does not directly activate TREM2 signaling via pSYK in this reporter system.

4.7 Antibody 4B2A3 has agonistic activity in TREM2-DAP12 reporter cells and iPSdMiG

Since the disease-associated variants studied here caused a partial or almost complete loss-of-function in signaling upon activation with PtdS, activation of TREM2-DAP12 signaling could potentially represent a therapeutic approach for the

treatment of neurodegenerative diseases. It seems reasonable that activation of TREM2 reduces amyloid deposition and thus has a positive effect on the progression of AD, as administration of bacterial lipopolysaccharide (LPS) activates microglia and leads to a decrease in amyloid deposits (DiCarlo et al., 2001). Moreover, agonistic antibodies have been used to activate TREM2 signaling (Cheng et al., 2018; Price et al., 2020; Schlepckow et al., 2020; S. Wang et al., 2020). In a transgenic mouse model with TREM2 R47H expression, the loss-of-myeloid cell function could be rescued by anti-TREM2 antibody application (Cheng et al., 2018). Membrane proximal signaling of TREM2 leads to survival, proliferation and phagocytosis and represents an important mechanism in the immune cell response to pathogens or, in the case of AD, amyloid deposits. Thus, the TREM2 specific antibody might also have a therapeutic effect on LOAD patients without rare variants of TREM2 (Cheng et al., 2018).

A promising candidate for the treatment of AD is the AL002 anti-TREM2 specific antibody developed by Alector. Currently, the antibody is in phase I clinical trials, including tests for safety, tolerability, pharmacokinetics, pharmacodynamics and immunogenicity (https://clinicaltrials.gov/ct2/show/NCT03635047). A variant of this antibody is AL002a, which showed to activate TREM2 signaling *in vitro* and *in vivo* upon intracranial and intraperitoneal injection of mice (Price et al., 2020). Interestingly, administration of the antibody resulted in enhanced clustering of microglia around amyloid plaques and eventually a reduced plaque deposition. A possible mode of action could be the stabilization of the TREM2 receptor on the cell surface, as in another study the anti-TREM2 antibody 4D9 specifically generated against the cleavage site for ADAM proteases in the TREM2 ectodomain resulted in enhanced microglial activity and reduced amyloid deposits (Schlepckow et al., 2020). The 4D9 antibody significantly enhanced the membrane concentration of TREM2, as it showed to prevent shedding of TREM2 by ADAM proteases (Schlepckow et al., 2020). AL002a increased pro-inflammatory and anti-inflammatory gene expression and thus possibly leads to a more homeostatic inflammatory response due to the reduction in amyloid deposits and the subsequent milder damage of the surrounding tissue (Price et al., 2020). At the behavioral level, AL002a showed to prevent progression of cognitive decline in a 5xFAD mouse model and even enhanced cognition (Price et al., 2020). Another variant of the AL002 is the mouse anti-human

TREM2 AL002c, which was studied in a transgenic mouse model expressing hTREM2 wt and R47H variants (Song et al., 2018; S. Wang et al., 2020). AL002c activated the metabolic activity and proliferation of microglia *in vivo* and had a clear effect on neurite dystrophy and behavior. However, the anti-TREM2 antibody could not change the amyloid plaque load (S. Wang et al., 2020). Several factors might contribute to the different effects of the described anti-TREM2 antibodies. The mouse models and experimental parameters used for their investigations were not comparable, as mice were analyzed at different ages and thus showed variable accumulation of amyloid plaques. Interestingly, AL002c had a more impressive impact on TREM2 activation in R47H expressing mice than in TREM2 wt mice (S. Wang et al., 2020). The authors explain this by the continuous binding and activation of TREM2 wt by endogenous ligands, whereas the R47H variant impairs ligand binding and is thus more responsive to antibody cross-linking.

The antibody 4B2A3 used in this study had agonistic effects on TREM2-DAP12 signaling. This antibody does not bind to the ligand binding domain, however, it still stimulated TREM2 signaling through binding to the stalk region of TREM2 within amino acids 131-148 and activated TREM2 through receptor cross-linking. 4B2A3 fragment $F(ab')_2$ even showed stronger stimulation of TREM2 signaling in TREM2-DAP12 reporter cells (Figure 26). This effect might be explained by the smaller size of the $F(ab')_2$ fragment. As the whole IgG is more bulky, $F(ab')_2$ could more easily reach and bind to TREM2 und thus might facilitate a stronger induction of TREM2-DAP12 signaling. Receptor cross-linking could also be confirmed with iPSdMiG expressing endogenous TREM2, albeit the overall stimulation of SYK phosphorylation was much lower as compared to the HEK 293 reporter line (Figures 33). As HEK 293 cells are overexpressing TREM2 and DAP12, cross-linking might be easier as there is presumably more protein on the cell surface. Recently, some other anti-TREM2 antibodies showed to bind to the same region of the receptor as the 4B2A3 antibody (Price et al., 2020; Schlepckow et al., 2020; S. Wang et al., 2020). Thus, the stalk region of TREM2 appears to have a high antigenicity.

Notably, besides the T66M variant, stimulation by the 4B2A3 antibody was observed for the other disease-associated variants, even though to a lower extent as compared to the stimulation of the common TREM2 variant in both, HEK 293 and iPSdMiG (Figures 27 and 34). Previously, a slight but significantly measurable conformational

change was detected for TREM2 R47H (Kober et al., 2016). This altered conformation might influence the stimulation of TREM2 R47H with the 4B2A3 antibody, even though it binds to the stalk region instead of the Ig-domain. The stalk region is directly affected by TREM2 variant G145W and possibly also H157Y, which might explain the decreased stimulation of pSYK levels by antibody treatment for these variants or affect the binding of the antibodies (Karsak et al., 2020). However, all disease-associated TREM2 variants result in a decreased cell surface expression of TREM2, most likely affecting the overall stimulation of SYK phosphorylation as compared to the common TREM2 variant.

4.8 Relevance

Several variants of TREM2 have been associated with neurological disorders in the recent years. The receptor interacts with a variety of ligands that are hallmarks of tissue damage, restricting the injured area and amongst others, inducing phagocytosis of possible harmful material. For instance, microglia have been involved in the clearance of Aβ plaques in hippocampal brain slices (Hellwig et al., 2015). The exact pathways and mechanisms of TREM2 signaling involved in the pathogenesis of neurodegenerative diseases still remain largely unknown. Therefore, selected variants of TREM2 were investigated to gain better insight into the receptor's function. All tested variants showed a partial or total loss-of-function compared to the wt TREM2 protein. The lowered surface levels potentially result from different mechanisms, including impaired transport (e.g. TREM2 T66M) or enhanced shedding by ADAM proteases (e.g. TREM2 H157Y). The TREM2 T66M variant has been identified in patients with NHD and FTD and is the cause for the disease in homozygous carriers (Guerreiro et al., 2013; Le Ber et al., 2014). Our results confirmed previous studies showing deficiency of mature TREM2 at the plasma membrane of cells expressing TREM2 T66M (Kleinberger et al., 2014; Kober et al., 2016). Consequently, missing TREM2-DAP12 signaling leads a decreased phagocytic activity of *E.coli* conjugated pHrodo particles and aggregated Aβ (Kleinberger et al., 2014). A recently established TREM2 T66M knock-in mouse revealed diminished microglial activity and glucose brain metabolism as compared to wt littermates (Kleinberger et al., 2017). Due to the lack of mature TREM2 at the cell surface, sTREM2 could not be observed in CSF or plasma (Henjum et al., 2016; Kleinberger et al., 2014) or in supernatants of TREM2 T66M expressing cells

observed by us and other groups (Kleinberger et al., 2014). Interestingly, TREM2 KO and T66M knock-in mice showed an elevated inflammatory response upon LPS challenge (Kleinberger et al., 2017; Turnbull et al., 2006), highlighting the involvement of TREM2 in inflammatory pathways.

The best-investigated TREM2 variant associated with an increased risk of developing AD is TREM2 R47H (Guerreiro et al., 2013). The R→H substitution leads to decreased ligand binding, due to a change in charge but also in conformation. In mouse models for AD, TREM2 R47H expression resulted in decreased plaque-associated microglia and consequently less dense core plaques, accompanied by increased plaque-associated neuritic dystrophy (Cheng-Hathaway et al., 2018; Yuan et al., 2016). Although TREM2 R47H is expressed at the cell surface, it shows a significant reduction of TREM2-dependent phagocytosis of fluorescent latex beads or aggregated Aβ (Kleinberger et al., 2014). Furthermore, LPS stimulation resulted in attenuated expression of pro-inflammatory cytokines in microglial cell cultures (Yin et al., 2016). It seems reasonable that, in addition to the shortened IDR in TREM2 G145W, proteolytic processing and secretion of sTREM2 was diminished and thus possibly contributes to AD-like pathology. TREM2 H157Y was differently glycosylated and indicated enhanced binding to ligands. Glycosylation is known to have an important impact on ligand binding, thus sTREM2 harboring the H157Y mutation should be particularly investigated for its effect on microglial activation.

Upon shedding by ADAM proteases, sTREM2 is released from the cell (Schlepckow et al., 2017; Thornton et al., 2017). Levels of sTREM2 in the cerebrospinal fluid showed correlation with AD pathogenesis and most studies demonstrated that sTREM2 was found to be increased in AD patients, thus representing a measure of microglial activity (Heslegrave et al., 2016; Piccio et al., 2008, 2016; Suárez‐Calvet et al., 2016). However, the increased levels of CSF sTREM2 showed variations regarding disease stages (Carmona et al., 2018; Knapskog et al., 2020). Interestingly, a very recent study compared AD patients with cognitively unimpaired controls. Here, association of increased sTREM2 with increased age and tauopathy was described, strengthening the relation of sTREM2 with tauopathy, independent of amyloid pathology and clinical symptoms (Knapskog et al., 2020). These observations showed to be in line with other studies (Heslegrave et al., 2016; Piccio

et al., 2016; Suárez-Calvet et al., 2019). In early phases of AD, levels of CSF sTREM2 for variants R47H and H157Y showed to be increased as compared to carriers of the common TREM2 variant (Suárez-Calvet et al., 2019). In the reporter cell system described here, sTREM2 levels were decreased for all disease-associated variants, suggesting that the mutations result in decreased processing of TREM2 variants by ADAM proteases and do not necessarily reflect the processing and presence of sTREM2 in AD conditions.

Notably, sTREM2 enhanced microglial survival, proliferation and migration as well as clustering around Aβ plaques and thus suggests a protective role against amyloid pathology (Zhong et al., 2017, 2019; Zhong & Chen, 2019). The production of inflammatory cytokines was stimulated in microglia upon exposure to sTREM2, which was independent of full-length TREM2 (Zhong et al., 2017). Microglia proliferation and clustering around plaques was induced by wt sTREM2 but not induced by R47H, encouraging an important protective role for sTREM2 in AD (Zhong et al., 2019). Indeed, patients with elevated levels of CSF sTREM2 developed a slower rate of decline in the hippocampal volume during AD progression (Ewers et al., 2019). In conclusion, strong evidence suggests a loss-of-function of FTD- and AD-associated TREM2 variants. Therefore, activation of TREM2-DAP12 signaling supposedly has beneficial effects on disease progression (Lewcock et al., 2020).

The reporter cell model described here represents a suitable system for studying cellular transport and metabolism of TREM2 and DAP12 and effects of disease associated TREM2 mutations. This system allows the identification and characterization of compounds that modulate TREM2 activity for the development of future therapeutic strategies for AD and other neurodegenerative diseases. It is interesting to note, that the effect of the 4B2A3 anti-TREM2 antibody is stronger than that of the physiological ligand PtdS. However, despite the strength of the signal, the effect on TREM2 disease-associated variants as compared to the common variant shows the same trend. These results indicate that the receptor conformation and glycosylation also has an impact on activation of the TREM2 signaling pathway by anti-TREM2 antibodies. Thus, 4B2A3 could be further explored as a potential therapeutic application, as it specifically activates TREM2. Nevertheless, microglia have various functions in the brain, depending on the CNS region, age of the individual and conditions of health and disease (Stratoulias et al., 2019). In mouse

models of AD, upregulation of TREM2 in early stages of amyloidogenesis showed to result in synaptic loss, whereas in later stages, the same approach had beneficial effects on disease progression (Sheng et al., 2019). The exact time point for activation of TREM2 thus needs to be determined. In addition, TREM2 is also expressed in myeloid cells of the periphery (Colonna, 2003b). Effects of TREM2 activating antibodies should be investigated in other TREM2 expressing tissues, including lung and adipose tissue (Jaitin et al., 2019; Wu et al., 2015), which might also have a beneficial effect on metabolic diseases (Deczkowska et al., 2020; Lewcock et al., 2020).

Bibliography

Alexandru, A., Jagla, W., Graubner, S., Becker, A., Bauscher, C., Kohlmann, S., Sedlmeier, R., Raber, K. A., Cynis, H., Ronicke, R., Reymann, K. G., Petrasch-Parwez, E., Hartlage-Rubsamen, M., Waniek, A., Rossner, S., Schilling, S., Osmand, A. P., Demuth, H.-U., & von Horsten, S. (2011). Selective Hippocampal Neurodegeneration in Transgenic Mice Expressing Small Amounts of Truncated A Is Induced by Pyroglutamate-A Formation. *Journal of Neuroscience*, *31*(36), 12790–12801. https://doi.org/10.1523/JNEUROSCI.1794-11.2011

Allcock, R. J. N., Barrow, A. D., Forbes, S., Beck, S., & Trowsdale, J. (2003). The human TREM gene cluster at 6p21.1 encodes both activating and inhibitory single IgV domain receptors and includes NKp44. *European Journal of Immunology*, *33*(2), 567–577. https://doi.org/10.1002/immu.200310033

Allinson, T. M. J., Parkin, E. T., Turner, A. J., & Hooper, N. M. (2003). ADAMs family members as amyloid precursor protein alpha-secretases. *Journal of Neuroscience Research*, *74*(3), 342–352. https://doi.org/10.1002/jnr.10737

Amore, A., Knott, B. C., Supekar, N. T., Shajahan, A., Azadi, P., Zhao, P., Wells, L., Linger, J. G., Hobdey, S. E., Vander Wall, T. A., Shollenberger, T., Yarbrough, J. M., Tan, Z., Crowley, M. F., Himmel, M. E., Decker, S. R., Beckham, G. T., & Taylor, L. E. (2017). Distinct roles of N- and O-glycans in cellulase activity and stability. *Proceedings of the National Academy of Sciences*, *114*(52), 13667–13672. https://doi.org/10.1073/pnas.1714249114

Appenzeller-Herzog, C., & Hauri, H.-P. (2006). The ER-Golgi intermediate compartment (ERGIC): in search of its identity and function. *Journal of Cell Science*, *119*(11), 2173–2183. https://doi.org/10.1242/jcs.03019

Atagi, Y., Liu, C.-C., Painter, M. M., Chen, X.-F., Verbeeck, C., Zheng, H., Li, X., Rademakers, R., Kang, S. S., Xu, H., Younkin, S., Das, P., Fryer, J. D., & Bu, G. (2015). Apolipoprotein E Is a Ligand for Triggering Receptor Expressed on Myeloid Cells 2 (TREM2). *Journal of Biological Chemistry*, *290*(43), 26043–26050. https://doi.org/10.1074/jbc.M115.679043

Bailey, C. C., DeVaux, L. B., & Farzan, M. (2015). The Triggering Receptor Expressed on Myeloid Cells 2 Binds Apolipoprotein E. *Journal of Biological Chemistry*, *290*(43), 26033–26042. https://doi.org/10.1074/jbc.M115.677286

Balch, W. E., Morimoto, R. I., Dillin, A., & Kelly, J. W. (2008). Adapting proteostasis for disease intervention. *Science (New York, N.Y.)*, *319*(5865), 916–919. https://doi.org/10.1126/science.1141448

Barlowe, C., & Helenius, A. (2016). Cargo Capture and Bulk Flow in the Early Secretory Pathway. *Annual Review of Cell and Developmental Biology*, *32*(1), 197–222. https://doi.org/10.1146/annurev-cellbio-111315-125016

Barlowe, C., Orci, L., Yeung, T., Hosobuchi, M., Hamamoto, S., Salama, N., Rexach, M. F., Ravazzola, M., Amherdt, M., & Schekman, R. (1994). COPII: a membrane coat formed by Sec proteins that drive vesicle budding from the endoplasmic reticulum. *Cell*, *77*(6), 895–907. https://doi.org/10.1016/0092-8674(94)90138-4

Barrow, C. J., Yasuda, A., Kenny, P. T. M., & Zagorski, M. G. (1992). Solution conformations and aggregational properties of synthetic amyloid β-peptides of Alzheimer's disease. *Journal of Molecular Biology*, *225*(4), 1075–1093. https://doi.org/10.1016/0022-2836(92)90106-T

Baumeister, W., Walz, J., Zühl, F., & Seemüller, E. (1998). The Proteasome: Paradigm of a Self-Compartmentalizing Protease. *Cell*, *92*(3), 367–380. https://doi.org/10.1016/S0092-8674(00)80929-0

Bellenguez, C., Charbonnier, C., Grenier-Boley, B., Quenez, O., Le Guennec, K., Nicolas, G., Chauhan, G., Wallon, D., Rousseau, S., Richard, A. C., Boland, A., Bourque, G., Munter, H. M., Olaso, R., Meyer, V., Rollin-Sillaire, A., Pasquier, F., Letenneur, L., Redon, R., … Jurici, S. (2017). Contribution to Alzheimer's disease risk of rare variants

in TREM2, SORL1, and ABCA7 in 1779 cases and 1273 controls. *Neurobiology of Aging*, *59*, 220.e1-220.e9. https://doi.org/10.1016/j.neurobiolaging.2017.07.001

Bence, N. F. (2001). Impairment of the Ubiquitin-Proteasome System by Protein Aggregation. *Science*, *292*(5521), 1552–1555. https://doi.org/10.1126/science.292.5521.1552

Bennett, E. P., Mandel, U., Clausen, H., Gerken, T. A., Fritz, T. A., & Tabak, L. A. (2012). Control of mucin-type O-glycosylation: A classification of the polypeptide GalNAc-transferase gene family. *Glycobiology*, *22*(6), 736–756. https://doi.org/10.1093/glycob/cwr182

Bertram, L., Lange, C., Mullin, K., Parkinson, M., Hsiao, M., Hogan, M. F., Schjeide, B. M. M., Hooli, B., DiVito, J., Ionita, I., Jiang, H., Laird, N., Moscarillo, T., Ohlsen, K. L., Elliott, K., Wang, X., Hu-Lince, D., Ryder, M., Murphy, A., … Tanzi, R. E. (2008). Genome-wide Association Analysis Reveals Putative Alzheimer's Disease Susceptibility Loci in Addition to APOE. *The American Journal of Human Genetics*, *83*(5), 623–632. https://doi.org/10.1016/j.ajhg.2008.10.008

Blobel, G., & Sabatini, D. (1971). Dissociation of Mammalian Polyribosomes into Subunits by Puromycin. *Proceedings of the National Academy of Sciences*, *68*(2), 390–394. https://doi.org/10.1073/pnas.68.2.390

Blobel, Günter, & Dobberstein, B. (1975). Transfer of proteins across membranes. I. Presence of proteolytically processed and unprocessed nascent immunoglobulin light chains on membrane-bound ribosomes of murine myeloma. *Journal of Cell Biology*, *67*(3), 835–851. https://doi.org/10.1083/jcb.67.3.835

Block, M. L., Zecca, L., & Hong, J.-S. (2007). Microglia-mediated neurotoxicity: uncovering the molecular mechanisms. *Nature Reviews Neuroscience*, *8*(1), 57–69. https://doi.org/10.1038/nrn2038

Bouchon, A., Facchetti, F., Weigand, M. A., & Colonna, M. (2001). TREM-1 amplifies inflammation and is a crucial mediator of septic shock. *Nature*, *410*(6832), 1103–1107. https://doi.org/10.1038/35074114

Boza-Serrano, A., Ruiz, R., Sanchez-Varo, R., García-Revilla, J., Yang, Y., Jimenez-Ferrer, I., Paulus, A., Wennström, M., Vilalta, A., Allendorf, D., Davila, J. C., Stegmayr, J., Jiménez, S., Roca-Ceballos, M. A., Navarro-Garrido, V., Swanberg, M., Hsieh, C. L., Real, L. M., Englund, E., … Deierborg, T. (2019). Galectin-3, a novel endogenous TREM2 ligand, detrimentally regulates inflammatory response in Alzheimer's disease. *Acta Neuropathologica*, *138*(2), 251–273. https://doi.org/10.1007/s00401-019-02013-z

Braak, H., & Braak, E. (1991). Neuropathological stageing of Alzheimer-related changes. *Acta Neuropathologica*, *82*(4), 239–259. https://doi.org/10.1007/BF00308809

Bradshaw, E. M., Chibnik, L. B., Keenan, B. T., Ottoboni, L., Raj, T., Tang, A., Rosenkrantz, L. L., Imboywa, S., Lee, M., Von Korff, A., Morris, M. C., Evans, D. A., Johnson, K., Sperling, R. A., Schneider, J. A., Bennett, D. A., & De Jager, P. L. (2013). CD33 Alzheimer's disease locus: altered monocyte function and amyloid biology. *Nature Neuroscience*, *16*(7), 848–850. https://doi.org/10.1038/nn.3435

Breuza, L., Halbeisen, R., Jenö, P., Otte, S., Barlowe, C., Hong, W., & Hauri, H.-P. (2004). Proteomics of Endoplasmic Reticulum-Golgi Intermediate Compartment (ERGIC) Membranes from Brefeldin A-treated HepG2 Cells Identifies ERGIC-32, a New Cycling Protein That Interacts with Human Erv46. *Journal of Biological Chemistry*, *279*(45), 47242–47253. https://doi.org/10.1074/jbc.M406644200

Brion, J. P., Couck, A. M., Passareiro, E., & Flament-Durand, J. (1985). Neurofibrillary tangles of Alzheimer's disease: an immunohistochemical study. *Journal of Submicroscopic Cytology*, *17*(1), 89–96.

Brodsky, J. L. (2012). Cleaning Up: ER-Associated Degradation to the Rescue. *Cell*, *151*(6), 1163–1167. https://doi.org/10.1016/j.cell.2012.11.012

Brookes, P. S., Yoon, Y., Robotham, J. L., Anders, M. W., & Sheu, S.-S. (2004). Calcium, ATP, and ROS: a mitochondrial love-hate triangle. *American Journal of Physiology-Cell Physiology*, *287*(4), C817–C833. https://doi.org/10.1152/ajpcell.00139.2004

Brosseron, F., Krauthausen, M., Kummer, M., & Heneka, M. T. (2014). Body Fluid Cytokine Levels in Mild Cognitive Impairment and Alzheimer's Disease: a Comparative Overview.

Molecular Neurobiology, *50*(2), 534–544. https://doi.org/10.1007/s12035-014-8657-1

Brown, M. C., Joaquim, T. R., Chambers, R., Onisk, D. V., Yin, F., Moriango, J. M., Xu, Y., Fancy, D. A., Crowgey, E. L., He, Y., Stave, J. W., & Lindpaintner, K. (2011). Impact of Immunization Technology and Assay Application on Antibody Performance – A Systematic Comparative Evaluation. *PLoS ONE*, *6*(12), e28718. https://doi.org/10.1371/journal.pone.0028718

Burgess, T. L., & Kelly, R. B. (1987). Constitutive and Regulated Secretion of Proteins. *Annual Review of Cell Biology*, *3*(1), 243–293. https://doi.org/10.1146/annurev.cb.03.110187.001331

Burnette, W. N. (1981). "Western Blotting": Electrophoretic transfer of proteins from sodium dodecyl sulfate-polyacrylamide gels to unmodified nitrocellulose and radiographic detection with antibody and radioiodinated protein A. *Analytical Biochemistry*, *112*(2), 195–203. https://doi.org/10.1016/0003-2697(81)90281-5

Carbon, S., Dietze, H., Lewis, S. E., Mungall, C. J., Munoz-Torres, M. C., Basu, S., Chisholm, R. L., Dodson, R. J., Fey, P., Thomas, P. D., Mi, H., Muruganujan, A., Huang, X., Poudel, S., Hu, J. C., Aleksander, S. A., McIntosh, B. K., Renfro, D. P., Siegele, D. A., … Westerfield, M. (2017). Expansion of the Gene Ontology knowledgebase and resources. *Nucleic Acids Research*, *45*(D1), D331–D338. https://doi.org/10.1093/nar/gkw1108

Carmona, S., Zahs, K., Wu, E., Dakin, K., Bras, J., & Guerreiro, R. (2018). The role of TREM2 in Alzheimer's disease and other neurodegenerative disorders. *The Lancet Neurology*, *17*(8), 721–730. https://doi.org/10.1016/S1474-4422(18)30232-1

Charles, J. F., Humphrey, M. B., Zhao, X., Quarles, E., Nakamura, M. C., Aderem, A., Seaman, W. E., & Smith, K. D. (2008). The Innate Immune Response to Salmonella enterica Serovar Typhimurium by Macrophages Is Dependent on TREM2-DAP12. *Infection and Immunity*, *76*(6), 2439–2447. https://doi.org/10.1128/IAI.00115-08

Cheng-Hathaway, P. J., Reed-Geaghan, E. G., Jay, T. R., Casali, B. T., Bemiller, S. M., Puntambekar, S. S., von Saucken, V. E., Williams, R. Y., Karlo, J. C., Moutinho, M., Xu, G., Ransohoff, R. M., Lamb, B. T., & Landreth, G. E. (2018). The Trem2 R47H variant confers loss-of-function-like phenotypes in Alzheimer's disease. *Molecular Neurodegeneration*, *13*(1), 29. https://doi.org/10.1186/s13024-018-0262-8

Cheng, Q., Danao, J., Talreja, S., Wen, P., Yin, J., Sun, N., Li, C.-M., Chui, D., Tran, D., Koirala, S., Chen, H., Foltz, I. N., Wang, S., & Sambashivan, S. (2018). TREM2-activating antibodies abrogate the negative pleiotropic effects of the Alzheimer's disease variant Trem2R47H on murine myeloid cell function. *Journal of Biological Chemistry*, *293*(32), 12620–12633. https://doi.org/10.1074/jbc.RA118.001848

Citron, M., Diehl, T. S., Gordon, G., Biere, A. L., Seubert, P., & Selkoe, D. J. (1996). Evidence that the 42- and 40-amino acid forms of amyloid protein are generated from the -amyloid precursor protein by different protease activities. *Proceedings of the National Academy of Sciences*, *93*(23), 13170–13175. https://doi.org/10.1073/pnas.93.23.13170

Colonna, M. (2003a). DAP12 signaling: from immune cells to bone modeling and brain myelination. *Journal of Clinical Investigation*, *111*(3), 313–314. https://doi.org/10.1172/JCI200317745

Colonna, M. (2003b). TREMs in the immune system and beyond. *Nature Reviews Immunology*, *3*(6), 445–453. https://doi.org/10.1038/nri1106

Colonna, M., & Wang, Y. (2016). TREM2 variants: new keys to decipher Alzheimer disease pathogenesis. *Nature Reviews Neuroscience*, *17*(4), 201–207. https://doi.org/10.1038/nrn.2016.7

Colton, C. A. (2009). Heterogeneity of Microglial Activation in the Innate Immune Response in the Brain. *Journal of Neuroimmune Pharmacology*, *4*(4), 399–418. https://doi.org/10.1007/s11481-009-9164-4

Condello, C., Yuan, P., Schain, A., & Grutzendler, J. (2015). Microglia constitute a barrier that prevents neurotoxic protofibrillar Aβ42 hotspots around plaques. *Nature Communications*, *6*(1), 6176. https://doi.org/10.1038/ncomms7176

Corder, E. H., Saunders, A. M., Risch, N. J., Strittmatter, W. J., Schmechel, D. E., Gaskell, P.

C., Rimmler, J. B., Locke, P. A., Conneally, P. M., Schmader, K. E., Small, G. W., Roses, A. D., Haines, J. L., & Pericak-Vance, M. A. (1994). Protective effect of apolipoprotein E type 2 allele for late onset Alzheimer disease. *Nature Genetics*, *7*(2), 180–184. https://doi.org/10.1038/ng0694-180

Coughlan, C. M., Walker, J. L., Cochran, J. C., Wittrup, K. D., & Brodsky, J. L. (2004). Degradation of Mutated Bovine Pancreatic Trypsin Inhibitor in the Yeast Vacuole Suggests Post-endoplasmic Reticulum Protein Quality Control. *Journal of Biological Chemistry*, *279*(15), 15289–15297. https://doi.org/10.1074/jbc.M309673200

Coux, O., Tanaka, K., & Goldberg, a L. (1996). Structure and functions of the 20S and 26S proteasomes. *Annual Review of Biochemistry*, *65*, 801–847. https://doi.org/10.1146/annurev.biochem.65.1.801

Cunningham, C. L., Martinez-Cerdeno, V., & Noctor, S. C. (2013). Microglia Regulate the Number of Neural Precursor Cells in the Developing Cerebral Cortex. *Journal of Neuroscience*, *33*(10), 4216–4233. https://doi.org/10.1523/JNEUROSCI.3441-12.2013

De Strooper, B. (2003). Aph-1, Pen-2, and Nicastrin with Presenilin Generate an Active γ-Secretase Complex. *Neuron*, *38*(1), 9–12. https://doi.org/10.1016/S0896-6273(03)00205-8

Deane, R., Wu, Z., Sagare, A., Davis, J., Du Yan, S., Hamm, K., Xu, F., Parisi, M., LaRue, B., Hu, H. W., Spijkers, P., Guo, H., Song, X., Lenting, P. J., Van Nostrand, W. E., & Zlokovic, B. V. (2004). LRP/Amyloid β-Peptide Interaction Mediates Differential Brain Efflux of Aβ Isoforms. *Neuron*, *43*(3), 333–344. https://doi.org/10.1016/j.neuron.2004.07.017

Deczkowska, A., Weiner, A., & Amit, I. (2020). The Physiology, Pathology, and Potential Therapeutic Applications of the TREM2 Signaling Pathway. *Cell*, *181*(6), 1207–1217. https://doi.org/10.1016/j.cell.2020.05.003

Deming, Y., Filipello, F., Cignarella, F., Cantoni, C., Hsu, S., Mikesell, R., Li, Z., Del-Aguila, J. L., Dube, U., Farias, F. G., Bradley, J., Budde, J., Ibanez, L., Fernandez, M. V., Blennow, K., Zetterberg, H., Heslegrave, A., Johansson, P. M., Svensson, J., … Cruchaga, C. (2019). The MS4A gene cluster is a key modulator of soluble TREM2 and Alzheimer's disease risk. *Science Translational Medicine*, *11*(505), eaau2291. https://doi.org/10.1126/scitranslmed.aau2291

Di Meco, A., Curtis, M. E., Lauretti, E., & Praticò, D. (2020). Autophagy Dysfunction in Alzheimer's Disease: Mechanistic Insights and New Therapeutic Opportunities. *Biological Psychiatry*, *87*(9), 797–807. https://doi.org/10.1016/j.biopsych.2019.05.008

DiCarlo, G., Wilcock, D., Henderson, D., Gordon, M., & Morgan, D. (2001). Intrahippocampal LPS injections reduce Abeta load in APP+PS1 transgenic mice. *Neurobiology of Aging*, *22*(6), 1007–1012. https://doi.org/10.1016/s0197-4580(01)00292-5

Doens, D., & Fernández, P. L. (2014). Microglia receptors and their implications in the response to amyloid β for Alzheimer's disease pathogenesis. *Journal of Neuroinflammation*, *11*(1), 48. https://doi.org/10.1186/1742-2094-11-48

Dyrks, T., Weidemann, A., Multhaup, G., Salbaum, J. M., Lemaire, H. G., Kang, J., Müller-Hill, B., Masters, C. L., & Beyreuther, K. (1988). Identification, transmembrane orientation and biogenesis of the amyloid A4 precursor of Alzheimer's disease. *The EMBO Journal*, *7*(4), 949–957. https://doi.org/10.1002/j.1460-2075.1988.tb02900.x

Edbauer, D., Winkler, E., Regula, J. T., Pesold, B., Steiner, H., & Haass, C. (2003). Reconstitution of γ-secretase activity. *Nature Cell Biology*, *5*(5), 486–488. https://doi.org/10.1038/ncb960

El Khoury, J. B., Moore, K. J., Means, T. K., Leung, J., Terada, K., Toft, M., Freeman, M. W., & Luster, A. D. (2003). CD36 Mediates the Innate Host Response to β-Amyloid. *Journal of Experimental Medicine*, *197*(12), 1657–1666. https://doi.org/10.1084/jem.20021546

Esch, F., Keim, P., Beattie, E., Blacher, R., Culwell, A., Oltersdorf, T., McClure, D., & Ward, P. (1990). Cleavage of amyloid beta peptide during constitutive processing of its precursor. *Science*, *248*(4959), 1122–1124. https://doi.org/10.1126/science.2111583

Ewers, M., Franzmeier, N., Suárez-Calvet, M., Morenas-Rodriguez, E., Caballero, M. A. A., Kleinberger, G., Piccio, L., Cruchaga, C., Deming, Y., Dichgans, M., Trojanowski, J. Q., Shaw, L. M., Weiner, M. W., & Haass, C. (2019). Increased soluble TREM2 in

cerebrospinal fluid is associated with reduced cognitive and clinical decline in Alzheimer's disease. *Science Translational Medicine*, *11*(507), eaav6221. https://doi.org/10.1126/scitranslmed.aav6221

Fadok, V. A., Voelker, D. R., Campbell, P. A., Cohen, J. J., Bratton, D. L., & Henson, P. M. (1992). Exposure of phosphatidylserine on the surface of apoptotic lymphocytes triggers specific recognition and removal by macrophages. *Journal of Immunology*, *148*(7), 2207–2216.

Fan, T., Huang, Z., Wang, W., Zhang, B., Xu, Y., Mao, Z., Chen, L., Hu, H., & Geng, Q. (2018). Proteasome inhibition promotes autophagy and protects from endoplasmic reticulum stress in rat alveolar macrophages exposed to hypoxia-reoxygenation injury. *Journal of Cellular Physiology*, *233*(10), 6748–6758. https://doi.org/10.1002/jcp.26516

Fantin, A., Vieira, J. M., Gestri, G., Denti, L., Schwarz, Q., Prykhozhij, S., Peri, F., Wilson, S. W., & Ruhrberg, C. (2010). Tissue macrophages act as cellular chaperones for vascular anastomosis downstream of VEGF-mediated endothelial tip cell induction. *Blood*, *116*(5), 829–840. https://doi.org/10.1182/blood-2009-12-257832

Farfara, D., Trudler, D., Segev-Amzaleg, N., Galron, R., Stein, R., & Frenkel, D. (2011). γ-Secretase component presenilin is important for microglia β-amyloid clearance. *Annals of Neurology*, *69*(1), 170–180. https://doi.org/10.1002/ana.22191

Farris, W., Schütz, S. G., Cirrito, J. R., Shankar, G. M., Sun, X., George, A., Leissring, M. A., Walsh, D. M., Qiu, W. Q., Holtzman, D. M., & Selkoe, D. J. (2007). Loss of Neprilysin Function Promotes Amyloid Plaque Formation and Causes Cerebral Amyloid Angiopathy. *The American Journal of Pathology*, *171*(1), 241–251. https://doi.org/10.2353/ajpath.2007.070105

Fernández-Vizarra, P., Fernández, A. P., Castro-Blanco, S., Encinas, J. M., Serrano, J., Bentura, M. L., Muñoz, P., Martínez-Murillo, R., & Rodrigo, J. (2004). Expression of nitric oxide system in clinically evaluated cases of Alzheimer's disease. *Neurobiology of Disease*, *15*(2), 287–305. https://doi.org/10.1016/j.nbd.2003.10.010

Feuerbach, D., Schindler, P., Barske, C., Joller, S., Beng-Louka, E., Worringer, K. A., Kommineni, S., Kaykas, A., Ho, D. J., Ye, C., Welzenbach, K., Elain, G., Klein, L., Brzak, I., Mir, A. K., Farady, C. J., Aichholz, R., Popp, S., George, N., & Neumann, U. (2017). ADAM17 is the main sheddase for the generation of human triggering receptor expressed in myeloid cells (hTREM2) ectodomain and cleaves TREM2 after Histidine 157. *Neuroscience Letters*, *660*, 109–114. https://doi.org/10.1016/j.neulet.2017.09.034

Forno, L. S. (1996). Neuropathology of Parkinson's Disease. *Journal of Neuropathology and Experimental Neurology*, *55*(3), 259–272. https://doi.org/10.1097/00005072-199603000-00001

Forsström, B., Bisławska Axnäs, B., Rockberg, J., Danielsson, H., Bohlin, A., & Uhlen, M. (2015). Dissecting Antibodies with Regards to Linear and Conformational Epitopes. *PLoS ONE*, *10*(3), e0121673. https://doi.org/10.1371/journal.pone.0121673

Frautschy, S. A., Yang, F., Irrizarry, M., Hyman, B., Saido, T. C., Hsiao, K., & Cole, G. M. (1998). Microglial response to amyloid plaques in APPsw transgenic mice. *The American Journal of Pathology*, *152*(1), 307–317.

Freeze, H. H., & Kranz, C. (2010). Endoglycosidase and Glycoamidase Release of N-Linked Glycans. *Current Protocols in Molecular Biology*, *89*(1). https://doi.org/10.1002/0471142727.mb1713as89

Fukuda, M., Dell, A., Oates, J. E., & Fukuda, M. N. (1984). Structure of branched lactosaminoglycan, the carbohydrate moiety of band 3 isolated from adult human erythrocytes. *Journal of Biological Chemistry*, *259*(13), 8260–8273. https://doi.org/10.1016/S0021-9258(17)39722-3

Furukawa, K., Sopher, B. L., Rydel, R. E., Begley, J. G., Pham, D. G., Martin, G. M., Fox, M., & Mattson, M. P. (2002). Increased Activity-Regulating and Neuroprotective Efficacy of α-Secretase-Derived Secreted Amyloid Precursor Protein Conferred by a C-Terminal Heparin-Binding Domain. *Journal of Neurochemistry*, *67*(5), 1882–1896. https://doi.org/10.1046/j.1471-4159.1996.67051882.x

Ge, P., Zhang, J., Wang, X., Meng, F., Li, W., Luan, Y., Ling, F., & Luo, Y. (2009). Inhibition of autophagy induced by proteasome inhibition increases cell death in human SHG-44

glioma cells. *Acta Pharmacologica Sinica*, *30*(7), 1046–1052. https://doi.org/10.1038/aps.2009.71

Gibson, D. G., Young, L., Chuang, R.-Y., Venter, J. C., Hutchison, C. A., & Smith, H. O. (2009). Enzymatic assembly of DNA molecules up to several hundred kilobases. *Nature Methods*, *6*(5), 343–345. https://doi.org/10.1038/nmeth.1318

Ginhoux, F., Greter, M., Leboeuf, M., Nandi, S., See, P., Gokhan, S., Mehler, M. F., Conway, S. J., Ng, L. G., Stanley, E. R., Samokhvalov, I. M., & Merad, M. (2010). Fate Mapping Analysis Reveals That Adult Microglia Derive from Primitive Macrophages. *Science*, *330*(6005), 841–845. https://doi.org/10.1126/science.1194637

Glebov, K., Wunderlich, P., Karaca, I., & Walter, J. (2016). Functional involvement of γ-secretase in signaling of the triggering receptor expressed on myeloid cells-2 (TREM2). *Journal of Neuroinflammation*, *13*(1), 17. https://doi.org/10.1186/s12974-016-0479-9

Glickman, M. H., & Ciechanover, A. (2002). The Ubiquitin-Proteasome Proteolytic Pathway: Destruction for the Sake of Construction. *Physiological Reviews*, *82*(2), 373–428. https://doi.org/10.1152/physrev.00027.2001

Goate, A., Chartier-Harlin, M.-C., Mullan, M., Brown, J., Crawford, F., Fidani, L., Giuffra, L., Haynes, A., Irving, N., James, L., Mant, R., Newton, P., Rooke, K., Roques, P., Talbot, C., Pericak-Vance, M., Roses, A., Williamson, R., Rossor, M., … Hardy, J. (1991). Segregation of a missense mutation in the amyloid precursor protein gene with familial Alzheimer's disease. *Nature*, *349*(6311), 704–706. https://doi.org/10.1038/349704a0

Goldberg, D., Bern, M., North, S. J., Haslam, S. M., & Dell, A. (2009). Glycan family analysis for deducing N-glycan topology from single MS. *Bioinformatics*, *25*(3), 365–371. https://doi.org/10.1093/bioinformatics/btn636

Grant, B. D., & Donaldson, J. G. (2009). Pathways and mechanisms of endocytic recycling. *Nature Reviews Molecular Cell Biology*, *10*(9), 597–608. https://doi.org/10.1038/nrm2755

Groll, M., Bajorek, M., Köhler, A., Moroder, L., Rubin, D. M., Huber, R., Glickman, M. H., & Finley, D. (2000). A gated channel into the proteasome core particle. *Nature Structural Biology*, *7*(11), 1062–1067. https://doi.org/10.1038/80992

Grundke-Iqbal, I., Iqbal, K., Tung, Y.-C., Quinlan, M., Wisniewski, H., & Binder, L. (1987). Abnormal phosphorylation of the microtubule-associated protein? (tau) in Alzheimer cytoskeletal pathology. *Alzheimer Disease & Associated Disorders*, *1*(3), 202. https://doi.org/10.1097/00002093-198701030-00020

Guerreiro, R., & Hardy, J. (2013). TREM2 and Neurodegenerative Disease. *New England Journal of Medicine*, *369*(16), 1564–1570. https://doi.org/10.1056/NEJMc1306509

Guerreiro, R., Wojtas, A., Bras, J., Carrasquillo, M., Rogaeva, E., Majounie, E., Cruchaga, C., Sassi, C., Kauwe, J. S. K., Younkin, S., Hazrati, L., Collinge, J., Pocock, J., Lashley, T., Williams, J., Lambert, J.-C., Amouyel, P., Goate, A., Rademakers, R., … Hardy, J. (2013). TREM2 Variants in Alzheimer's Disease. *New England Journal of Medicine*, *368*(2), 117–127. https://doi.org/10.1056/NEJMoa1211851

Güntert, A., Döbeli, H., & Bohrmann, B. (2006). High sensitivity analysis of amyloid-beta peptide composition in amyloid deposits from human and PS2APP mouse brain. *Neuroscience*, *143*(2), 461–475. https://doi.org/10.1016/j.neuroscience.2006.08.027

Haass, C., & De Strooper, B. (1999). The Presenilins in Alzheimer's Disease--Proteolysis Holds the Key. *Science*, *286*(5441), 916–919. https://doi.org/10.1126/science.286.5441.916

Haass, C., Hung, A. Y., Schlossmacher, M. G., Teplow, D. B., & Selkoe, D. J. (1993). beta-Amyloid peptide and a 3-kDa fragment are derived by distinct cellular mechanisms. *Journal of Biological Chemistry*, *268*(5), 3021–3024. https://doi.org/10.1016/S0021-9258(18)53650-4

Haass, C., & Selkoe, D. J. (2007). Soluble protein oligomers in neurodegeneration: lessons from the Alzheimer's amyloid β-peptide. *Nature Reviews Molecular Cell Biology*, *8*(2), 101–112. https://doi.org/10.1038/nrm2101

Hakola, H. P. A., Järvi, O. H., & Sourander, P. (2009). Osteodysplasia Polycystica Hereditaria Combined with Sclerosing Leucoencephalopathy. *Acta Neurologica Scandinavica*, *46*(S43), 79–80. https://doi.org/10.1111/j.1600-0404.1970.tb02161.x

Hammond, C., & Helenius, A. (1994). Quality control in the secretory pathway: retention of a misfolded viral membrane glycoprotein involves cycling between the ER, intermediate compartment, and Golgi apparatus. *Journal of Cell Biology*, *126*(1), 41–52. https://doi.org/10.1083/jcb.126.1.41

Hara, T., Nakamura, K., Matsui, M., Yamamoto, A., Nakahara, Y., Suzuki-Migishima, R., Yokoyama, M., Mishima, K., Saito, I., Okano, H., & Mizushima, N. (2006). Suppression of basal autophagy in neural cells causes neurodegenerative disease in mice. *Nature*, *441*(7095), 885–889. https://doi.org/10.1038/nature04724

Hardy, J., & Higgins, G. (1992). Alzheimer's disease: the amyloid cascade hypothesis. *Science*, *256*(5054), 184–185. https://doi.org/10.1126/science.1566067

He, W., & Barrow, C. J. (1999). The Aβ 3-Pyroglutamyl and 11-Pyroglutamyl Peptides Found in Senile Plaque Have Greater β-Sheet Forming and Aggregation Propensities in Vitro than Full-Length Aβ. *Biochemistry*, *38*(33), 10871–10877. https://doi.org/10.1021/bi990563r

Hebert, L. E., Weuve, J., Scherr, P. A., & Evans, D. A. (2013). Alzheimer disease in the United States (2010-2050) estimated using the 2010 census. *Neurology*, *80*(19), 1778–1783. https://doi.org/10.1212/WNL.0b013e31828726f5

Heinemeyer, W., Ramos, P. C., & Dohmen, R. J. (2004). Ubiquitin-proteasome system. *Cellular and Molecular Life Sciences*, *61*(13), 1562–1578. https://doi.org/10.1007/s00018-004-4130-z

Helenius, A., & Aebi, M. (2001). Intracellular Functions of N-Linked Glycans. *Science*, *291*(5512), 2364–2369. https://doi.org/10.1126/science.291.5512.2364

Helenius, A., & Aebi, M. (2004). Roles of N-Linked Glycans in the Endoplasmic Reticulum. *Annual Review of Biochemistry*, *73*(1), 1019–1049. https://doi.org/10.1146/annurev.biochem.73.011303.073752

Hellwig, S., Masuch, A., Nestel, S., Katzmarski, N., Meyer-Luehmann, M., & Biber, K. (2015). Forebrain microglia from wild-type but not adult 5xFAD mice prevent amyloid-β plaque formation in organotypic hippocampal slice cultures. *Scientific Reports*, *5*(1), 14624. https://doi.org/10.1038/srep14624

Heneka, M. T., Carson, M. J., Khoury, J. El, Landreth, G. E., Brosseron, F., Feinstein, D. L., Jacobs, A. H., Wyss-Coray, T., Vitorica, J., Ransohoff, R. M., Herrup, K., Frautschy, S. A., Finsen, B., Brown, G. C., Verkhratsky, A., Yamanaka, K., Koistinaho, J., Latz, E., Halle, A., … Kummer, M. P. (2015). Neuroinflammation in Alzheimer's disease. *The Lancet Neurology*, *14*(4), 388–405. https://doi.org/10.1016/S1474-4422(15)70016-5

Heneka, M. T., Wiesinger, H., Dumitrescu-Ozimek, L., Riederer, P., Feinstein, D. L., & Klockgether, T. (2001). Neuronal and Glial Coexpression of Argininosuccinate Synthetase and Inducible Nitric Oxide Synthase in Alzheimer Disease. *Journal of Neuropathology & Experimental Neurology*, *60*(9), 906–916. https://doi.org/10.1093/jnen/60.9.906

Henjum, K., Almdahl, I. S., Årskog, V., Minthon, L., Hansson, O., Fladby, T., & Nilsson, L. N. G. (2016). Cerebrospinal fluid soluble TREM2 in aging and Alzheimer's disease. *Alzheimer's Research & Therapy*, *8*(1), 17. https://doi.org/10.1186/s13195-016-0182-1

Heppner, F. L., Ransohoff, R. M., & Becher, B. (2015). Immune attack: the role of inflammation in Alzheimer disease. *Nature Reviews Neuroscience*, *16*(6), 358–372. https://doi.org/10.1038/nrn3880

Hershko, a, & Ciechanover, a. (1992). The ubiquitin system for protein degradation. *Annual Review of Biochemistry*, *61*, 761–807. https://doi.org/10.1146/annurev.biochem.61.1.761

Heslegrave, A., Heywood, W., Paterson, R., Magdalinou, N., Svensson, J., Johansson, P., Öhrfelt, A., Blennow, K., Hardy, J., Schott, J., Mills, K., & Zetterberg, H. (2016). Increased cerebrospinal fluid soluble TREM2 concentration in Alzheimer's disease. *Molecular Neurodegeneration*, *11*(1), 3. https://doi.org/10.1186/s13024-016-0071-x

Hippius, H., & Neundörfer, G. (2003). The discovery of Alzheimer's disease. *Dialogues in Clinical Neuroscience*, *5*(1), 101–108. https://doi.org/10.31887/DCNS.2003.5.1/hhippius

Hollingworth, P., Harold, D., Sims, R., Gerrish, A., Lambert, J.-C., Carrasquillo, M. M., Abraham, R., Hamshere, M. L., Pahwa, J. S., Moskvina, V., Dowzell, K., Jones, N.,

Stretton, A., Thomas, C., Richards, A., Ivanov, D., Widdowson, C., Chapman, J., Lovestone, S., … Williams, J. (2011). Common variants at ABCA7, MS4A6A/MS4A4E, EPHA1, CD33 and CD2AP are associated with Alzheimer's disease. *Nature Genetics*, *43*(5), 429–435. https://doi.org/10.1038/ng.803

Hopkins, C. R., Miller, K., & Beardmore, J. M. (1985). Receptor-Mediated Endocytosis of Transferrin and Epidermal Growth Factor Receptors: A Comparison of Constitutive and Ligand-Induced Uptake. *Journal of Cell Science*, *1985*(Supplement_3), 173–186. https://doi.org/10.1242/jcs.1985.Supplement_3.17

Hou, L., Kang, I., Marchant, R. E., & Zagorski, M. G. (2002). Methionine 35 Oxidation Reduces Fibril Assembly of the Amyloid Aβ-(1–42) Peptide of Alzheimer's Disease. *Journal of Biological Chemistry*, *277*(43), 40173–40176. https://doi.org/10.1074/jbc.C200338200

Hsieh, C. L., Koike, M., Spusta, S. C., Niemi, E. C., Yenari, M., Nakamura, M. C., & Seaman, W. E. (2009). A role for TREM2 ligands in the phagocytosis of apoptotic neuronal cells by microglia. *Journal of Neurochemistry*, *109*(4), 1144–1156. https://doi.org/10.1111/j.1471-4159.2009.06042.x

Humphrey, M. B., Xing, J., & Titus, A. (2015). The TREM2-DAP12 signaling pathway in Nasu-Hakola disease: a molecular genetics perspective. *Research and Reports in Biochemistry*, *5*, 89. https://doi.org/10.2147/RRBC.S58057

Iwata, N., Tsubuki, S., Takaki, Y., Shirotani, K., Lu, B., Gerard, N. P., Gerard, C., Hama, E., Lee, H. J., & Saido, T. C. (2001). Metabolic Regulation of Brain Abeta by Neprilysin. *Science*, *292*(5521), 1550–1552. https://doi.org/10.1126/science.1059946

Iwata, N., Tsubuki, S., Takaki, Y., Watanabe, K., Sekiguchi, M., Hosoki, E., Kawashima-Morishima, M., Lee, H.-J., Hama, E., Sekine-Aizawa, Y., & Saido, T. C. (2000). Identification of the major Aβ1–42-degrading catabolic pathway in brain parenchyma: Suppression leads to biochemical and pathological deposition. *Nature Medicine*, *6*(2), 143–150. https://doi.org/10.1038/72237

Jaeger, P. A., Pickford, F., Sun, C.-H., Lucin, K. M., Masliah, E., & Wyss-Coray, T. (2010). Regulation of Amyloid Precursor Protein Processing by the Beclin 1 Complex. *PLoS ONE*, *5*(6), e11102. https://doi.org/10.1371/journal.pone.0011102

Jaitin, D. A., Adlung, L., Thaiss, C. A., Weiner, A., Li, B., Descamps, H., Lundgren, P., Bleriot, C., Liu, Z., Deczkowska, A., Keren-Shaul, H., David, E., Zmora, N., Eldar, S. M., Lubezky, N., Shibolet, O., Hill, D. A., Lazar, M. A., Colonna, M., … Amit, I. (2019). Lipid-Associated Macrophages Control Metabolic Homeostasis in a Trem2-Dependent Manner. *Cell*, *178*(3), 686-698.e14. https://doi.org/10.1016/j.cell.2019.05.054

Jäkel, S., & Dimou, L. (2017). Glial Cells and Their Function in the Adult Brain: A Journey through the History of Their Ablation. *Frontiers in Cellular Neuroscience*, *11*, 24. https://doi.org/10.3389/fncel.2017.00024

Jansen, I. E., Savage, J. E., Watanabe, K., Bryois, J., Williams, D. M., Steinberg, S., Sealock, J., Karlsson, I. K., Hägg, S., Athanasiu, L., Voyle, N., Proitsi, P., Witoelar, A., Stringer, S., Aarsland, D., Almdahl, I. S., Andersen, F., Bergh, S., Bettella, F., … Posthuma, D. (2019). Genome-wide meta-analysis identifies new loci and functional pathways influencing Alzheimer's disease risk. *Nature Genetics*, *51*(3), 404–413. https://doi.org/10.1038/s41588-018-0311-9

Jarrett, J. T., Berger, E. P., & Lansbury, P. T. (1993). The C-terminus of the beta protein is critical in amyloidogenesis. *Annals of the New York Academy of Sciences*, *695*(1), 144–148. https://doi.org/10.1111/j.1749-6632.1993.tb23043.x

Jay, T. R., von Saucken, V. E., & Landreth, G. E. (2017). TREM2 in Neurodegenerative Diseases. *Molecular Neurodegeneration*, *12*(1), 56. https://doi.org/10.1186/s13024-017-0197-5

Jiang, T., Hou, J.-K., Gao, Q., Yu, J.-T., Zhou, J.-S., Zhao, H.-D., & Zhang, Y.-D. (2016). TREM2 p.H157Y Variant and the Risk of Alzheimer's Disease: A Meta-Analysis Involving 14,510 Subjects. *Current Neurovascular Research*, *13*(4), 318–320. https://doi.org/10.2174/1567202613666160808095530

Jiang, T., Tan, L., Chen, Q., Tan, M.-S., Zhou, J.-S., Zhu, X.-C., Lu, H., Wang, H.-F., Zhang, Y.-D., & Yu, J.-T. (2016). A rare coding variant in TREM2 increases risk for Alzheimer's

disease in Han Chinese. *Neurobiology of Aging*, *42*, 217.e1-217.e3. https://doi.org/10.1016/j.neurobiolaging.2016.02.023

Jin, S. C., Benitez, B. A., Karch, C. M., Cooper, B., Skorupa, T., Carrell, D., Norton, J. B., Hsu, S., Harari, O., Cai, Y., Bertelsen, S., Goate, A. M., & Cruchaga, C. (2014). Coding variants in TREM2 increase risk for Alzheimer's disease. *Human Molecular Genetics*, *23*(21), 5838–5846. https://doi.org/10.1093/hmg/ddu277

Jonsson, T., Stefansson, H., Steinberg, S., Jonsdottir, I., Jonsson, P. V., Snaedal, J., Bjornsson, S., Huttenlocher, J., Levey, A. I., Lah, J. J., Rujescu, D., Hampel, H., Giegling, I., Andreassen, O. A., Engedal, K., Ulstein, I., Djurovic, S., Ibrahim-Verbaas, C., Hofman, A., … Stefansson, K. (2013). Variant of TREM2 Associated with the Risk of Alzheimer's Disease. *New England Journal of Medicine*, *368*(2), 107–116. https://doi.org/10.1056/NEJMoa1211103

Jovic, M., Sharma, M., Rahajeng, J., & Caplan, S. (2010). The early endosome: a busy sorting station for proteins at the crossroads. *Histology and Histopathology*, *25*(1), 99–112. https://doi.org/10.14670/HH-25.99

Kabeya, Y., Mizushima, N., Ueno, T., Yamamoto, A., Kirisako, T., Noda, T., Kominami, E., Ohsumi, Y., & Yoshimori, T. (2003). Corrigenda. *The EMBO Journal*, *22*(17), 4577–4577. https://doi.org/10.1093/emboj/cdg454

Kaneko, M., Sano, K., Nakayama, J., & Amano, N. (2010). Nasu-Hakola disease: The first case reported by Nasu and review. *Neuropathology*, *30*(5), 463–470. https://doi.org/10.1111/j.1440-1789.2010.01127.x

Kang, J., Lemaire, H.-G., Unterbeck, A., Salbaum, J. M., Masters, C. L., Grzeschik, K.-H., Multhaup, G., Beyreuther, K., & Müller-Hill, B. (1987). The precursor of Alzheimer's disease amyloid A4 protein resembles a cell-surface receptor. *Nature*, *325*(6106), 733–736. https://doi.org/10.1038/325733a0

Karsak, M., Glebov, K., Scheffold, M., Bajaj, T., Kawalia, A., Karaca, I., Rading, S., Kornhuber, J., Peters, O., Diez-Fairen, M., Frölich, L., Hüll, M., Wiltfang, J., Scherer, M., Riedel-Heller, S., Schneider, A., Heneka, M. T., Fliessbach, K., Sharaf, A., … Ramirez, A. (2020). A rare heterozygous TREM2 coding variant identified in familial clustering of dementia affects an intrinsically disordered protein region and function of TREM2. *Human Mutation*, *41*(1), 169–181. https://doi.org/10.1002/humu.23904

Kelly, R. (1985). Pathways of protein secretion in eukaryotes. *Science*, *230*(4721), 25–32. https://doi.org/10.1126/science.2994224

Kemmerling, N., Wunderlich, P., Theil, S., Linnartz-Gerlach, B., Hersch, N., Hoffmann, B., Heneka, M. T., de Strooper, B., Neumann, H., & Walter, J. (2017). Intramembranous processing by γ-secretase regulates reverse signaling of ephrin-B2 in migration of microglia. *Glia*, *65*(7), 1103–1118. https://doi.org/10.1002/glia.23147

Khaminets, A., Behl, C., & Dikic, I. (2016). Ubiquitin-Dependent And Independent Signals In Selective Autophagy. *Trends in Cell Biology*, *26*(1), 6–16. https://doi.org/10.1016/j.tcb.2015.08.010

Kim, G. H., Kim, J. E., Rhie, S. J., & Yoon, S. (2015). The Role of Oxidative Stress in Neurodegenerative Diseases. *Experimental Neurobiology*, *24*(4), 325–340. https://doi.org/10.5607/en.2015.24.4.325

Kleinberger, G., Brendel, M., Mracsko, E., Wefers, B., Groeneweg, L., Xiang, X., Focke, C., Deußing, M., Suárez-Calvet, M., Mazaheri, F., Parhizkar, S., Pettkus, N., Wurst, W., Feederle, R., Bartenstein, P., Mueggler, T., Arzberger, T., Knuesel, I., Rominger, A., & Haass, C. (2017). The FTD-like syndrome causing TREM2 T66M mutation impairs microglia function, brain perfusion, and glucose metabolism. *The EMBO Journal*, *36*(13), 1837–1853. https://doi.org/10.15252/embj.201796516

Kleinberger, G., Yamanishi, Y., Suarez-Calvet, M., Czirr, E., Lohmann, E., Cuyvers, E., Struyfs, H., Pettkus, N., Wenninger-Weinzierl, A., Mazaheri, F., Tahirovic, S., Lleo, A., Alcolea, D., Fortea, J., Willem, M., Lammich, S., Molinuevo, J. L., Sanchez-Valle, R., Antonell, A., … Haass, C. (2014). TREM2 mutations implicated in neurodegeneration impair cell surface transport and phagocytosis. *Science Translational Medicine*, *6*(243), 243ra86-243ra86. https://doi.org/10.1126/scitranslmed.3009093

Klesney-Tait, J., Turnbull, I. R., & Colonna, M. (2006). The TREM receptor family and signal

integration. *Nature Immunology*, *7*(12), 1266–1273. https://doi.org/10.1038/ni1411

Klionsky, D. J. (2007). Autophagy: from phenomenology to molecular understanding in less than a decade. *Nature Reviews Molecular Cell Biology*, *8*(11), 931–937. https://doi.org/10.1038/nrm2245

Klionsky, D. J., Baehrecke, E. H., Brumell, J. H., Chu, C. T., Codogno, P., Cuervo, A. M., Debnath, J., Deretic, V., Elazar, Z., Eskelinen, E.-L., Finkbeiner, S., Fueyo-Margareto, J., Gewirtz, D., Jäättelä, M., Kroemer, G., Levine, B., Melia, T. J., Mizushima, N., Rubinsztein, D. C., … Tooze, S. A. (2011). A comprehensive glossary of autophagy-related molecules and processes (2nd edition). *Autophagy*, *7*(11), 1273–1294. https://doi.org/10.4161/auto.7.11.17661

Klionsky, D. J., & Emr, S. D. (2000). Autophagy as a regulated pathway of cellular degradation. *Science (New York, N.Y.)*, *290*(5497), 1717–1721. https://doi.org/10.1126/science.290.5497.1717

Klumperman, J. (2011). Architecture of the Mammalian Golgi. *Cold Spring Harbor Perspectives in Biology*, *3*(7), a005181–a005181. https://doi.org/10.1101/cshperspect.a005181

Knapskog, A.-B., Henjum, K., Idland, A.-V., Eldholm, R. S., Persson, K., Saltvedt, I., Watne, L. O., Engedal, K., & Nilsson, L. N. G. (2020). Cerebrospinal fluid sTREM2 in Alzheimer's disease: comparisons between clinical presentation and AT classification. *Scientific Reports*, *10*(1), 15886. https://doi.org/10.1038/s41598-020-72878-8

Knoblich, K., Park, S., Lutfi, M., van 't Hag, L., Conn, C. E., Seabrook, S. A., Newman, J., Czabotar, P. E., Im, W., Call, M. E., & Call, M. J. (2015). Transmembrane Complexes of DAP12 Crystallized in Lipid Membranes Provide Insights into Control of Oligomerization in Immunoreceptor Assembly. *Cell Reports*, *11*(8), 1184–1192. https://doi.org/10.1016/j.celrep.2015.04.045

Kober, D. L., Alexander-Brett, J. M., Karch, C. M., Cruchaga, C., Colonna, M., Holtzman, M. J., & Brett, T. J. (2016). Neurodegenerative disease mutations in TREM2 reveal a functional surface and distinct loss-of-function mechanisms. *ELife*, *5*, 1–24. https://doi.org/10.7554/eLife.20391

Komatsu, M., Waguri, S., Chiba, T., Murata, S., Iwata, J., Tanida, I., Ueno, T., Koike, M., Uchiyama, Y., Kominami, E., & Tanaka, K. (2006). Loss of autophagy in the central nervous system causes neurodegeneration in mice. *Nature*, *441*(7095), 880–884. https://doi.org/10.1038/nature04723

Köpke, E., Tung, Y. C., Shaikh, S., Alonso, A. C., Iqbal, K., & Grundke-Iqbal, I. (1993). Microtubule-associated protein tau. Abnormal phosphorylation of a non-paired helical filament pool in Alzheimer disease. *Journal of Biological Chemistry*, *268*(32), 24374–24384. https://doi.org/10.1016/S0021-9258(20)80536-5

Korolchuk, V. I., Mansilla, A., Menzies, F. M., & Rubinsztein, D. C. (2009). Autophagy Inhibition Compromises Degradation of Ubiquitin-Proteasome Pathway Substrates. *Molecular Cell*, *33*(4), 517–527. https://doi.org/10.1016/j.molcel.2009.01.021

Kosik, K. S., Joachim, C. L., & Selkoe, D. J. (1986). Microtubule-associated protein tau (tau) is a major antigenic component of paired helical filaments in Alzheimer disease. *Proceedings of the National Academy of Sciences*, *83*(11), 4044–4048. https://doi.org/10.1073/pnas.83.11.4044

Krabbe, G., Halle, A., Matyash, V., Rinnenthal, J. L., Eom, G. D., Bernhardt, U., Miller, K. R., Prokop, S., Kettenmann, H., & Heppner, F. L. (2013). Functional Impairment of Microglia Coincides with Beta-Amyloid Deposition in Mice with Alzheimer-Like Pathology. *PLoS ONE*, *8*(4), e60921. https://doi.org/10.1371/journal.pone.0060921

Kraft, C., & Martens, S. (2012). Mechanisms and regulation of autophagosome formation. In *Current Opinion in Cell Biology* (Vol. 24, Issue 4, pp. 496–501). https://doi.org/10.1016/j.ceb.2012.05.001

Kraft, C., Reggiori, F., & Peter, M. (2009). Selective types of autophagy in yeast. *Biochimica et Biophysica Acta (BBA) - Molecular Cell Research*, *1793*(9), 1404–1412. https://doi.org/10.1016/j.bbamcr.2009.02.006

Krstic, D., Madhusudan, A., Doehner, J., Vogel, P., Notter, T., Imhof, C., Manalastas, A., Hilfiker, M., Pfister, S., Schwerdel, C., Riether, C., Meyer, U., & Knuesel, I. (2012).

Systemic immune challenges trigger and drive Alzheimer-like neuropathology in mice. *Journal of Neuroinflammation*, *9*(1), 699. https://doi.org/10.1186/1742-2094-9-151

Kruse, K. B., Brodsky, J. L., & McCracken, A. A. (2006). Characterization of an ERAD Gene as VPS30/ATG6 Reveals Two Alternative and Functionally Distinct Protein Quality Control Pathways: One for Soluble Z Variant of Human α-1 Proteinase Inhibitor (A1PiZ) and Another for Aggregates of A1PiZ. *Molecular Biology of the Cell*, *17*(1), 203–212. https://doi.org/10.1091/mbc.e04-09-0779

Kumar, S., Rezaei-Ghaleh, N., Terwel, D., Thal, D. R., Richard, M., Hoch, M., Mc Donald, J. M., Wüllner, U., Glebov, K., Heneka, M. T., Walsh, D. M., Zweckstetter, M., & Walter, J. (2011). Extracellular phosphorylation of the amyloid β-peptide promotes formation of toxic aggregates during the pathogenesis of Alzheimer's disease. *The EMBO Journal*, *30*(11), 2255–2265. https://doi.org/10.1038/emboj.2011.138

Kumar, S., Wirths, O., Stüber, K., Wunderlich, P., Koch, P., Theil, S., Rezaei-Ghaleh, N., Zweckstetter, M., Bayer, T. A., Brüstle, O., Thal, D. R., & Walter, J. (2016). Phosphorylation of the amyloid β-peptide at Ser26 stabilizes oligomeric assembly and increases neurotoxicity. *Acta Neuropathologica*, *131*(4), 525–537. https://doi.org/10.1007/s00401-016-1546-0

Kumar, S., Wirths, O., Theil, S., Gerth, J., Bayer, T. A., & Walter, J. (2013). Early intraneuronal accumulation and increased aggregation of phosphorylated Abeta in a mouse model of Alzheimer's disease. *Acta Neuropathologica*, *125*(5), 699–709. https://doi.org/10.1007/s00401-013-1107-8

Kummer, M. P., & Heneka, M. T. (2014). Truncated and modified amyloid-beta species. *Alzheimer's Research & Therapy*, *6*(3), 28. https://doi.org/10.1186/alzrt258

Kummer, M. P., Hermes, M., Delekarte, A., Hammerschmidt, T., Kumar, S., Terwel, D., Walter, J., Pape, H.-C., König, S., Roeber, S., Jessen, F., Klockgether, T., Korte, M., & Heneka, M. T. (2011). Nitration of Tyrosine 10 Critically Enhances Amyloid β Aggregation and Plaque Formation. *Neuron*, *71*(5), 833–844. https://doi.org/10.1016/j.neuron.2011.07.001

Kyrychenko, V. O., Nagibin, V. S., Tumanovska, L. V., Pashevin, D. O., Gurianova, V. L., Moibenko, A. A., Dosenko, V. E., & Klionsky, D. J. (2014). Knockdown of PSMB7 Induces Autophagy in Cardiomyocyte Cultures: Possible Role in Endoplasmic Reticulum Stress. *Pathobiology*, *81*(1), 8–14. https://doi.org/10.1159/000350704

LaFerla, F. M., Green, K. N., & Oddo, S. (2007). Intracellular amyloid-β in Alzheimer's disease. *Nature Reviews Neuroscience*, *8*(7), 499–509. https://doi.org/10.1038/nrn2168

Le Ber, I., De Septenville, A., Guerreiro, R., Bras, J., Camuzat, A., Caroppo, P., Lattante, S., Couarch, P., Kabashi, E., Bouya-Ahmed, K., Dubois, B., & Brice, A. (2014). Homozygous TREM2 mutation in a family with atypical frontotemporal dementia. *Neurobiology of Aging*, *35*(10), 2419.e23-2419.e25. https://doi.org/10.1016/j.neurobiolaging.2014.04.010

Lecker, S. H., Goldberg, A. L., & Mitch, W. E. (2006). Protein degradation by the ubiquitin-proteasome pathway in normal and disease states. *Journal of the American Society of Nephrology : JASN*, *17*(7), 1807–1819. https://doi.org/10.1681/ASN.2006010083

Lee, C. Y. D., & Landreth, G. E. (2010). The role of microglia in amyloid clearance from the AD brain. *Journal of Neural Transmission*, *117*(8), 949–960. https://doi.org/10.1007/s00702-010-0433-4

Lee, D. H., & Goldberg, A. L. (1998). Proteasome inhibitors: valuable new tools for cell biologists. *Trends in Cell Biology*, *8*(10), 397–403. https://doi.org/10.1016/S0962-8924(98)01346-4

Lee, J.-H., Yu, W. H., Kumar, A., Lee, S., Mohan, P. S., Peterhoff, C. M., Wolfe, D. M., Martinez-Vicente, M., Massey, A. C., Sovak, G., Uchiyama, Y., Westaway, D., Cuervo, A. M., & Nixon, R. A. (2010). Lysosomal Proteolysis and Autophagy Require Presenilin 1 and Are Disrupted by Alzheimer-Related PS1 Mutations. *Cell*, *141*(7), 1146–1158. https://doi.org/10.1016/j.cell.2010.05.008

Leissring, M. A., Farris, W., Chang, A. Y., Walsh, D. M., Wu, X., Sun, X., Frosch, M. P., & Selkoe, D. J. (2003). Enhanced Proteolysis of β-Amyloid in APP Transgenic Mice Prevents Plaque Formation, Secondary Pathology, and Premature Death. *Neuron*,

40(6), 1087–1093. https://doi.org/10.1016/S0896-6273(03)00787-6

Leslie, R. G. Q., Melamed, M. D., & Cohen, S. (1971). The products from papain and pepsin hydrolyses of guinea-pig immunoglobulins γ1G and γ2G. *Biochemical Journal*, *121*(5), 829–837. https://doi.org/10.1042/bj1210829

Lessard, C. B., Malnik, S. L., Zhou, Y., Ladd, T. B., Cruz, P. E., Ran, Y., Mahan, T. E., Chakrabaty, P., Holtzman, D. M., Ulrich, J. D., Colonna, M., & Golde, T. E. (2018). High-affinity interactions and signal transduction between Aβ oligomers and TREM2. *EMBO Molecular Medicine*, *10*(11), e9027. https://doi.org/10.15252/emmm.201809027

Lewcock, J. W., Schlepckow, K., Di Paolo, G., Tahirovic, S., Monroe, K. M., & Haass, C. (2020). Emerging Microglia Biology Defines Novel Therapeutic Approaches for Alzheimer's Disease. *Neuron*, *108*(5), 801–821. https://doi.org/10.1016/j.neuron.2020.09.029

Linnartz-Gerlach, B., Bodea, L., Klaus, C., Ginolhac, A., Halder, R., Sinkkonen, L., Walter, J., Colonna, M., & Neumann, H. (2019). TREM2 triggers microglial density and age-related neuronal loss. *Glia*, *67*(3), 539–550. https://doi.org/10.1002/glia.23563

Lu, H., Khurana, S., Verma, N., Manischewitz, J., King, L., Beigel, J. H., & Golding, H. (2011). A Rapid Flp-In System for Expression of Secreted H5N1 Influenza Hemagglutinin Vaccine Immunogen in Mammalian Cells. *PLoS ONE*, *6*(2), e17297. https://doi.org/10.1371/journal.pone.0017297

Lúcio, M., Nunes, C., Gaspar, D., Ferreira, H., Lima, J. L. F. C., & Reis, S. (2009). Antioxidant Activity of Vitamin E and Trolox: Understanding of the Factors that Govern Lipid Peroxidation Studies In Vitro. *Food Biophysics*, *4*(4), 312–320. https://doi.org/10.1007/s11483-009-9129-4

Ma, Q.-L., Chan, P., Yoshii, M., & Uéda, K. (2003). α-Synuclein aggregation and neurodegenerative diseases. *Journal of Alzheimer's Disease*, *5*(2), 139–148. https://doi.org/10.3233/JAD-2003-5208

Mandelkow, E.-M., & Mandelkow, E. (2012). Biochemistry and Cell Biology of Tau Protein in Neurofibrillary Degeneration. *Cold Spring Harbor Perspectives in Medicine*, *2*(7), a006247–a006247. https://doi.org/10.1101/cshperspect.a006247

Mandrekar, S., Jiang, Q., Lee, C. Y. D., Koenigsknecht-Talboo, J., Holtzman, D. M., & Landreth, G. E. (2009). Microglia Mediate the Clearance of Soluble A through Fluid Phase Macropinocytosis. *Journal of Neuroscience*, *29*(13), 4252–4262. https://doi.org/10.1523/JNEUROSCI.5572-08.2009

Mattson, M. P. (1997). Cellular actions of beta-amyloid precursor protein and its soluble and fibrillogenic derivatives. *Physiological Reviews*, *77*(4), 1081–1132. https://doi.org/10.1152/physrev.1997.77.4.1081

Mauthe, M., Orhon, I., Rocchi, C., Zhou, X., Luhr, M., Hijlkema, K.-J., Coppes, R. P., Engedal, N., Mari, M., & Reggiori, F. (2018). Chloroquine inhibits autophagic flux by decreasing autophagosome-lysosome fusion. *Autophagy*, *14*(8), 1435–1455. https://doi.org/10.1080/15548627.2018.1474314

Mazaheri, F., Snaidero, N., Kleinberger, G., Madore, C., Daria, A., Werner, G., Krasemann, S., Capell, A., Trümbach, D., Wurst, W., Brunner, B., Bultmann, S., Tahirovic, S., Kerschensteiner, M., Misgeld, T., Butovsky, O., & Haass, C. (2017). TREM2 deficiency impairs chemotaxis and microglial responses to neuronal injury. *EMBO Reports*, *18*(7), 1186–1198. https://doi.org/10.15252/embr.201743922

Menzies, F. M., Fleming, A., Caricasole, A., Bento, C. F., Andrews, S. P., Ashkenazi, A., Füllgrabe, J., Jackson, A., Jimenez Sanchez, M., Karabiyik, C., Licitra, F., Lopez Ramirez, A., Pavel, M., Puri, C., Renna, M., Ricketts, T., Schlotawa, L., Vicinanza, M., Won, H., … Rubinsztein, D. C. (2017). Autophagy and Neurodegeneration: Pathogenic Mechanisms and Therapeutic Opportunities. *Neuron*, *93*(5), 1015–1034. https://doi.org/10.1016/j.neuron.2017.01.022

Menzies, F. M., Moreau, K., & Rubinsztein, D. C. (2011). Protein misfolding disorders and macroautophagy. *Current Opinion in Cell Biology*, *23*(2), 190–197. https://doi.org/10.1016/j.ceb.2010.10.010

Mettlen, M., Chen, P.-H., Srinivasan, S., Danuser, G., & Schmid, S. L. (2018). Regulation of Clathrin-Mediated Endocytosis. *Annual Review of Biochemistry*, *87*(1), 871–896.

https://doi.org/10.1146/annurev-biochem-062917-012644
Milton, N. G. N. (2001). Phosphorylation of amyloid-β at the serine 26 residue by human cdc2 kinase. *Neuroreport*, *12*(17), 3839–3844. https://doi.org/10.1097/00001756-200112040-00047
Mori, H., Takio, K., Ogawara, M., & Selkoe, D. J. (1992). Mass spectrometry of purified amyloid beta protein in Alzheimer's disease. *Journal of Biological Chemistry*, *267*(24), 17082–17086. https://doi.org/10.1016/S0021-9258(18)41896-0
Mukherjee, S., Ghosh, R. N., & Maxfield, F. R. (1997). Endocytosis. *Physiological Reviews*, *77*(3), 759–803. https://doi.org/10.1152/physrev.1997.77.3.759
Mulrooney, T. J., Posch, P. E., & Hurley, C. K. (2013). DAP12 impacts trafficking and surface stability of killer immunoglobulin-like receptors on natural killer cells. *Journal of Leukocyte Biology*, *94*(2), 301–313. https://doi.org/10.1189/jlb.0213093
Murata, S., Yashiroda, H., & Tanaka, K. (2009). Molecular mechanisms of proteasome assembly. *Nature Reviews Molecular Cell Biology*, *10*(2), 104–115. https://doi.org/10.1038/nrm2630
Nabi, I. R., & Dennis, J. W. (1998). The extent of polylactosamine glycosylation of MDCK LAMP-2 is determined by its Golgi residence time. *Glycobiology*, *8*(9), 947–953. https://doi.org/10.1093/glycob/8.9.947
Nadler, Y., Alexandrovich, A., Grigoriadis, N., Hartmann, T., Rao, K. S. J., Shohami, E., & Stein, R. (2008). Increased expression of the γ-secretase components presenilin-1 and nicastrin in activated astrocytes and microglia following traumatic brain injury. *Glia*, *56*(5), 552–567. https://doi.org/10.1002/glia.20638
Naj, A. C., Jun, G., Beecham, G. W., Wang, L.-S., Vardarajan, B. N., Buros, J., Gallins, P. J., Buxbaum, J. D., Jarvik, G. P., Crane, P. K., Larson, E. B., Bird, T. D., Boeve, B. F., Graff-Radford, N. R., De Jager, P. L., Evans, D., Schneider, J. A., Carrasquillo, M. M., Ertekin-Taner, N., … Schellenberg, G. D. (2011). Common variants at MS4A4/MS4A6E, CD2AP, CD33 and EPHA1 are associated with late-onset Alzheimer's disease. *Nature Genetics*, *43*(5), 436–441. https://doi.org/10.1038/ng.801
Nasu, T., Tsukahara, Y., & Terayama, K. (1973). A lipid metabolic disease -"Membraneous lipodystrophy"- an autopsy case demonstrating numerous peculiar membrane-structures composed of compound lipid in bone and bone marrow and various adipose tissues. *Pathology International*, *23*(3), 539–558.
Nelson, P. T., Alafuzoff, I., Bigio, E. H., Bouras, C., Braak, H., Cairns, N. J., Castellani, R. J., Crain, B. J., Davies, P., Tredici, K. Del, Duyckaerts, C., Frosch, M. P., Haroutunian, V., Hof, P. R., Hulette, C. M., Hyman, B. T., Iwatsubo, T., Jellinger, K. A., Jicha, G. A., … Beach, T. G. (2012). Correlation of Alzheimer Disease Neuropathologic Changes With Cognitive Status: A Review of the Literature. *Journal of Neuropathology & Experimental Neurology*, *71*(5), 362–381. https://doi.org/10.1097/NEN.0b013e31825018f7
Nimmerjahn, A., Kirchhoff, F., & Helmchen, F. (2005). Resting Microglial Cells Are Highly Dynamic Surveillants of Brain Parenchyma in Vivo. *Science*, *308*(5726), 1314–1318. https://doi.org/10.1126/science.1110647
Nixon, R. A., Wegiel, J., Kumar, A., Yu, W. H., Peterhoff, C., Cataldo, A., & Cuervo, A. M. (2005). Extensive Involvement of Autophagy in Alzheimer Disease: An Immuno-Electron Microscopy Study. *Journal of Neuropathology & Experimental Neurology*, *64*(2), 113–122. https://doi.org/10.1093/jnen/64.2.113
Nyathi, Y., Wilkinson, B. M., & Pool, M. R. (2013). Co-translational targeting and translocation of proteins to the endoplasmic reticulum. *Biochimica et Biophysica Acta (BBA) - Molecular Cell Research*, *1833*(11), 2392–2402. https://doi.org/10.1016/j.bbamcr.2013.02.021
O'Gorman, S., Fox, D., & Wahl, G. (1991). Recombinase-mediated gene activation and site-specific integration in mammalian cells. *Science*, *251*(4999), 1351–1355. https://doi.org/10.1126/science.1900642
Orre, M., Kamphuis, W., Osborn, L. M., Jansen, A. H. P., Kooijman, L., Bossers, K., & Hol, E. M. (2014). Isolation of glia from Alzheimer's mice reveals inflammation and dysfunction. *Neurobiology of Aging*, *35*(12), 2746–2760. https://doi.org/10.1016/j.neurobiolaging.2014.06.004

Owen, D. J., & Evans, P. R. (1998). A Structural Explanation for the Recognition of Tyrosine-Based Endocytotic Signals. *Science*, *282*(5392), 1327–1332. https://doi.org/10.1126/science.282.5392.1327

Palade, G. (1975). Intracellular Aspects of the Process of Protein Synthesis. *Science*, *189*(4206), 867–867. https://doi.org/10.1126/science.189.4206.867-b

Palmblad, M., Westlind-Danielsson, A., & Bergquist, J. (2002). Oxidation of Methionine 35 Attenuates Formation of Amyloid β-Peptide 1–40 Oligomers. *Journal of Biological Chemistry*, *277*(22), 19506–19510. https://doi.org/10.1074/jbc.M112218200

Paloneva, J., Mandelin, J., Kiialainen, A., Böhling, T., Prudlo, J., Hakola, P., Haltia, M., Konttinen, Y. T., & Peltonen, L. (2003). DAP12/TREM2 Deficiency Results in Impaired Osteoclast Differentiation and Osteoporotic Features. *Journal of Experimental Medicine*, *198*(4), 669–675. https://doi.org/10.1084/jem.20030027

Paloneva, J., Manninen, T., Christman, G., Hovanes, K., Mandelin, J., Adolfsson, R., Bianchin, M., Bird, T., Miranda, R., Salmaggi, A., Tranebjærg, L., Konttinen, Y., & Peltonen, L. (2002). Mutations in Two Genes Encoding Different Subunits of a Receptor Signaling Complex Result in an Identical Disease Phenotype. *The American Journal of Human Genetics*, *71*(3), 656–662. https://doi.org/10.1086/342259

Pang, Y., Fan, L.-W., Tien, L.-T., Dai, X., Zheng, B., Cai, Z., Lin, R. C. S., & Bhatt, A. (2013). Differential roles of astrocyte and microglia in supporting oligodendrocyte development and myelination in vitro. *Brain and Behavior*, *3*(5), 503–514. https://doi.org/10.1002/brb3.152

Pankiv, S., Clausen, T. H., Lamark, T., Brech, A., Bruun, J.-A., Outzen, H., Øvervatn, A., Bjørkøy, G., & Johansen, T. (2007). p62/SQSTM1 Binds Directly to Atg8/LC3 to Facilitate Degradation of Ubiquitinated Protein Aggregates by Autophagy. *Journal of Biological Chemistry*, *282*(33), 24131–24145. https://doi.org/10.1074/jbc.M702824200

Pardossi-Piquard, R., & Checler, F. (2012). The physiology of the β-amyloid precursor protein intracellular domain AICD. *Journal of Neurochemistry*, *120*, 109–124. https://doi.org/10.1111/j.1471-4159.2011.07475.x

Park, J.-S., Ji, I. J., An, H. J., Kang, M.-J., Kang, S.-W., Kim, D.-H., & Yoon, S.-Y. (2015). Disease-Associated Mutations of TREM2 Alter the Processing of N-Linked Oligosaccharides in the Golgi Apparatus. *Traffic*, *16*(5), 510–518. https://doi.org/10.1111/tra.12264

Pasquier, B. (2016). Autophagy inhibitors. *Cellular and Molecular Life Sciences*, *73*(5), 985–1001. https://doi.org/10.1007/s00018-015-2104-y

Paula, V. de J. R. de, Guimarães, F. M., Diniz, B. S., & Forlenza, O. V. (2009). Neurobiological pathways to Alzheimer's disease: Amyloid-beta, TAU protein or both? *Dementia & Neuropsychologia*, *3*(3), 188–194. https://doi.org/10.1590/S1980-57642009DN30300003

Peng, H., Yang, J., Li, G., You, Q., Han, W., Li, T., Gao, D., Xie, X., Lee, B.-H., Du, J., Hou, J., Zhang, T., Rao, H., Huang, Y., Li, Q., Zeng, R., Hui, L., Wang, H., Xia, Q., … Hu, R. (2017). Ubiquitylation of p62/sequestosome1 activates its autophagy receptor function and controls selective autophagy upon ubiquitin stress. *Cell Research*, *27*(5), 657–674. https://doi.org/10.1038/cr.2017.40

Perry, V. H. (1998). A revised view of the central nervous system microenvironment and major histocompatibility complex class II antigen presentation. *Journal of Neuroimmunology*, *90*(2), 113–121. https://doi.org/10.1016/S0165-5728(98)00145-3

Perry, V. H., Nicoll, J. A. R., & Holmes, C. (2010). Microglia in neurodegenerative disease. *Nature Reviews Neurology*, *6*(4), 193–201. https://doi.org/10.1038/nrneurol.2010.17

Piccio, L., Buonsanti, C., Cella, M., Tassi, I., Schmidt, R. E., Fenoglio, C., Rinker, J., Naismith, R. T., Panina-Bordignon, P., Passini, N., Galimberti, D., Scarpini, E., Colonna, M., & Cross, A. H. (2008). Identification of soluble TREM-2 in the cerebrospinal fluid and its association with multiple sclerosis and CNS inflammation. *Brain*, *131*(11), 3081–3091. https://doi.org/10.1093/brain/awn217

Piccio, L., Deming, Y., Del-Águila, J. L., Ghezzi, L., Holtzman, D. M., Fagan, A. M., Fenoglio, C., Galimberti, D., Borroni, B., & Cruchaga, C. (2016). Cerebrospinal fluid soluble TREM2 is higher in Alzheimer disease and associated with mutation status. *Acta*

Neuropathologica, *131*(6), 925–933. https://doi.org/10.1007/s00401-016-1533-5

Pickford, F., Masliah, E., Britschgi, M., Lucin, K., Narasimhan, R., Jaeger, P. a., Small, S., Spencer, B., Rockenstein, E., Levine, B., & Wyss-Coray, T. (2008). The autophagy-related protein beclin 1 shows reduced expression in early Alzheimer disease and regulates amyloid β accumulation in mice. *Journal of Clinical Investigation*, *118*(6), 2190–2199. https://doi.org/10.1172/JCI33585

Piers, T. M., Cosker, K., Mallach, A., Johnson, G. T., Guerreiro, R., Hardy, J., & Pocock, J. M. (2020). A locked immunometabolic switch underlies TREM2 R47H loss of function in human iPSC-derived microglia. *The FASEB Journal*, *34*(2), 2436–2450. https://doi.org/10.1096/fj.201902447R

Pike, C. J., Overman, M. J., & Cotman, C. W. (1995). Amino-terminal Deletions Enhance Aggregation of β-Amyloid Peptides in Vitro. *Journal of Biological Chemistry*, *270*(41), 23895–23898. https://doi.org/10.1074/jbc.270.41.23895

Plummer, T. H., Elder, J. H., Alexander, S., Phelan, A. W., & Tarentino, A. L. (1984). Demonstration of peptide:N-glycosidase F activity in endo-beta-N-acetylglucosaminidase F preparations. *Journal of Biological Chemistry*, *259*(17), 10700–10704. https://doi.org/10.1016/S0021-9258(18)90568-5

Ponomarev, E. D., Maresz, K., Tan, Y., & Dittel, B. N. (2007). CNS-Derived Interleukin-4 Is Essential for the Regulation of Autoimmune Inflammation and Induces a State of Alternative Activation in Microglial Cells. *Journal of Neuroscience*, *27*(40), 10714–10721. https://doi.org/10.1523/JNEUROSCI.1922-07.2007

Ponte, P., DeWhitt, P. G., Schilling, J., Miller, J., Hsu, D., Greenberg, B., Davis, K., Wallace, W., Lieberburg, I., Fuller, F., & Cordell, B. (1988). A new A4 amyloid mRNA contains a domain homologous to serine proteinase inhibitors. *Nature*, *331*(6156), 525–527. https://doi.org/10.1038/331525a0

Pottier, C., Hannequin, D., Coutant, S., Rovelet-Lecrux, A., Wallon, D., Rousseau, S., Legallic, S., Paquet, C., Bombois, S., Pariente, J., Thomas-Anterion, C., Michon, A., Croisile, B., Etcharry-Bouyx, F., Berr, C., Dartigues, J.-F., Amouyel, P., Dauchel, H., Boutoleau-Bretonnière, C., … Campion, D. (2012). High frequency of potentially pathogenic SORL1 mutations in autosomal dominant early-onset Alzheimer disease. *Molecular Psychiatry*, *17*(9), 875–879. https://doi.org/10.1038/mp.2012.15

Prada, I., Ongania, G. N., Buonsanti, C., Panina-Bordignon, P., & Meldolesi, J. (2006). Triggering receptor expressed in myeloid cells 2 (TREM2) trafficking in microglial cells: Continuous shuttling to and from the plasma membrane regulated by cell stimulation. *Neuroscience*, *140*(4), 1139–1148. https://doi.org/10.1016/j.neuroscience.2006.03.058

Presley, J. F., Cole, N. B., Schroer, T. A., Hirschberg, K., Zaal, K. J. M., & Lippincott-Schwartz, J. (1997). ER-to-Golgi transport visualized in living cells. *Nature*, *389*(6646), 81–85. https://doi.org/10.1038/38001

Price, B. R., Sudduth, T. L., Weekman, E. M., Johnson, S., Hawthorne, D., Woolums, A., & Wilcock, D. M. (2020). Therapeutic Trem2 activation ameliorates amyloid-beta deposition and improves cognition in the 5XFAD model of amyloid deposition. *Journal of Neuroinflammation*, *17*(1), 238. https://doi.org/10.1186/s12974-020-01915-0

Priller, C., Bauer, T., Mitteregger, G., Krebs, B., Kretzschmar, H. A., & Herms, J. (2006). Synapse Formation and Function Is Modulated by the Amyloid Precursor Protein. *Journal of Neuroscience*, *26*(27), 7212–7221. https://doi.org/10.1523/JNEUROSCI.1450-06.2006

Prince, M., Wimo, A., Guerchet, M., Ali, G.-C., Wu, Y.-T., & Prina, M. (2015). *World Alzheimer Report 2015*.

Qi-Takahara, Y. (2005). Longer Forms of Amyloid Protein: Implications for the Mechanism of Intramembrane Cleavage by -Secretase. *Journal of Neuroscience*, *25*(2), 436–445. https://doi.org/10.1523/JNEUROSCI.1575-04.2005

Qiu, W. Q., & Folstein, M. F. (2006). Insulin, insulin-degrading enzyme and amyloid-β peptide in Alzheimer's disease: review and hypothesis. *Neurobiology of Aging*, *27*(2), 190–198. https://doi.org/10.1016/j.neurobiolaging.2005.01.004

Ransohoff, R. M., & Cardona, A. E. (2010). The myeloid cells of the central nervous system parenchyma. *Nature*, *468*(7321), 253–262. https://doi.org/10.1038/nature09615

Ravikumar, B., Vacher, C., Berger, Z., Davies, J. E., Luo, S., Oroz, L. G., Scaravilli, F., Easton, D. F., Duden, R., O'Kane, C. J., & Rubinsztein, D. C. (2004). Inhibition of mTOR induces autophagy and reduces toxicity of polyglutamine expansions in fly and mouse models of Huntington disease. *Nature Genetics*, *36*(6), 585–595. https://doi.org/10.1038/ng1362

Reily, C., Stewart, T. J., Renfrow, M. B., & Novak, J. (2019). Glycosylation in health and disease. *Nature Reviews Nephrology*, *15*(6), 346–366. https://doi.org/10.1038/s41581-019-0129-4

Rezaei-Ghaleh, N., Amininasab, M., Giller, K., Kumar, S., Stündl, A., Schneider, A., Becker, S., Walter, J., & Zweckstetter, M. (2014). Turn Plasticity Distinguishes Different Modes of Amyloid-β Aggregation. *Journal of the American Chemical Society*, *136*(13), 4913–4919. https://doi.org/10.1021/ja411707y

Rhein, V., & Eckert, A. (2007). Effects of Alzheimer's amyloid-beta and tau protein on mitochondrial function—role of glucose metabolism and insulin signalling. *Archives of Physiology and Biochemistry*, *113*(3), 131–141. https://doi.org/10.1080/13813450701572288

Rijal Upadhaya, A., Kosterin, I., Kumar, S., von Arnim, C. A. F., Yamaguchi, H., Fändrich, M., Walter, J., & Thal, D. R. (2014). Biochemical stages of amyloid-β peptide aggregation and accumulation in the human brain and their association with symptomatic and pathologically preclinical Alzheimer's disease. *Brain*, *137*(3), 887–903. https://doi.org/10.1093/brain/awt362

Roberts, G. W., Gentleman, S. M., Lynch, A., Murray, L., Landon, M., & Graham, D. I. (1994). Beta amyloid protein deposition in the brain after severe head injury: implications for the pathogenesis of Alzheimer's disease. *Journal of Neurology, Neurosurgery & Psychiatry*, *57*(4), 419–425. https://doi.org/10.1136/jnnp.57.4.419

Rock, K. L., Gramm, C., Rothstein, L., Clark, K., Stein, R., Dick, L., Hwang, D., & Goldberg, A. L. (1994). Inhibitors of the proteasome block the degradation of most cell proteins and the generation of peptides presented on MHC class I molecules. *Cell*, *78*(5), 761–771. https://doi.org/10.1016/S0092-8674(94)90462-6

Rosen, D. R., Siddique, T., Patterson, D., Figlewicz, D. A., Sapp, P., Hentati, A., Donaldson, D., Goto, J., O'Regan, J. P., Deng, H.-X., Rahmani, Z., Krizus, A., McKenna-Yasek, D., Cayabyab, A., Gaston, S. M., Berger, R., Tanzi, R. E., Halperin, J. J., Herzfeldt, B., … Brown, R. H. (1993). Mutations in Cu/Zn superoxide dismutase gene are associated with familial amyotrophic lateral sclerosis. *Nature*, *362*(6415), 59–62. https://doi.org/10.1038/362059a0

Ross, C. A., & Poirier, M. A. (2004). Protein aggregation and neurodegenerative disease. *Nature Medicine*, *10*(S7), S10–S17. https://doi.org/10.1038/nm1066

Rudd, P. M., & Dwek, R. A. (1997). Glycosylation: Heterogeneity and the 3D Structure of Proteins. *Critical Reviews in Biochemistry and Molecular Biology*, *32*(1), 1–100. https://doi.org/10.3109/10409239709085144

Saido, T. C., Iwatsubo, T., Mann, D. M. A., Shimada, H., Ihara, Y., & Kawashima, S. (1995). Dominant and differential deposition of distinct β-amyloid peptide species, AβN3(pE), in senile plaques. *Neuron*, *14*(2), 457–466. https://doi.org/10.1016/0896-6273(95)90301-1

Saiki, M., Honda, S., Kawasaki, K., Zhou, D., Kaito, A., Konakahara, T., & Morii, H. (2005). Higher-order molecular packing in amyloid-like fibrils constructed with linear arrangements of hydrophobic and hydrogen-bonding side-chains. *Journal of Molecular Biology*, *348*(4), 983–998. https://doi.org/10.1016/j.jmb.2005.03.022

Sarkar, S. (2013). Regulation of autophagy by mTOR-dependent and mTOR-independent pathways: autophagy dysfunction in neurodegenerative diseases and therapeutic application of autophagy enhancers. *Biochemical Society Transactions*, *41*(5), 1103–1130. https://doi.org/10.1042/BST20130134

Satoh, J., Tabunoki, H., Ishida, T., Yagishita, S., Jinnai, K., Futamura, N., Kobayashi, M., Toyoshima, I., Yoshioka, T., Enomoto, K., Arai, N., & Arima, K. (2011). Immunohistochemical characterization of microglia in Nasu-Hakola disease brains. *Neuropathology*, *31*(4), 363–375. https://doi.org/10.1111/j.1440-1789.2010.01174.x

Satpute-Krishnan, P., DeGiorgis, J. A., Conley, M. P., Jang, M., & Bearer, E. L. (2006). A

peptide zipcode sufficient for anterograde transport within amyloid precursor protein. *Proceedings of the National Academy of Sciences*, *103*(44), 16532–16537. https://doi.org/10.1073/pnas.0607527103

Schieb, H., Kratzin, H., Jahn, O., Möbius, W., Rabe, S., Staufenbiel, M., Wiltfang, J., & Klafki, H. W. (2011). β-Amyloid Peptide Variants in Brains and Cerebrospinal Fluid from Amyloid Precursor Protein (APP) Transgenic Mice. *Journal of Biological Chemistry*, *286*(39), 33747–33758. https://doi.org/10.1074/jbc.M111.246561

Schlepckow, K., Kleinberger, G., Fukumori, A., Feederle, R., Lichtenthaler, S. F., Steiner, H., & Haass, C. (2017). An Alzheimer-associated TREM2 variant occurs at the ADAM cleavage site and affects shedding and phagocytic function. *EMBO Molecular Medicine*, *9*(10), 1356–1365. https://doi.org/10.15252/emmm.201707672

Schlepckow, K., Monroe, K. M., Kleinberger, G., Cantuti-Castelvetri, L., Parhizkar, S., Xia, D., Willem, M., Werner, G., Pettkus, N., Brunner, B., Sülzen, A., Nuscher, B., Hampel, H., Xiang, X., Feederle, R., Tahirovic, S., Park, J. I., Prorok, R., Mahon, C., … Haass, C. (2020). Enhancing protective microglial activities with a dual function TREM2 antibody to the stalk region. *EMBO Molecular Medicine*, *12*(4), e11227. https://doi.org/10.15252/emmm.201911227

Selkoe, D. J. (2001). Alzheimer's Disease: Genes, Proteins, and Therapy. *Physiological Reviews*, *81*(2), 741–766. https://doi.org/10.1152/physrev.2001.81.2.741

Sergeant, N., Bombois, S., Ghestem, A., Drobecq, H., Kostanjevecki, V., Missiaen, C., Wattez, A., David, J.-P., Vanmechelen, E., Sergheraert, C., & Delacourte, A. (2003). Truncated beta-amyloid peptide species in pre-clinical Alzheimer's disease as new targets for the vaccination approach. *Journal of Neurochemistry*, *85*(6), 1581–1591. https://doi.org/10.1046/j.1471-4159.2003.01818.x

Sethi, M., & Fanayan, S. (2015). Mass Spectrometry-Based N-Glycomics of Colorectal Cancer. *International Journal of Molecular Sciences*, *16*(12), 29278–29304. https://doi.org/10.3390/ijms161226165

Shakin-Eshleman, S. H., Spitalnik, S. L., & Kasturi, L. (1996). The Amino Acid at the X Position of an Asn-X-Ser Sequon Is an Important Determinant of N-Linked Core-glycosylation Efficiency. *Journal of Biological Chemistry*, *271*(11), 6363–6366. https://doi.org/10.1074/jbc.271.11.6363

Sheng, L., Chen, M., Cai, K., Song, Y., Yu, D., Zhang, H., & Xu, G. (2019). Microglial Trem2 induces synaptic impairment at early stage and prevents amyloidosis at late stage in APP/PS1 mice. *The FASEB Journal*, *33*(9), 10425–10442. https://doi.org/10.1096/fj.201900527R

Shibata, M., Yamada, S., Kumar, S. R., Calero, M., Bading, J., Frangione, B., Holtzman, D. M., Miller, C. A., Strickland, D. K., Ghiso, J., & Zlokovic, B. V. (2000). Clearance of Alzheimer's amyloid-β1-40 peptide from brain by LDL receptor–related protein-1 at the blood-brain barrier. *Journal of Clinical Investigation*, *106*(12), 1489–1499. https://doi.org/10.1172/JCI10498

Shigemoto-Mogami, Y., Hoshikawa, K., Goldman, J. E., Sekino, Y., & Sato, K. (2014). Microglia Enhance Neurogenesis and Oligodendrogenesis in the Early Postnatal Subventricular Zone. *Journal of Neuroscience*, *34*(6), 2231–2243. https://doi.org/10.1523/JNEUROSCI.1619-13.2014

Sims, R., van der Lee, S. J., Naj, A. C., Bellenguez, C., Badarinarayan, N., Jakobsdottir, J., Kunkle, B. W., Boland, A., Raybould, R., Bis, J. C., Martin, E. R., Grenier-Boley, B., Heilmann-Heimbach, S., Chouraki, V., Kuzma, A. B., Sleegers, K., Vronskaya, M., Ruiz, A., Graham, R. R., … Schellenberg, G. D. (2017). Rare coding variants in PLCG2, ABI3, and TREM2 implicate microglial-mediated innate immunity in Alzheimer's disease. *Nature Genetics*, *49*(9), 1373–1384. https://doi.org/10.1038/ng.3916

Singh, A., Kukreti, R., Saso, L., & Kukreti, S. (2019). Oxidative Stress: A Key Modulator in Neurodegenerative Diseases. *Molecules*, *24*(8), 1583. https://doi.org/10.3390/molecules24081583

Sirkis, D. W., Aparicio, R. E., & Schekman, R. (2017). Neurodegeneration-associated mutant TREM2 proteins abortively cycle between the ER and ER–Golgi intermediate compartment. *Molecular Biology of the Cell*, *28*(20), 2723–2733.

https://doi.org/10.1091/mbc.e17-06-0423

Sladek, R., Rocheleau, G., Rung, J., Dina, C., Shen, L., Serre, D., Boutin, P., Vincent, D., Belisle, A., Hadjadj, S., Balkau, B., Heude, B., Charpentier, G., Hudson, T. J., Montpetit, A., Pshezhetsky, A. V., Prentki, M., Posner, B. I., Balding, D. J., … Froguel, P. (2007). A genome-wide association study identifies novel risk loci for type 2 diabetes. *Nature*, *445*(7130), 881–885. https://doi.org/10.1038/nature05616

Solito, E., & Sastre, M. (2012). Microglia Function in Alzheimer's Disease. *Frontiers in Pharmacology*, *3*, 14. https://doi.org/10.3389/fphar.2012.00014

Song, W. M., Hooli, B., Mullin, K., Jin, S. C., Cella, M., Ulland, T. K., Wang, Y., Tanzi, R. E., & Colonna, M. (2017). Alzheimer's disease-associated TREM2 variants exhibit either decreased or increased ligand-dependent activation. *Alzheimer's & Dementia*, *13*(4), 381–387. https://doi.org/10.1016/j.jalz.2016.07.004

Song, W. M., Joshita, S., Zhou, Y., Ulland, T. K., Gilfillan, S., & Colonna, M. (2018). Humanized TREM2 mice reveal microglia-intrinsic and -extrinsic effects of R47H polymorphism. *Journal of Experimental Medicine*, *215*(3), 745–760. https://doi.org/10.1084/jem.20171529

Soto, C. (2003). Unfolding the role of protein misfolding in neurodegenerative diseases. *Nature Reviews Neuroscience*, *4*(1), 49–60. https://doi.org/10.1038/nrn1007

Spiro, R. G. (2002). Protein glycosylation: nature, distribution, enzymatic formation, and disease implications of glycopeptide bonds. *Glycobiology*, *12*(4), 43R-56R. https://doi.org/10.1093/glycob/12.4.43R

Stanley, P. (2011). Golgi Glycosylation. *Cold Spring Harbor Perspectives in Biology*, *3*(4), a005199–a005199. https://doi.org/10.1101/cshperspect.a005199

Stanley, P., Schachter, H., & Taniguchi, N. (2009). N-Glycans. In *Essentials of Glycobiology*.

Steinberg, S., Stefansson, H., Jonsson, T., Johannsdottir, H., Ingason, A., Helgason, H., Sulem, P., Magnusson, O. T., Gudjonsson, S. A., Unnsteinsdottir, U., Kong, A., Helisalmi, S., Soininen, H., Lah, J. J., Aarsland, D., Fladby, T., Ulstein, I. D., Djurovic, S., Sando, S. B., … Stefansson, K. (2015). Loss-of-function variants in ABCA7 confer risk of Alzheimer's disease. *Nature Genetics*, *47*(5), 445–447. https://doi.org/10.1038/ng.3246

Steinman, R. M., Mellman, I. S., Muller, W. A., & Cohn, Z. A. (1983). Endocytosis and the recycling of plasma membrane. *Journal of Cell Biology*, *96*(1), 1–27. https://doi.org/10.1083/jcb.96.1.1

Stelzmann, R. A., Schnitzlein, H. N., & Murtagh, F. R. (1995). An english translation of alzheimer's 1907 paper, "über eine eigenartige erkankung der hirnrinde." *Clinical Anatomy*, *8*(6), 429–431. https://doi.org/10.1002/ca.980080612

Stephenson, J., Nutma, E., van der Valk, P., & Amor, S. (2018). Inflammation in CNS neurodegenerative diseases. *Immunology*, *154*(2), 204–219. https://doi.org/10.1111/imm.12922

Stevens, B., Allen, N. J., Vazquez, L. E., Howell, G. R., Christopherson, K. S., Nouri, N., Micheva, K. D., Mehalow, A. K., Huberman, A. D., Stafford, B., Sher, A., Litke, A. M., Lambris, J. D., Smith, S. J., John, S. W. M., & Barres, B. A. (2007). The Classical Complement Cascade Mediates CNS Synapse Elimination. *Cell*, *131*(6), 1164–1178. https://doi.org/10.1016/j.cell.2007.10.036

Stewart, C. R., Stuart, L. M., Wilkinson, K., van Gils, J. M., Deng, J., Halle, A., Rayner, K. J., Boyer, L., Zhong, R., Frazier, W. A., Lacy-Hulbert, A., Khoury, J. El, Golenbock, D. T., & Moore, K. J. (2010). CD36 ligands promote sterile inflammation through assembly of a Toll-like receptor 4 and 6 heterodimer. *Nature Immunology*, *11*(2), 155–161. https://doi.org/10.1038/ni.1836

Stratoulias, V., Venero, J. L., Tremblay, M., & Joseph, B. (2019). Microglial subtypes: diversity within the microglial community. *The EMBO Journal*, *38*(17), e101997. https://doi.org/10.15252/embj.2019101997

Strittmatter, W. J., Saunders, A. M., Schmechel, D., Pericak-Vance, M., Enghild, J., Salvesen, G. S., & Roses, A. D. (1993). Apolipoprotein E: high-avidity binding to beta-amyloid and increased frequency of type 4 allele in late-onset familial Alzheimer disease. *Proceedings of the National Academy of Sciences*, *90*(5), 1977–1981.

https://doi.org/10.1073/pnas.90.5.1977

Suárez-Calvet, M., Araque Caballero, M. A., Kleinberger, G., Bateman, R. J., Fagan, A. M., Morris, J. C., Levin, J., Danek, A., Ewers, M., & Haass, C. (2016). Early changes in CSF sTREM2 in dominantly inherited Alzheimers disease occur after amyloid deposition and neuronal injury. *Science Translational Medicine*, *8*(369), 369ra178-369ra178. https://doi.org/10.1126/scitranslmed.aag1767

Suárez-Calvet, M., Morenas-Rodríguez, E., Kleinberger, G., Schlepckow, K., Araque Caballero, M. Á., Franzmeier, N., Capell, A., Fellerer, K., Nuscher, B., Eren, E., Levin, J., Deming, Y., Piccio, L., Karch, C. M., Cruchaga, C., Shaw, L. M., Trojanowski, J. Q., Weiner, M., Ewers, M., & Haass, C. (2019). Early increase of CSF sTREM2 in Alzheimer's disease is associated with tau related-neurodegeneration but not with amyloid-β pathology. *Molecular Neurodegeneration*, *14*(1), 1. https://doi.org/10.1186/s13024-018-0301-5

Suárez-Calvet, M., Kleinberger, G., Araque Caballero, M. Á., Brendel, M., Rominger, A., Alcolea, D., Fortea, J., Lleó, A., Blesa, R., Gispert, J. D., Sánchez-Valle, R., Antonell, A., Rami, L., Molinuevo, J. L., Brosseron, F., Traschütz, A., Heneka, M. T., Struyfs, H., Engelborghs, S., … Haass, C. (2016). sTREM2 cerebrospinal fluid levels are a potential biomarker for microglia activity in early-stage Alzheimer's disease and associate with neuronal injury markers. *EMBO Molecular Medicine*, *8*(5), 466–476. https://doi.org/10.15252/emmm.201506123

Sudom, A., Talreja, S., Danao, J., Bragg, E., Kegel, R., Min, X., Richardson, J., Zhang, Z., Sharkov, N., Marcora, E., Thibault, S., Bradley, J., Wood, S., Lim, A. C., Chen, H., Wang, S., Foltz, I. N., Sambashivan, S., & Wang, Z. (2018). Molecular basis for the loss-of-function effects of the Alzheimer's disease-associated R47H variant of the immune receptor TREM2. *Journal of Biological Chemistry*, *293*(32), 12634–12646. https://doi.org/10.1074/jbc.RA118.00235

Sumer-Bayraktar, Z., Kolarich, D., Campbell, M. P., Ali, S., Packer, N. H., & Thaysen-Andersen, M. (2011). N-Glycans Modulate the Function of Human Corticosteroid-Binding Globulin. *Molecular & Cellular Proteomics*, *10*(8), M111.009100. https://doi.org/10.1074/mcp.M111.009100

Takalo, M., Salminen, A., Soininen, H., Hiltunen, M., & Haapasalo, A. (2013). Protein aggregation and degradation mechanisms in neurodegenerative diseases. *American Journal of Neurodegenerative Disease*, *2*(1), 1–14.

Takei, N., & Nawa, H. (2014). mTOR signaling and its roles in normal and abnormal brain development. *Frontiers in Molecular Neuroscience*, *7*(April), 28. https://doi.org/10.3389/fnmol.2014.00028

Tang, B., Cai, J., Sun, L., Li, Y., Qu, J., Snider, B. J., & Wu, S. (2014). Proteasome Inhibitors Activate Autophagy Involving Inhibition of PI3K-Akt-mTOR Pathway as an Anti-Oxidation Defense in Human RPE Cells. *PLoS ONE*, *9*(7), e103364. https://doi.org/10.1371/journal.pone.0103364

Tanzi, R. E., & Bertram, L. (2001). New Frontiers in Alzheimer's Disease Genetics. *Neuron*, *32*(2), 181–184. https://doi.org/10.1016/S0896-6273(01)00476-7

Tarentino, A. L., & Plummer, T. H. (1994). Enzymatic deglycosylation of asparagine-linked glycans: purification, properties, and specificity of oligosaccharide-cleaving enzymes from Flavobacterium meningosepticum. *Methods in Enzymology*, *230*, 44–57. https://doi.org/10.1016/0076-6879(94)30006-2

Tarentino, A. L., Trimble, R. B., & Plummer, T. H. (1989). Enzymatic approaches for studying the structure, synthesis, and processing of glycoproteins. *Methods in Cell Biology*, *32*, 111–139. https://doi.org/10.1016/s0091-679x(08)61169-3

Tarkowski, E., Andreasen, N., Tarkowski, A., & Blennow, K. (2003). Intrathecal inflammation precedes development of Alzheimer's disease. *Journal of Neurology, Neurosurgery & Psychiatry*, *74*(9), 1200–1205. https://doi.org/10.1136/jnnp.74.9.1200

Taubes, G. (2003). NEUROSCIENCE: Insulin Insults May Spur Alzheimer's Disease. *Science*, *301*(5629), 40–41. https://doi.org/10.1126/science.301.5629.40

The Alzheimer's Association. (2020). 2020 Alzheimer's disease facts and figures. *Alzheimer's & Dementia*, *16*(3), 391–460. https://doi.org/10.1002/alz.12068

Thornton, P., Sevalle, J., Deery, M. J., Fraser, G., Zhou, Y., Ståhl, S., Franssen, E. H., Dodd, R. B., Qamar, S., Gomez Perez-Nievas, B., Nicol, L. S., Eketjäll, S., Revell, J., Jones, C., Billinton, A., St George-Hyslop, P. H., Chessell, I., & Crowther, D. C. (2017). TREM2 shedding by cleavage at the H157-S158 bond is accelerated for the Alzheimer's disease-associated H157Y variant. *EMBO Molecular Medicine*, *9*(10), 1366–1378. https://doi.org/10.15252/emmm.201707673

Tomlinson, B. E., Blessed, G., & Roth, M. (1970). Observations on the brains of demented old people. *Journal of the Neurological Sciences*, *11*(3), 205–242. https://doi.org/10.1016/0022-510X(70)90063-8

Traub, L. M. (2009). Tickets to ride: selecting cargo for clathrin-regulated internalization. *Nature Reviews Molecular Cell Biology*, *10*(9), 583–596. https://doi.org/10.1038/nrm2751

Tremblay, M.-È., Lowery, R. L., & Majewska, A. K. (2010). Microglial Interactions with Synapses Are Modulated by Visual Experience. *PLoS Biology*, *8*(11), e1000527. https://doi.org/10.1371/journal.pbio.1000527

Tremblay, M.-È., Stevens, B., Sierra, A., Wake, H., Bessis, A., & Nimmerjahn, A. (2011). The Role of Microglia in the Healthy Brain. *Journal of Neuroscience*, *31*(45), 16064–16069. https://doi.org/10.1523/JNEUROSCI.4158-11.2011

Tsubuki, S., Saito, Y., Tomioka, M., Ito, H., & Kawashima, S. (1996). Differential Inhibition of Calpain and Proteasome Activities by Peptidyl Aldehydes of Di-Leucine and Tri-Leucine. *Journal of Biochemistry*, *119*(3), 572–576. https://doi.org/10.1093/oxfordjournals.jbchem.a021280

Turnbull, I. R., Gilfillan, S., Cella, M., Aoshi, T., Miller, M., Piccio, L., Hernandez, M., & Colonna, M. (2006). Cutting Edge: TREM-2 Attenuates Macrophage Activation. *The Journal of Immunology*, *177*(6), 3520–3524. https://doi.org/10.4049/jimmunol.177.6.3520

Ueno, M., Fujita, Y., Tanaka, T., Nakamura, Y., Kikuta, J., Ishii, M., & Yamashita, T. (2013). Layer V cortical neurons require microglial support for survival during postnatal development. *Nature Neuroscience*, *16*(5), 543–551. https://doi.org/10.1038/nn.3358

Ulland, T. K., Song, W. M., Huang, S. C.-C., Ulrich, J. D., Sergushichev, A., Beatty, W. L., Loboda, A. A., Zhou, Y., Cairns, N. J., Kambal, A., Loginicheva, E., Gilfillan, S., Cella, M., Virgin, H. W., Unanue, E. R., Wang, Y., Artyomov, M. N., Holtzman, D. M., & Colonna, M. (2017). TREM2 Maintains Microglial Metabolic Fitness in Alzheimer's Disease. *Cell*, *170*(4), 649-663.e13. https://doi.org/10.1016/j.cell.2017.07.023

Varki, A., Cummings, R. D., Aebi, M., Packer, N. H., Seeberger, P. H., Esko, J. D., Stanley, P., Hart, G., Darvill, A., Kinoshita, T., Prestegard, J. J., Schnaar, R. L., Freeze, H. H., Marth, J. D., Bertozzi, C. R., Etzler, M. E., Frank, M., Vliegenthart, J. F. G., Lütteke, T., … Kornfeld, S. (2015). Symbol Nomenclature for Graphical Representations of Glycans. *Glycobiology*, *25*(12), 1323–1324. https://doi.org/10.1093/glycob/cwv091

Vassar, R., Bennett, B. D., Babu-Khan, S., Kahn, S., Mendiaz, E. A., Denis, P., Teplow, D. B., Ross, S., Amarante, P., Loeloff, R., Luo, Y., Fisher, S., Fuller, J., Edenson, S., Lile, J., Jarosinski, M. A., Biere, A. L., Curran, E., Burgess, T., … Citron, M. (1999). Beta-Secretase Cleavage of Alzheimer's Amyloid Precursor Protein by the Transmembrane Aspartic Protease BACE. *Science*, *286*(5440), 735–741. https://doi.org/10.1126/science.286.5440.735

Vasudevan, D., & Haltiwanger, R. S. (2014). Novel roles for O-linked glycans in protein folding. *Glycoconjugate Journal*, *31*(6–7), 417–426. https://doi.org/10.1007/s10719-014-9556-4

Vembar, S. S., & Brodsky, J. L. (2008). One step at a time: endoplasmic reticulum-associated degradation. *Nature Reviews Molecular Cell Biology*, *9*(12), 944–957. https://doi.org/10.1038/nrm2546

Viotti, C. (2016). ER to Golgi-Dependent Protein Secretion: The Conventional Pathway. In *Methods in Molecular Biology* (pp. 3–29). https://doi.org/10.1007/978-1-4939-3804-9_1

Voisine, C., Pedersen, J. S., & Morimoto, R. I. (2010). Chaperone networks: Tipping the balance in protein folding diseases. *Neurobiology of Disease*, *40*(1), 12–20. https://doi.org/10.1016/j.nbd.2010.05.007

Vonsattel, J. P., Myers, R. H., Stevens, T. J., Ferrante, R. J., Bird, E. D., & Richardson, E. P. (1985). Neuropathological Classification of Huntington's Disease. *Journal of Neuropathology and Experimental Neurology*, *44*(6), 559–577. https://doi.org/10.1097/00005072-198511000-00003

Walter, J. (2016). The Triggering Receptor Expressed on Myeloid Cells 2: A Molecular Link of Neuroinflammation and Neurodegenerative Diseases. *Journal of Biological Chemistry*, *291*(9), 4334–4341. https://doi.org/10.1074/jbc.R115.704981

Walter, J., Kemmerling, N., Wunderlich, P., & Glebov, K. (2017). γ-Secretase in microglia - implications for neurodegeneration and neuroinflammation. *Journal of Neurochemistry*, *143*(4), 445–454. https://doi.org/10.1111/jnc.14224

Walter, P., & Ron, D. (2011). The Unfolded Protein Response: From Stress Pathway to Homeostatic Regulation. *Science*, *334*(6059), 1081–1086. https://doi.org/10.1126/science.1209038

Wang, D., Peng, Z., Ren, G., & Wang, G. (2015). The different roles of selective autophagic protein degradation in mammalian cells. *Oncotarget*, *6*(35), 37098–37116. https://doi.org/10.18632/oncotarget.5776

Wang, P. (2005). Defective Neuromuscular Synapses in Mice Lacking Amyloid Precursor Protein (APP) and APP-Like Protein 2. *Journal of Neuroscience*, *25*(5), 1219–1225. https://doi.org/10.1523/JNEUROSCI.4660-04.2005

Wang, S., Mustafa, M., Yuede, C. M., Salazar, S. V., Kong, P., Long, H., Ward, M., Siddiqui, O., Paul, R., Gilfillan, S., Ibrahim, A., Rhinn, H., Tassi, I., Rosenthal, A., Schwabe, T., & Colonna, M. (2020). Anti-human TREM2 induces microglia proliferation and reduces pathology in an Alzheimer's disease model. *Journal of Experimental Medicine*, *217*(9), e20200785. https://doi.org/10.1084/jem.20200785

Wang, X., Wang, W., Li, L., Perry, G., Lee, H., & Zhu, X. (2014). Oxidative stress and mitochondrial dysfunction in Alzheimer's disease. *Biochimica et Biophysica Acta (BBA) - Molecular Basis of Disease*, *1842*(8), 1240–1247. https://doi.org/10.1016/j.bbadis.2013.10.015

Wang, Y., Cella, M., Mallinson, K., Ulrich, J. D., Young, K. L., Robinette, M. L., Gilfillan, S., Krishnan, G. M., Sudhakar, S., Zinselmeyer, B. H., Holtzman, D. M., Cirrito, J. R., & Colonna, M. (2015). TREM2 Lipid Sensing Sustains the Microglial Response in an Alzheimer's Disease Model. *Cell*, *160*(6), 1061–1071. https://doi.org/10.1016/j.cell.2015.01.049

Wang, Y., Ulland, T. K., Ulrich, J. D., Song, W., Tzaferis, J. A., Hole, J. T., Yuan, P., Mahan, T. E., Shi, Y., Gilfillan, S., Cella, M., Grutzendler, J., DeMattos, R. B., Cirrito, J. R., Holtzman, D. M., & Colonna, M. (2016). TREM2-mediated early microglial response limits diffusion and toxicity of amyloid plaques. *Journal of Experimental Medicine*, *213*(5), 667–675. https://doi.org/10.1084/jem.20151948

Weingarten, M. D., Lockwood, A. H., Hwo, S. Y., & Kirschner, M. W. (1975). A protein factor essential for microtubule assembly. *Proceedings of the National Academy of Sciences*, *72*(5), 1858–1862. https://doi.org/10.1073/pnas.72.5.1858

Werner, E. D., Brodsky, J. L., & McCracken, A. A. (1996). Proteasome-dependent endoplasmic reticulum-associated protein degradation: An unconventional route to a familiar fate. *Proceedings of the National Academy of Sciences*, *93*(24), 13797–13801. https://doi.org/10.1073/pnas.93.24.13797

Westerheide, S. D., & Morimoto, R. I. (2005). Heat shock response modulators as therapeutic tools for diseases of protein conformation. *The Journal of Biological Chemistry*, *280*(39), 33097–33100. https://doi.org/10.1074/jbc.R500010200

Wiltfang, J., Esselmann, H., Bibl, M., Smirnov, A., Otto, M., Paul, S., Schmidt, B., Klafki, H.-W., Maler, M., Dyrks, T., Bienert, M., Beyermann, M., Rüther, E., & Kornhuber, J. (2002). Highly conserved and disease-specific patterns of carboxyterminally truncated Aβ peptides 1-37/38/39 in addition to 1-40/42 in Alzheimer's disease and in patients with chronic neuroinflammation. *Journal of Neurochemistry*, *81*(3), 481–496. https://doi.org/10.1046/j.1471-4159.2002.00818.x

Winslow, A. R., Chen, C.-W., Corrochano, S., Acevedo-Arozena, A., Gordon, D. E., Peden, A. A., Lichtenberg, M., Menzies, F. M., Ravikumar, B., Imarisio, S., Brown, S., O'Kane,

C. J., & Rubinsztein, D. C. (2010). α-Synuclein impairs macroautophagy: implications for Parkinson's disease. *Journal of Cell Biology*, *190*(6), 1023–1037. https://doi.org/10.1083/jcb.201003122

Wirths, O., Breyhan, H., Cynis, H., Schilling, S., Demuth, H.-U., & Bayer, T. A. (2009). Intraneuronal pyroglutamate-Abeta 3–42 triggers neurodegeneration and lethal neurological deficits in a transgenic mouse model. *Acta Neuropathologica*, *118*(4), 487–496. https://doi.org/10.1007/s00401-009-0557-5

Wójcik, C., & DeMartino, G. N. (2003). Intracellular localization of proteasomes. *The International Journal of Biochemistry & Cell Biology*, *35*(5), 579–589. https://doi.org/10.1016/S1357-2725(02)00380-1

Wood, J. G., Mirra, S. S., Pollock, N. J., & Binder, L. I. (1986). Neurofibrillary tangles of Alzheimer disease share antigenic determinants with the axonal microtubule-associated protein tau. *Proceedings of the National Academy of Sciences*, *83*(11), 4040–4043. https://doi.org/10.1073/pnas.83.11.4040

Wormald, M. R., Petrescu, A. J., Pao, Y.-L., Glithero, A., Elliott, T., & Dwek, R. A. (2002). Conformational Studies of Oligosaccharides and Glycopeptides: Complementarity of NMR, X-ray Crystallography, and Molecular Modelling. *Chemical Reviews*, *102*(2), 371–386. https://doi.org/10.1021/cr990368i

Wright, P. E., & Dyson, H. J. (2015). Intrinsically disordered proteins in cellular signalling and regulation. *Nature Reviews Molecular Cell Biology*, *16*(1), 18–29. https://doi.org/10.1038/nrm3920

Wu, K., Byers, D. E., Jin, X., Agapov, E., Alexander-Brett, J., Patel, A. C., Cella, M., Gilfilan, S., Colonna, M., Kober, D. L., Brett, T. J., & Holtzman, M. J. (2015). TREM-2 promotes macrophage survival and lung disease after respiratory viral infection. *Journal of Experimental Medicine*, *212*(5), 681–697. https://doi.org/10.1084/jem.20141732

Wunderlich, P., Glebov, K., Kemmerling, N., Tien, N. T., Neumann, H., & Walter, J. (2013). Sequential Proteolytic Processing of the Triggering Receptor Expressed on Myeloid Cells-2 (TREM2) Protein by Ectodomain Shedding and γ-Secretase-dependent Intramembranous Cleavage. *Journal of Biological Chemistry*, *288*(46), 33027–33036. https://doi.org/10.1074/jbc.M113.517540

Wyss-Coray, T., & Mucke, L. (2002). Inflammation in Neurodegenerative Disease—A Double-Edged Sword. *Neuron*, *35*(3), 419–432. https://doi.org/10.1016/S0896-6273(02)00794-8

Yan, R., Bienkowski, M. J., Shuck, M. E., Miao, H., Tory, M. C., Pauley, A. M., Brashler, J. R., Stratman, N. C., Mathews, W. R., Buhl, A. E., Carter, D. B., Tomasselli, A. G., Parodi, L. A., Heinrikson, R. L., & Gurney, M. E. (1999). Membrane-anchored aspartyl protease with Alzheimer's disease β-secretase activity. *Nature*, *402*(6761), 533–537. https://doi.org/10.1038/990107

Yao, H., Coppola, K., Schweig, J. E., Crawford, F., Mullan, M., & Paris, D. (2019). Distinct Signaling Pathways Regulate TREM2 Phagocytic and NFκB Antagonistic Activities. *Frontiers in Cellular Neuroscience*, *13*, 457. https://doi.org/10.3389/fncel.2019.00457

Yeh, F. L., Hansen, D. V., & Sheng, M. (2017). TREM2, Microglia, and Neurodegenerative Diseases. *Trends in Molecular Medicine*, *23*(6), 512–533. https://doi.org/10.1016/j.molmed.2017.03.008

Yeh, F. L., Wang, Y., Tom, I., Gonzalez, L. C., & Sheng, M. (2016). TREM2 Binds to Apolipoproteins, Including APOE and CLU/APOJ, and Thereby Facilitates Uptake of Amyloid-Beta by Microglia. *Neuron*, *91*(2), 328–340. https://doi.org/10.1016/j.neuron.2016.06.015

Yin, J., Liu, X., He, Q., Zhou, L., Yuan, Z., & Zhao, S. (2016). Vps35-dependent recycling of Trem2 regulates microglial function. *Traffic*, *17*(12), 1286–1296. https://doi.org/10.1111/tra.12451

Yuan, P., Condello, C., Keene, C. D., Wang, Y., Bird, T. D., Paul, S. M., Luo, W., Colonna, M., Baddeley, D., & Grutzendler, J. (2016). TREM2 Haplodeficiency in Mice and Humans Impairs the Microglia Barrier Function Leading to Decreased Amyloid Compaction and Severe Axonal Dystrophy. *Neuron*, *90*(4), 724–739. https://doi.org/10.1016/j.neuron.2016.05.003

Zaffagnini, G., & Martens, S. (2016). Mechanisms of Selective Autophagy. *Journal of Molecular Biology*, *428*(9), 1714–1724. https://doi.org/10.1016/j.jmb.2016.02.004

Zerbinatti, C. V., & Bu, G. (2005). LRP and Alzheimer's Disease. *Reviews in the Neurosciences*, *16*(2). https://doi.org/10.1515/REVNEURO.2005.16.2.123

Zhang, B., Gaiteri, C., Bodea, L.-G., Wang, Z., McElwee, J., Podtelezhnikov, A. A., Zhang, C., Xie, T., Tran, L., Dobrin, R., Fluder, E., Clurman, B., Melquist, S., Narayanan, M., Suver, C., Shah, H., Mahajan, M., Gillis, T., Mysore, J., … Emilsson, V. (2013). Integrated Systems Approach Identifies Genetic Nodes and Networks in Late-Onset Alzheimer's Disease. *Cell*, *153*(3), 707–720. https://doi.org/10.1016/j.cell.2013.03.030

Zhao, J., & Goldberg, A. L. (2016). Coordinate regulation of autophagy and the ubiquitin proteasome system by MTOR. *Autophagy*, *12*(10), 1967–1970. https://doi.org/10.1080/15548627.2016.1205770

Zhao, J., Zhai, B., Gygi, S. P., & Goldberg, A. L. (2015). mTOR inhibition activates overall protein degradation by the ubiquitin proteasome system as well as by autophagy. *Proceedings of the National Academy of Sciences*, *112*(52), 15790–15797. https://doi.org/10.1073/pnas.1521919112

Zhao, Y., Li, X., Huang, T., Jiang, L., Tan, Z., Zhang, M., Cheng, I. H.-J., Wang, X., Bu, G., Zhang, Y., Wang, Q., & Xu, H. (2017). Intracellular trafficking of TREM2 is regulated by presenilin 1. *Experimental & Molecular Medicine*, *49*(12), e405–e405. https://doi.org/10.1038/emm.2017.200

Zhao, Y., Wu, X., Li, X., Jiang, L.-L., Gui, X., Liu, Y., Sun, Y., Zhu, B., Piña-Crespo, J. C., Zhang, M., Zhang, N., Chen, X., Bu, G., An, Z., Huang, T. Y., & Xu, H. (2018). TREM2 Is a Receptor for β-Amyloid that Mediates Microglial Function. *Neuron*, *97*(5), 1023-1031.e7. https://doi.org/10.1016/j.neuron.2018.01.031

Zhong, L., & Chen, X.-F. (2019). The Emerging Roles and Therapeutic Potential of Soluble TREM2 in Alzheimer's Disease. *Frontiers in Aging Neuroscience*, *11*, 328. https://doi.org/10.3389/fnagi.2019.00328

Zhong, L., Chen, X.-F., Wang, T., Wang, Z., Liao, C., Wang, Z., Huang, R., Wang, D., Li, X., Wu, L., Jia, L., Zheng, H., Painter, M., Atagi, Y., Liu, C.-C., Zhang, Y.-W., Fryer, J. D., Xu, H., & Bu, G. (2017). Soluble TREM2 induces inflammatory responses and enhances microglial survival. *Journal of Experimental Medicine*, *214*(3), 597–607. https://doi.org/10.1084/jem.20160844

Zhong, L., Chen, X.-F., Zhang, Z.-L., Wang, Z., Shi, X.-Z., Xu, K., Zhang, Y.-W., Xu, H., & Bu, G. (2015). DAP12 Stabilizes the C-terminal Fragment of the Triggering Receptor Expressed on Myeloid Cells-2 (TREM2) and Protects against LPS-induced Pro-inflammatory Response. *Journal of Biological Chemistry*, *290*(25), 15866–15877. https://doi.org/10.1074/jbc.M115.645986

Zhong, L., Wang, Z., Wang, D., Wang, Z., Martens, Y. A., Wu, L., Xu, Y., Wang, K., Li, J., Huang, R., Can, D., Xu, H., Bu, G., & Chen, X.-F. (2018). Amyloid-beta modulates microglial responses by binding to the triggering receptor expressed on myeloid cells 2 (TREM2). *Molecular Neurodegeneration*, *13*(1), 15. https://doi.org/10.1186/s13024-018-0247-7

Zhong, L., Xu, Y., Zhuo, R., Wang, T., Wang, K., Huang, R., Wang, D., Gao, Y., Zhu, Y., Sheng, X., Chen, K., Wang, N., Zhu, L., Can, D., Marten, Y., Shinohara, M., Liu, C., Du, D., Sun, H., … Chen, X.-F. (2019). Soluble TREM2 ameliorates pathological phenotypes by modulating microglial functions in an Alzheimer's disease model. *Nature Communications*, *10*(1), 1365. https://doi.org/10.1038/s41467-019-09118-9

Zhou, D. (2003). Why are Glycoproteins Modified by Poly-N-Acetyllactosamine Glycoconjugates? *Current Protein & Peptide Science*, *4*(1), 1–9. https://doi.org/10.2174/1389203033380304

Zhou, F., van Laar, T., Huang, H., & Zhang, L. (2011). APP and APLP1 are degraded through autophagy in response to proteasome inhibition in neuronal cells. *Protein & Cell*, *2*(5), 377–383. https://doi.org/10.1007/s13238-011-1047-9

Zhu, M., Li, D., Wu, Y., Huang, X., & Wu, M. (2014). TREM-2 Promotes Macrophage-Mediated Eradication of Pseudomonas aeruginosa via a PI3K/Akt Pathway. *Scandinavian Journal of Immunology*, *79*(3), 187–196. https://doi.org/10.1111/sji.12148

List of Figures

List of Tables

Abbreviations

%	Percent
°C	Degree Celsius
aa	Amino acid
AD	Alzheimer's disease
ADAM	A disintegrin and metalloprotease
ApoE	Apolipoprotein E
APP	Amyloid precursor protein
Aβ	β-Amyloid
BBB	Blood-brain-barrier
BSA	Bovine serum albumin
CNS	Central nervous system
conj.	Conjugated
CPS	Classical protein secretion
CSF	Cerebrospinal fluid
CTF	C-terminal fragment
DAP12	DNAX activation protein of 12 kDa
DAPI	4',6-Diamidin-2-phenylindol
DMEM	Dulbecco's modified eagle's medium
DMSO	Dimethyl sulfoxide
DNA	Deoxyribonucleic acid
dNTP	Deoxynucleotide triphosphate
DTT	Dithiothreitol
E.coli	Escherichia coli
EB	Embryoid body
ECL	Enhanced chemiluminescence
EDTA	Ethylenediaminetetraacetic acid
EOAD	Early-onset AD
ER	Endoplasmic reticulum
ERAD	ER-associated degradation
ERGIC	ER-Golgi-intermediate compartment
FCS	Fetal calf serum
FRT	Flp recombination target

FTD	Frontotemporal dementia
GA	Golgi apparatus
GalNAc	N-acetylgalactosamine
GlcNAc	N-acetylglucosamine
GWAS	Genome-wide association studies
HD	Huntington's disease
HEK	Human embryonic kidney cells
$H_2O_{dest.}$	Distilled water
HRP	Horseradish peroxidase
ICC	Immunocytochemistry
ICD	Intracellular domain
IDE	Insulin-degrading enzyme
IDR	Intrinsically disordered region
ITAM	Immunoreceptor tyrosine-based activation motif
iPSC	Induced pluripotent stem cells
iPSdMiG	iPS-derived microglia
kDa	Kilodalton
LB	Lysogeny Broth
LC3	Light chain 3
LOAD	Late-onset AD
LRP	Low-density lipoprotein receptor-related protein
MCI	Mild cognitive impairment
MS4A	Membrane-spanning 4-domains superfamily A
mTOR	mammalian target of rapamycin
NaDOC	Deoxycholic acid
Neu5Ac	N-acetylneuraminic acid
NEP	Neprilysin
NHD	Nasu-Hakola disease
NFT	Neurofibrillary tangles
PAGE	Polyacrylamide gel electrophoresis
PBS	Phosphate buffered saline
PCR	Polymerase chain reaction
PFA	Paraformaldehyde
PD	Parkinson's disease

PNS	Postnucleaur supernatant
PLL	Poly-L-Lysine
PS	Presenilin
PtdS	Phosphatidylserine
PTM	Post-translational modification
RNA	Ribonucleic acid
ROS	Reactive oxygen species
rpm	Revolutions per minute
RT	Room temperature
SD	Standard deviation
SDS	Sodium dodecyl sulfate
SEM	Standard error of mean
SOC	Super optimal broth with catabolite repression
SOD1	Superoxide dismutase 1
sTREM	soluble TREM
SYK	Spleen tyrosine kinase
TBE	Tris-borate-EDTA
TBST	Tris-buffered saline, Tween-20
TCA	Trichloroacetic acid
TGN	*Trans*-Golgi network
TREM	Triggering receptor expressed on myeloid cells
Ub	Ubiquitin
UPS	Ubiquitin-proteasome system
USP	Unconventional secretory pathway
UV	Ultraviolet
wt	Wild-type

Amino Acids

Amino acid	3-letter code	1-letter code
Alanine	Ala	A
Arginine	Arg	R
Asparagine	Asn	N
Aspartic acid	Asp	D
Cysteine	Cys	C
Glutamic acid	Glu	E
Glutamine	Gln	Q
Glycine	Gly	G
Histidine	His	H
Isoleucine	Ile	I
Leucine	Leu	L
Lysine	Lys	K
Methionine	Met	M
Phenylalanine	Phe	F
Proline	Pro	P
Serine	Ser	S
Threonine	Thr	T
Tryptophan	Trp	W
Tyrosine	Tyr	Y
Valine	Val	V

Publications and congress contributions

Publications

Ibach, M., Mathews, M., Linnartz-Gerlach, B., Theil, S., Kumar, S., Feederle, R., Brüstle, O., Neumann, H., & Walter, J. (2021). A reporter cell system for the triggering receptor expressed on myeloid cells 2 reveals differential effects of disease-associated variants on receptor signaling and activation by antibodies against the stalk region. *Glia*, *69*(5), 1126–1139. https://doi.org/10.1002/glia.23953

Posters

10/2017	PHAGO General Assembly Meeting 2, Paris, France
10/2018	PHAGO General Assembly Meeting 3, Ludwigshafen, Germany
12/2018	ASCB/EMBO Meeting, San Diego, CA, USA Travel Grant DAAD, IPID4all
10/2019	PHAGO General Assembly Meeting 4, London, UK
11/2019	Düsseldorf-Jülich Symposium on Neurodegenerative Diseases, Düsseldorf, Germany

Talks

10/2018	PHAGO General Assembly Meeting 3, Ludwigshafen, Germany
10/2019	PHAGO General Assembly Meeting 4, London, UK
11/2020	PHAGO General Assembly Meeting 5, Virtual Meeting